Dislocations in Strained-layer Semiconductor Heterostructures.

Thesis

UNRESTRICTED

Dislocations in Strained-layer Semiconductor Heterostructures

by

Xian Wei Liu

Thesis submitted for the degree of

Doctor of Philosophy

Faculty of Technology

The Open University

UK

DATE OF SUBMISSION : 17 SEPTEMBER 1999

DATE OF AWARD : 20 DECEMBER 1999

September 1999

ProQuest LLC.
789 East Eisenhower Parkway
P.O. Box 1346
Ann Arbor, MI 48106 – 1346

Abstract

The reliability of semiconductor devices depends upon the stability of the constituent materials. Strained-layer semiconductor structures contain a layer whose lattice constant differs from the surrounding layers, resulting in a misfit strain. As dislocations are the main failure mechanism in semiconductor lasers, it is essential to establish whether the stability of these structures is affected by the lattice mismatch and the possibility of relaxation by the formation of misfit dislocations. In this thesis, dislocations in strained-layer semiconductor structures are investigated.

Relaxation of strained-layer GaAs/$In_xGa_{1-x}As$/GaAs heterostructures through the formation of misfit dislocations is found to occur in stages. Firstly, generation and elongation of misfit dislocations on threading dislocations during molecular beam epitaxy (MBE) growth have been demonstrated with increasing strained-layer thickness. The onset of this stage has been shown to occur at strained-layer thicknesses below those predicted by the Matthews-Blakeslee (M-B) model. The second stage of relaxation is marked by the formation of a network of 60° misfit dislocations. A third stage of relaxation has been discovered, in which pure edge (i.e. 90°) misfit dislocations are formed in addition to the existing network of 60° misfit dislocations.

Different mechanisms are found to be responsible for the three stages of relaxation. The M-B model describes the transformation of threading dislocations to generate 60° misfit dislocations. As this affects individual dislocations, it results in only local relaxation. A separate mechanism, which remains unclear but is not dependent on the interactions of dislocations, dominates the formation of a 60° misfit dislocation network. The edge dislocations responsible for further relaxation of the structures are produced by vacancy-producing jogs. These protrude from pre-existing 60° dislocations and trail edge dislocation pairs as they climb.

It is shown here that as-grown structures with strained-layer thicknesses below the theoretical prediction can be relaxed by the formation of a 60° dislocation network during post-growth thermal processing and bending. Thus the first two stages of relaxation are dependent on both the strained-layer thickness during fabrication, and on the temperature and applied stress of as-grown structures.

Finally, dislocation motion in strained layer structures has been shown to be slower than that in unstrained structures. Thus the misfit stress acts as an additional resistant force to the displacement of atoms in non-misfit dislocations, even though it drives the formation of misfit dislocations.

Acknowledgements

This study of dislocations in strained-layer semiconductor heterostructures could not have been carried out without the help of numerous people. Fist of all, I would like to wholeheartedly thank my supervisors, Dr Adrian A Hopgood and Dr Nick St J Braithwaite for their tremendous help in all aspects of this work. Without this help and without the framework established by Dr Adrian A Hopgood, this PhD research would have been inconceivable. It was very inspiring and rewarding to have the privilege to work for my PhD under their supervision.

I greatly appreciate the help of Naomi Williams for the instruction in the use of electron microscopes and her help with my English. I am very grateful to Ian Norman, Colin Gagg, Jim Moffatt, Gordon Imlach, Pete Ledgard, John Bandy, and Richard Black for their technical assistance. Thank you also to the staff of the Department of Materials Engineering for their help throughout my doctoral research.

I am particularly grateful to Hong Wang in Singapore and Dr Brian F Usher in Australia for their kind provision of MBE InGaAs/GaAs specimens, and to Dr Peter Augustus in GEC for his kind help in the measurement of strained-layer thickness.

I would like to thank my family. My mother was very supportive of my efforts to come to the UK despite the fact that I was going to be so far away from her. It is a regret of mine for life that she could not see me finish my PhD research. My sister and brothers helped and supported me in various ways. I also owe a great deal to my wife and son who shared with me all of the times, good and not so good, here. Their encouragement and help have always made a great deal of difference.

Finally, this PhD research could not have been carried out without the funding provided by the Research Degrees Centre of The Open University.

List of Figures

Contents

Chapter 1: Introduction

The development of electronic and optoelectronic devices based on heteroepitaxial strained layers has attracted much attention in recent years. Semiconductors that are difficult to grow as bulk crystals may be obtained by forming heteroepitaxial films on dislocation-free single-crystal substrates [Nix_89]. Such structures allow a great variety of materials to be combined and exhibit unique properties due to the built-in strain and, in the case of semiconductors, they enable a wider range of electrical and optical properties than the lattice-matched structures [Drigo_89]. A great deal of attention has been focused on film/substrate systems of III-V compounds such as InGaAs/GaAs for optical applications. The fundamental materials challenge in the synthesis and application of such structures is the enormous strains and associated stresses generated by the lattice parameters mismatch [Hull_96]. While this misfit strain itself can be beneficial, there is often a large driving force for its relaxation through the formation of misfit dislocations at the film/substrate interface. Because the presence of dislocations often has adverse effects on the electrical properties of devices and degrades the electrical transport of carriers [Coleman_91, Fitzgerald_91], much effort has been made to understand the thermodynamics and kinetics of this relaxation process. However, strained-layer semiconductors are not presently well understood [Price_91, Dunstan_97], controlling the relaxation process and the effects of misfit stress on the reliability of the structure is still key to the development of reliable devices based on heteroepitaxial films.

1.1 Strained-layer structure, misfit dislocation, and critical thickness

Strained epitaxial layers are grown for one or more of three reasons [Goodhew_97]: to retain their strain in order to exploit the properties of strained materials; to relax their strain in order to provide a layer of different lattice parameter from its substrate; or, by accident.

If a pair of crystals with the same orientation but different lattice parameters are placed in perfect contact, the atoms near the interface will adjust their positions. This results in interfacial regions of good and bad register. The regions of bad register resemble crystal dislocations and, because of this, they are called interfacial or misfit dislocations. The existence of misfit dislocations was predicted by Frank and van der Merwe 50 years ago[Frank_49]. In the case of a layer of crystal growing onto a substrate with the same orientation but different lattice parameter, if the thickness of the layer and the misfit between the stress-free lattice parameters of the two crystals are both sufficiently small, the crystal of the layer is strained to bring its lattice into register at the interface, and all misfit is accommodated by elastic strain. Crystals strained in this way are described as pseudomorphic [Pashley_65] or coherent [Kelly_63]. When the thickness of the layer becomes large enough the misfit will be accommodated by both the elastic strain and the formation of misfit dislocations. It is called a relaxed structure. The boundary between these two structures is estimated by the concept of critical thickness. The strained-layer structures of which the strained-layer thicknesses are below the critical thickness are thought to be thermodynamically stable [Dunstan_97].

There are several considerations about the definition of critical thickness. Matthews [Matthews_79] defined the critical thickness as the thickness of the overgrowth at which the generation of misfit dislocations will begin. According to his model, as soon as the bowing of threading dislocations in a strained-layer structure

begins under the effects of misfit stress, that means the critical thickness for the relaxation of the structure has been reached. Cohen-Solal *et al* [Cohen_94] and Pinardi *et al* [Pinardi_98] suggested that the critical thickness is the thickness at which the homogeneous strain energy and the energy of the totally relaxed layer are equal. Dunstan [Dunstan_97] thought that a critical thickness is the thickness at which the fully strained layer becomes unstable (or metastable).

The distinction between dislocations and misfit-dislocations is important. Dislocations in an unstrained crystal always increase the energy of the crystal and they are not required by thermodynamics. Misfit dislocations are present in an elastically strained crystal and relax misfit strain. Therefore, misfit dislocations decrease the total energy of the crystal and are required by thermodynamics [Jain_94].

1.2 Device applications of strained InGaAs layers

1.2.1 Device applications

Strained-layer quantum well (QW) semiconductor lasers were fabricated for the first time in 1984 [Laidig_84] by adding indium to GaAs layers in order to bridge the 880 to 1100 nm wavelength gap left by the lower and higher wavelength limits of AlGaAs/GaAs and InGaAsP/InP, respectively. The research was extended to the other group III-V material systems after theoretical predictions of improved performance for QW semiconductor lasers with the active material deliberately grown in a state of compressive strain [Adams_86, Yablonovitch_86]. In 1989, the first successful application of compressive strain in 1.5 μm wavelength $In_{0.8}Ga_{0.2}As$/InGaAsP MQW semiconductor lasers was reported [Thijs_89]. And in the same year, strained InGaAs quantum wells were reported to be used for 980 nm pumping of Er^{3+}-doped optical fibre amplifiers [Vodhanel_89]. To date, enhanced and reliable performance of strained-layer QW semiconductor lasers has been reported for InGaAs(P)/InP and AlGaInAs/InP telecommunication lasers, AlGaInP/GaAs visible-light emitting lasers, and

AlGa(In)As(P)/GaAs near-infrared emitting lasers. The dramatic impact of strained-layer QWs is best illustrated by the fact that they are now commercially available [Thijs_95].

There are other applications that make use of relaxed films as buffer layers for the growth of other heteroepitaxial layers [Fitzgerald_91]. For this type of application, a buffer layer as fully relaxed as possible is desired.

1.2.2 Reliability worries

The presence of a strained layer in structure raises questions over the reliability of these lasers. Simple elasticity theory gives the misfit stress, σ_ε, generated by a lattice mismatch strain, ε, as

$$\sigma_\varepsilon = 2G\varepsilon(1+\nu)/(1-\nu), \tag{1.1}$$

where G is the epilayer shear modulus (typically of order 50 GPa), ν is the Poisson ratio (≈ 0.33), and ε is the lattice mismatch strain. Thus a lattice mismatch parameter difference of 1% between substrate and epilayer generates a stress of ≈ 2 GPa in the structure. There is no doubt that this stress will have effects on nucleation and propagation of dislocations which are one of the main mechanisms of the material failure [Petroff_73, Hutchinson_75, Ueda_88].

Some phenomena have been observed showing the difference in dislocation propagation between unstrained AlGaAs and strained InGaAs and InAlGaAs quantum well semiconductor lasers [Waters_90, Waters_91]. In unstrained AlGaAs quantum well semiconductor lasers, dark line defects (DLDs), which are three-dimensional dislocation networks, grew predominantly in <100> directions. The growth along <110> directions was much slower. However, in strained InGaAs and InAlGaAs quantum well heterostructure lasers, DLD growth along <100> directions was practically eliminated while the much slower growth along <110> still occurred. It is generally accepted that <100> DLDs propagate by dislocation climb and <110> DLDs

propagate by dislocation glide [Ueda_88]. It is unclear why the climb mechanism but not the glide mechanism would be affected by the strained-layer, but a vacancy-controlled model has been proposed by Hopgood [Hopgood_94] as a possible explanation.

1.3 Strain relaxation through the formation of misfit dislocations

1.3.1 Mechanisms for the relaxation

Several mechanisms have been proposed for relaxation of a strained-layer structure [Hull_96], including roughening of the epitaxial layer surface, interdiffusion between epilayer and substrate, and introduction of misfit dislocations. This thesis only concerns misfit dislocations.

1.3.2 Theoretical models

The model based on energy consideration

The concept of an equilibrium critical thickness was initiated by Frank and van der Merwe based on the energy balance approach in which a Frenkel-Kontorowa potential was employed to determine the energy expressions describing the misfit between a crystalline epitaxial layer and a crystalline substrate with different lattice constants [Frank_49_A, Frank_49_B]. The theory shows that the interfacial energy for a film of finite thickness is nearly the same as that for an infinitely thick film, the difference only being significant when the misfit is small. In the case of small misfit, the minimum-energy state is one in which the overlayer is deformed to fit the substrate. The relative hardness between the overlayer and substrate, the strength of the bonding between the overlayer and substrate, and the film thickness all affect the critical misfit value for defect formation [Fox_90, E.A.Fitzgerald_91].

From van der Merwe's model, the interfacial energy E_I between film and substrate was assumed the minimum energy available for generation of dislocations. The approximate expression for E_I, in the limit of moderate misfit ($f < 4\%$), is

$$E_I \approx 9.5 f(Gb / 4\pi^2), \tag{1.2}$$

where b is the slip distance (i.e., b = magnitude of the Burgers vector). Note that E_I is independent of film thickness. The strain energy per unit area associated with a film of thickness h is given by

$$E_H = 2G\left(\frac{1+\nu}{1-\nu}\right)hf^2, \tag{1.3}$$

and increases linearly from zero with h. Equating Eqs. (1.2) and (1.3) and setting $h = h_c$, one obtains the critical thickness

$$h_c \approx \left(\frac{1}{8\pi^2}\right)\left(\frac{1+\nu}{1-\nu}\right)\frac{a_0}{f}, \tag{1.4}$$

where a_0 is the bulk lattice constant of the substrate [People_85]

The theory by van der Merwe qualitatively describes misfit epitaxy, and proves to be somewhat valid for high-misfit metal systems with thin overlayers. However, it was thought to be not valid for lower misfit or thick overlayers [E.A.Fitzgerald_91]. Jesser and Matthews [Jesser_67] showed experimentally that thin layers of iron on copper, cobalt on copper [Jesser_68_A] and iron on hot copper [Jesser_68_B] did approximately agree with van der Merwe's theory, but thicker films retained much higher elastic strain than expected by this same theory [Matthews_70_A, Matthews_70_B]. The energy-minimisation model by van der Merwe allows one to estimate the lowest-energy state of the system, but the theory does not consider the actual mechanism of film relaxation [Fitzgerald_91].

The model based on force balance

For semiconductor strained layers, the most generally used model for predicting critical thickness is the mechanical equilibrium (force balance) theory of Matthews-Blakeslee (M-B model) [HullR_92, Fitzgerald_91, Downes_94].

The M-B theory [Matthews_79, Matthews_76, Matthews_74, Matthews_75_A, Jesser_67, Matthews_66] presupposes the existence of grown-in threading dislocations and it is the interaction of these dislocations with the misfit strain field that generates misfit dislocations at the epitaxial film/substrate interface.

Bicrystals contain dislocation lines which extend from the substrate, through the interface, and through the overgrowth layer. Some of these threading dislocations are able to move by glide to generate lengths of misfit dislocation line. Interface structure can be predicted from the forces on dislocation lines. Two of the important forces are F_ε, the force exerted by misfit strain as the driving force for the formation of misfit dislocation and increasing with the strained-layer thickness, and F_l, the tension in the dislocation line which opposes the motion of misfit dislocation, as illustrated in Fig. 1.1 (a). Assuming the elastic constant of the two media, A and B are equal, the force exerted by misfit strain is given as

$$F_\varepsilon = \frac{2G(1+\nu)}{(1-\nu)} bh\varepsilon \cos\lambda \ , \tag{1.5}$$

where b is the magnitude of the Burgers vector, h is the strained-layer thickness, and λ is the angle between the slip direction and that direction in the film plane which is perpendicular to the line of intersection of the slip plane and the interface. The tension in the dislocation line is

$$F_l = \frac{Gb^2}{4\pi(1-\nu)}(1-\nu\cos^2\alpha)(\ln\frac{h}{b}+1), \tag{1.6}$$

where α is the angle between the dislocation line and its Burgers vector.

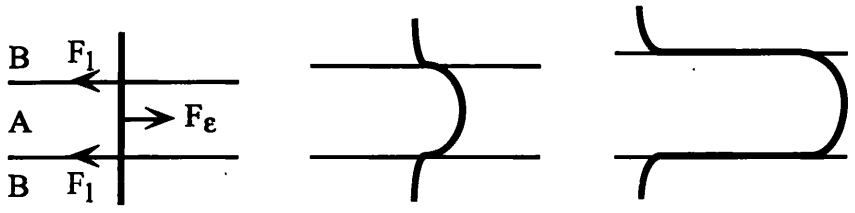

(a) (b) (c)

Fig. 1.1. Different geometries of threading dislocations marking the interfacial structures in a double heterostructures predicted by the Matthews-Blakeslee model. The layer A is a strained layer. (a) coherent when $F_\varepsilon < F_l$, (b) critical when $F_\varepsilon = F_l$, and (c) incoherent. when $F_\varepsilon > F_l$,

For the single heterostructure, if $F_\varepsilon = F_l$, threading dislocations will have the geometry shown by Fig. 1.1 (b) where a threading dislocation has bowed under the influence of the misfit strain. If $F_\varepsilon > F_l$, the dislocation will elongate at the plane of the interface, thereby producing a length of misfit dislocation, as in Fig. 1.1 (c). This motion reduces ε and destroys the coherence of the interface between layers. Equating (1.5) and (1.6), and making the replacement $\varepsilon = f$, one obtains the critical thickness, h_c,

$$h_c = \frac{b(1-\nu\cos^2\alpha)}{8\pi f\cos\lambda(1+\nu)}(\ln\frac{h_c}{b}+1). \tag{1.7}$$

For the single quantum wells, due to the existence of two interfaces, the driving force needs to overcome two line tensions to extend the misfit dislocation at the interfaces. Twigg [Twigg_90, Zuo_93] pointed out that if the capping layer thickness is more than twice that of the strained-layer, the capping layer thickness can be considered to be infinite. Then the critical thickness H_c for the single quantum well system is obtained from $F_\varepsilon = 2F_l$ and so

$$H_c = \frac{b(1-\nu\cos^2\alpha)}{4\pi f\cos\lambda(1+\nu)}(\ln\frac{H_c}{b}+1). \tag{1.8}$$

The People and Bean's consideration

The equilibrium model of Matthews-Blakeslee assumes that misfit dislocations are formed by glide of pre-existing threading dislocations. In carefully grown semiconductor crystals on low-defect substrate the number of available threading dislocations might not be sufficient. In that case, new dislocations must nucleate before misfit segments can be formed[Maree_87]. People and Bean [People_85, People_86] developed an empirical model for critical thickness which considered the nucleation of dislocations. They defined critical thickness by equating the strain energy per unit area of the layer with the energy per unit area of an array of misfit dislocations. It is assumed that the growing film is initially free of threading dislocations, and that interfacial misfit dislocations will be generated when the strain energy per unit area exceeds the self-energy of an isolated dislocation of a given type (e.g., screw, edge, etc.). The strain energy per unit area associated with a film of thickness h is given by

$$E_H = 2G\left(\frac{1+\nu}{1-\nu}\right)hf^2, \tag{1.15}$$

and increases linearly from zero with h. The energy per unit area associated with an isolated dislocation at a distance h from a free surface is approximately

$$E_D = \left(\frac{Gb^2}{8\pi\sqrt{2}a(x)}\right)\ln\left(\frac{h}{b}\right), \tag{1.16}$$

where $a(x)$ is the bulk lattice constant of the film. Equating (1.15) and (1.16) and setting $h = h_c$, one obtains

$$h_c \cong \left(\frac{1-\nu}{1+\nu}\right)\left(\frac{1}{16\pi\sqrt{2}}\right)\left(\frac{b^2}{a(x)}\right)\left[\left(\frac{1}{f^2}\right)\ln\left(\frac{h_c}{b}\right)\right]. \tag{1.17}$$

The excess stress

The concept of excess stress for the formation of misfit dislocations was proposed by Dodson and Tsao[Dodson_87, Dodson_88, Tsao_87, Tsao 88]. The excess, or net, stress σ_{ex} on the dislocation is given by

$$\sigma_{ex} = \sigma_M - \sigma_D$$

$$= \frac{G\cos\Phi}{1-\nu}\left[2\varepsilon(1+\nu)\cos\lambda - \frac{b(1-\nu\cos^2\theta)}{4\pi h}\ln\left(\frac{\alpha h}{b}\right)\right]. \qquad (1.18)$$

This means that the stress which actually drives dislocation motion is the difference between the usual stress σ_M due to misfit strain and "effective" stress σ_D due to dislocation-line tension. This excess stress is a measure of the driving force for strain relief, and hence both for the deviation from equilibrium and for the degree of metastability.

The concept of this excess stress as the driving force is considered to be of considerable significance for dislocation dynamics in lattice-mismatched films [HullR_92]. This model predicts the stages in strain relaxation. There is no strain relaxation until the critical thickness is reached. After the critical thickness has just been passed, strain relaxation is initially very slow. This incubation period arises because the excess stress at this stage is relatively low and dislocation multiplication is retarded by the low initial source density. As the epilayer thickness increases, the excess stress gets progressively larger. This increases dislocation propagation velocity and thus strain relaxation rates, effectively producing an approximately exponential increase in the number of dislocations. Hence, the strain relaxation rate dramatically increases. Eventually, a large fraction of the original lattice mismatch strain is relaxed. The excess stress decreases and, because dislocations are now moving more slowly, they interact less frequently and thus dislocation multiplication slows. The structure now asymptotically approaches its equilibrium strain state, ε_0. Note that ε_0 is not equal to zero, as may be confirmed by setting the excess stress to zero. For a given lattice

mismatch in a given system, the magnitude of ε_0 asymptotically approaches zero as the layer thickness approaches infinity.

1.3.3 Disparity between models and experimental observations

There has been much comparison of experimental data with the critical thickness as calculated using Matthews-Blakeslee's theory. Some experiments yield critical thicknesses greater than the value given by the theory [People_85, People_86], whereas others agree well with the theory [Grundmann_89].

The discrepancy between theory and experimental data has, in some cases, been attributed to the different sensitivity of the experimental method used to detect the onset of interface-dislocation formation [Fitzgerald_91, Fritz_87_A]. As pointed out by Fritz [Fritz_87_B], the observed critical thickness will crucially depend on the minimum detectable strain relaxation or misfit dislocation density for a given technique. This reflects the absence of experimental evidence on the onset of misfit dislocation formation in investigation of strained-layer structures. Most misfit dislocations that can be seen in publications are ones which have developed far beyond their stages of initialisation.

The fact that some strained-layer structures relax at greater thickness than that expected by the equilibrium theory indicates that dislocation nucleation and/or propagation may be inhibited [Fitzgerald_91]. It suggests the existence of a kinetic barrier to the generation of misfit dislocations in semiconductors [Maree_87]. Neither van der Merwe's nor Matthews-Blakeslee's theory attempts to describe the nucleation and propagation processes of the misfit dislocations [LeGoues_96].

The ability to grow greater thicknesses of strained epilayer than predicted by the MB theory before misfit dislocations are observed has led to the concept of metastability of strained layer structures [HullR_92].

1.3.4 Temperature dependence of critical thickness

It was suggested [Price_91] that to obtain the correct value of the critical thickness at high temperature (~530°C) other forces should be included where appropriate, such as the creation or loss of surface and the forces between gliding dislocations, dislocations and obstacles. Fox and Jesser[Fox_90] modified the Matthews-Blakeslee model to explain the discrepancy between the theory and experimental results by including the frictional force on a dislocation. They proposed that the effective force on the threading dislocation is the driving force due to the lattice mismatch F_ε less the barrier forces due to the Peierls force F_p, the line tension F_l, and the forces F_a due to a dislocation atmosphere or other dislocations,

$$F_{eff} = F_\varepsilon - F_p - F_l - F_a. \tag{1.9}$$

This gives a critical thickness, $h_c^{'}$, when the frictional force is included can be obtained as

$$h_c^{'} = \frac{C}{D(f - \varepsilon_U - \varepsilon_a)}\left[\ln\left(\frac{h_c^{'}}{b}\right)+1\right], \tag{1.10}$$

where

$$C = \frac{Gb^2(1-\nu\cos^2\psi)}{2\pi G(1-\nu)} \tag{1.11}$$

and

$$D = \frac{2G(1+\nu)b\cos\lambda}{(1-\nu)}. \tag{1.12}$$

Here,

$$\varepsilon_U = \frac{A}{D}\exp\left(\frac{U_i}{kT}\right) \tag{1.13}$$

is independent of thickness and represents an amount of elastic strain that cannot be accommodated by the generation of misfit dislocations and is a direct result of the Peierls barriers, and

$$\varepsilon_a = \frac{E}{D}\exp\left(\frac{W_i}{kT}\right), \tag{1.14}$$

is due to the additional barrier which results from the locking of a dislocation by the dislocation atmosphere. Comparing with the critical thickness given by Matthews-Blakeslee's model, h_c' increases by $\frac{1}{f-\varepsilon_U-\varepsilon_a}-\frac{1}{f}$ due to Peierls force and dislocation atmosphere.

This modification makes critical thickness become a function of temperature. The value of critical thickness given by the M-B model is now becoming a low limit and will be approaching by the modified value from upwards with the increase of temperature, as shown in Fig. 1.2. In this way, the theoretical value was modified to become higher and fitted the experimental results quite well [Price_91].

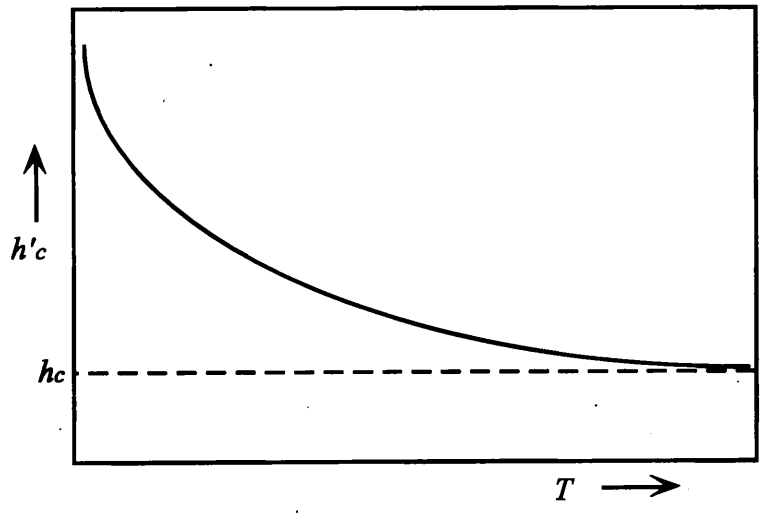

Fig. 1.2. Temperature dependence of h'_c. h_c is the value given by the M-B model

Some experimental results [Radulescu_89, Whaley_90, Price_91] were reported showing that the critical thickness is temperature dependent and decreases with the

increase of temperature in a good agreement with the prediction given by the equation (1.10), as shown in Fig. 1.3.

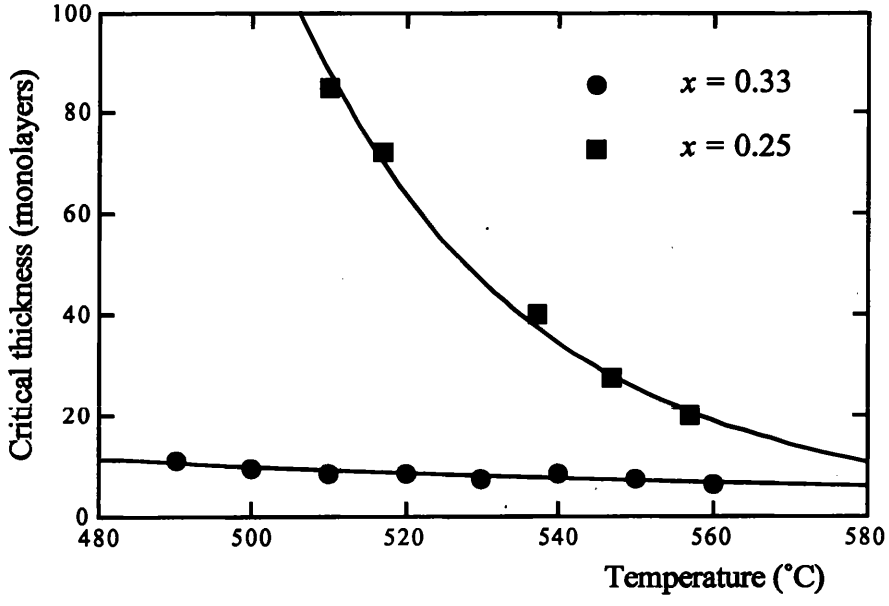

Fig. 1.3. Plots of critical thickness against temperature predicted by the equation (1.10) and the temperature dependence of critical thickness obtained experimentally for $In_xGa_{1-x}As$ on GaAs.

1.3.5 Limitation of the M-B model and different phases of relaxation

The M-B model has been regarded as a basic mechanism for the critical thickness and it is expected to accurately predict the critical thickness for strains of order of 1% or less [HullR_96]. Pichaud et al [Pichaud_99] recently claimed that the mechanism proposed by the M-B model could actually be observed in low misfit systems.

However, as pointed out by Dunstan [Dunstan_97], although equilibrium theory predicts when a threader could be turned over to form a misfit dislocation, what actually happens after that is highly adventitious. Dixon and Goodhew [Dixon_90] found that, in $In_xGa_{1-x}As$ grown on GaAs by molecular-beam epitaxy (MBE), threading dislocations were turned over at a thickness near the equilibrium critical thickness, but generation of fresh dislocations did not take place until a much greater thickness. Whitehouse and co-

workers [Whitehouse_93] found that, in $In_xGa_{1-x}As$ grown on GaAs by both liquid encapsulated Czochralski (LEC) and vertical-gradient freeze Bridgmann (VGFB), there were different phases of relaxation. Threading dislocations played the dominant role in the first phase; after all 1/2<110> type dislocations had been activated, a significant increase in the epilayer thickness was required to initiate a second phase of stress-relief resulting from other dislocation generation processes. P. Kidd and co-workers [Kidd_93] illustrated the transition from the appearance of the first dislocations in thin layers, which only provided localised relaxation, to the condition where the dislocation density was sufficient to relax all regions of the layer.

Relaxation of strained-layer structures, as pointed out by Goodhew [Goodhew_99, Goodhew_94], never can be complete, and strained layers never relax fully to give a strain-free surface. This arises the necessary that relaxation should be investigated with the consideration that this relaxation may be a process with different stages.

1.4 Misfit dislocations

1.4.1 Geometry

Almost all heteroepitaxial semiconductor systems investigated today are diamond or zinc-blende crystal systems, and by far the most common interface orientation is (001). In these crystal structures, the slip system is {111}/<110>, and the shortest possible Burgers vectors for perfect dislocations are of type $\frac{1}{2}<110>$. There are two types of (111) glide planes which are denoted as I and II in Fig. 1.4. The operation of the type I glide plane (shuffle set) implies the breaking of the smallest number of covalent bonds between layers with the same letters. Glide along type II planes (glide set) requires the breaking of three times more bonds, however, since glide takes place between close-packed planes dissociation into partial dislocations can readily be visualised.

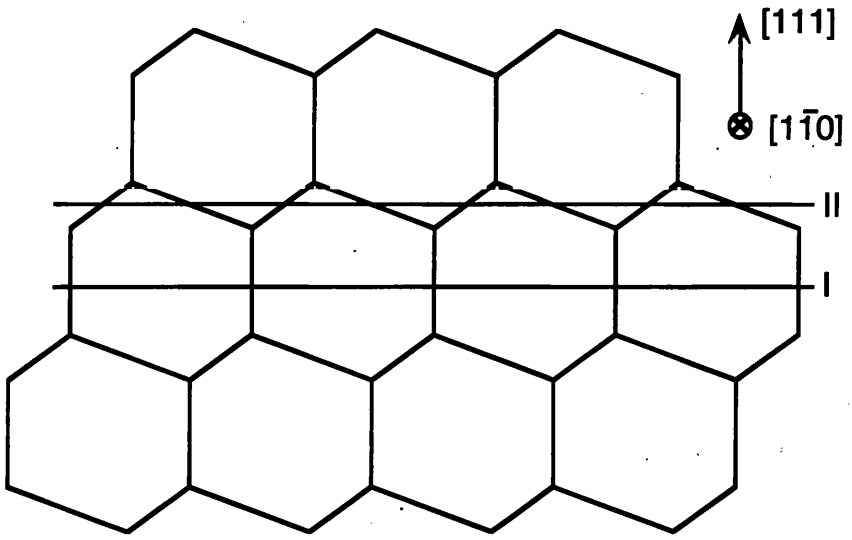

Fig. 1.4. Two possible locations I and II of slip plane in diamond structure

For the (001) orientation, the four possible {111} glide planes intersect the (001) interfaces along orthogonal in-plane <110> directions. Therefore, if a (001) mismatched interface is fabricated, an orthogonal set of misfit dislocations can be expected to form at the intersections of the {111} slip planes with the (001) interface, thus producing a square mesh of interface dislocations along <110> directions as illustrated in Fig. 1.5.

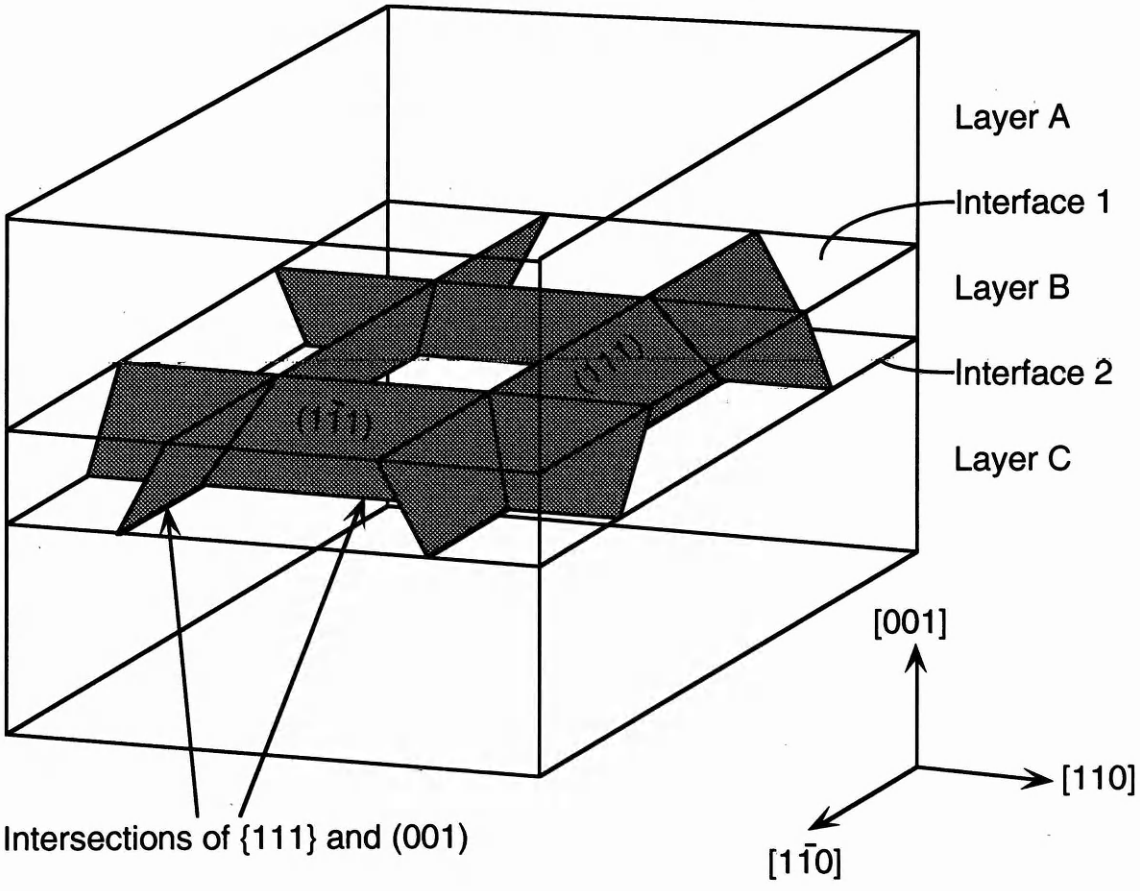

Fig. 1.5. Schematic illustration of the geometry of (001) interfaces, {111} slip planes, and intersections of {111} and (001) in a fcc multilayer structure.

A dislocation qualifies as misfit dislocation provided its Burgers vector has a nonzero component in the interface plane normal to the dislocation line. Only this component can accommodate misfit. Accordingly, misfit dislocations are most efficient (100%) in accommodating misfit when they have the Burgers vector lying within the interfacial plane and perpendicular to the dislocation line. However, such an edge dislocation cannot glide to the interface since their glide plane is {100}. These dislocations must move by far slower climb processes. Only dislocations with Burgers vectors lying within {111} planes will be able to move by glide. The most prominent of these are the 60°, or mixed, dislocations, corresponding to an angle of 60° between the dislocation-line direction and their Burgers vector. Only 50% of the magnitude of their

Burgers vectors projects onto the interfacial plane; thus, they are only 50% effective at relieving lattice-mismatch [Merwe_91].

When the lattice mismatch is negative, epilayers are subjected to tensile stress, extra half planes are produced on the epilayer side of the interface as a consequence of misfit stress relaxation. The misfit dislocations in the tensile films form straight lines and a number of stacking faults are expected to be observed. In contrast, when the lattice mismatch is positive, extra planes are produced on the substrate side of the interface. The misfit dislocations in this case are much more curved, cross slip will occur and fewer stacking faults are expected to be observed. A schematic model of the dislocation introduction for both cases is shown in Figure 1.5 [Maree_87, Sugiura_94].

Pure edge dislocations, with their Burgers vector perpendicular to their line direction can be formed from reactions between 60° dislocations. Occasionally, dislocations were observed to adopt <100> line directions [Goodhew_94], implying that other slip system could operate, or, dislocation climb might be involved[Goodhew_97].

1.4.2 Kinetics aspect

The precise mechanisms of nucleation of misfit dislocations remain elusive and controversial. They can be heterogeneous nucleation at specific local stress concentration due, for example, to growth artifacts or pre-existing substrate defects, homogeneous or spontaneous nucleation of dislocation loops or half-loops, and multiplication mechanism arising from dislocation pinning and/or interaction processes [HullR_92].

The M-B model [Matthews_79, Matthews_76, Matthews_75_A] suggests that misfit dislocations are generated from threading dislocations. However, only a very few experimental results have been reported to prove the generation of misfit dislocations on threading dislocations [Zuo_93]. Most misfit dislocations were observed with a fully developed geometry, well past their onset [Matthews_79, Matthews_76,

Matthews_75_B, Fitzgerald_89, Bouillet_93, Dunstan_97]. It remains unclear how misfit dislocations develop from individual ones to a misfit dislocation network.

It is obvious that the model based on elongation of threading dislocations to form misfit dislocations cannot explain the massive formation of misfit dislocations in a structure with rather low density of threading dislocations. There must be some mechanisms involving dislocation interaction and multiplication.

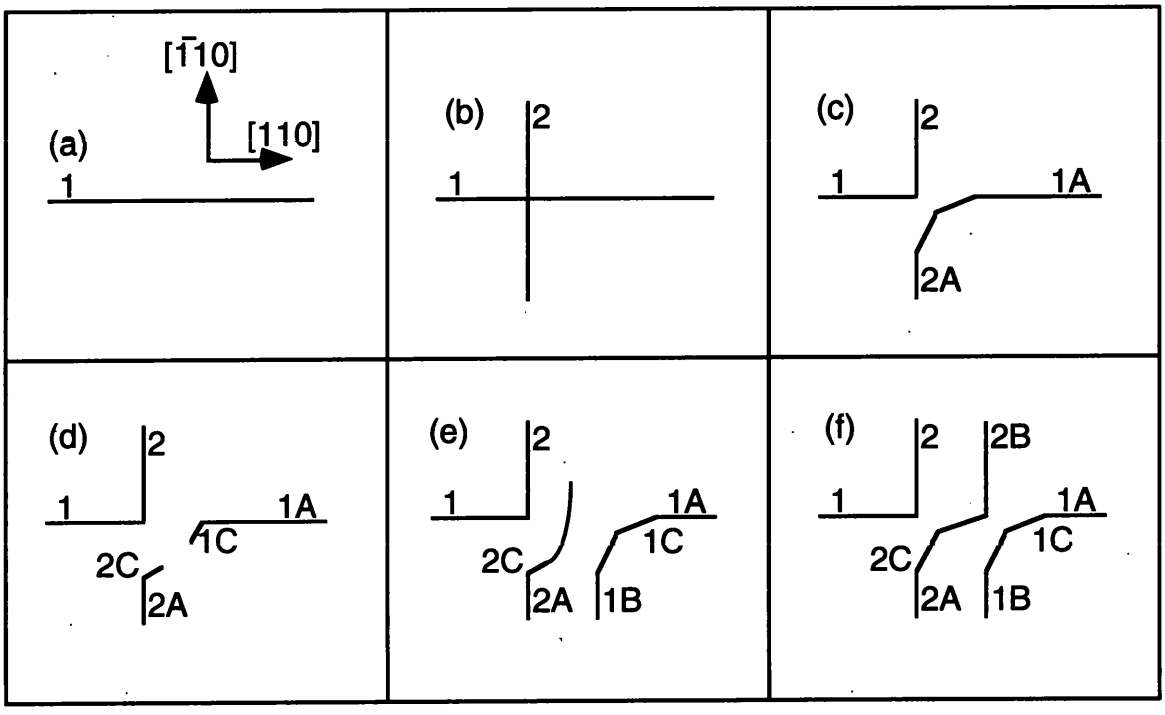

Fig. 1.6. Schematic diagram of the Hagen-Strunk dislocation multiplication mechanism. The misfit dislocations (1 and 2) are 60° type with identical Burgers vectors. The inclined transition segments are marked 1C and 2C. (b) is an unstable arrangement.

A multiplication mechanism of misfit dislocations was proposed by Hagen and Strunk as illustrated in Fig. 1.6 [Hagen_78, Strunk_79, Rajan_87] for growth of Ge on GaAs. There will be two possible configurations when a mixed dislocation line as shown in Fig. 1.6 (a) meets another one at a (001) interface. No (or only weak) reaction will occur upon the crossing of two dislocations with the Burgers vectors perpendicular

to each other, as shown in (b). If their Burgers vectors are identical, the interaction of these two dislocation lines can lead to the elimination of the intersection point. The high configuration energy at the initially sharp intersection is lowered by formation of interfacial segments with localised glide of dislocation, producing rounding near the original intersection, as shown in (c). The tip of one of the L-shaped dislocations glides toward the film surface under the presence of a surface image force. When the tip intersects the surface, as in the case of (d), two new dislocation segments are formed that may continually move, thereby producing regenerative dislocations, as shown in Fig. 1.6 (e) and (f).

The efficiency of the multiplication process was thought to be limited [Maree_87], since the (001) interface is not a glide plane, the misfit segments cannot separate as proposed by Hagen-Strunk mechanism. Lefebvre et al [Lefebvre_91] theoretically and experimentally demonstrated that the Hagen-Strunk source did not operate in the $In_xGa_{1-x}As/GaAs$ system (x = 0.08 to 0.18) and, indeed, dislocation tips in stages Fig. 1.6(c) and Fig.1.6(d) actually moved away from, rather than toward, the surface.

1.5 Post-growth relaxation of strained layers

There should be two different processes of relaxation for a strained-layer structure. One is the relaxation which might occur while the structure is being fabricated, this process deactivates with the finish of structure fabrication. The other is the relaxation which might occur after the structure has been build up, this is a process of life-span for the structure. For practical applications the latter is much more important.

All theoretical models only gave a description of thermodynamic equilibrium for a strained layer and predict the boundary condition for relaxation of a strained layer while the structure is being built up. Because energetic barriers (typically very much

greater than the thermal energy, kT) exist for the formation and motion of misfit dislocations at finite crystal growth temperature, the kinetic development of the misfit dislocation generally lags behind the equilibrium misfit dislocation density [Hull_96]. Therefore, two characteristics have been ascribed to the stability of a strained-layer structure according to the theoretical model. The structure was thought to be fully stable if the thickness of strained layer is below the critical thickness given by the model [Lourenco_94]. A strained layer was also thought to be stable if it has been relaxed by the introduction of misfit dislocations, the thickness of such a strained layer must have exceeded the critical thickness. The dividing of these two states is a strained layer whose thickness has exceeded the critical thickness but interfacial structure still keeps coherent, no relaxation. This structure is classified as metastable [Hull_96].

The metastability of strained layers is generally investigated by post-growth annealing. Lourenco *et al* [Lourenco_94] measured the residual strain in InGaAs/GaAs using double-crystal X-ray diffraction to follow the relaxation of $In_{0.1}Ga_{0.9}As/GaAs$ as a function of anneal time and temperature. The results showed a strong systematic dependence of the relaxation rate on anneal temperature, confirming that these layers were indeed metastable. A linear relationship between temperature T and normalized strain η was found to be

$$\eta = -0.0018T + 2.76. \tag{1.19}$$

The high temperature required to obtain appreciable relaxation suggested that these layers might still be sufficiently robust for applications.

Even for the structure which has been relaxed by the introduction of 60° dislocations, its stability is also questionable. Beanland et al [Beanland_97] proposed that the structure would relax towards a lower energy configuration and found that $\sqrt{2}$ times more misfit relief was produced by rotation of 60° dislocations into edge orientation in $In_{0.1}Ga_{0.9}As/GaAs$ layers during annealing.

1.6 Dislocation motion and relaxation under applied stress

Dislocations move at velocities which depend on the applied shear stress and temperature. The type of dislocation, purity of crystal, and, especially for strained-layer structure, misfit stress associated with lattice mismatch are also the factors which may influence dislocation motion.

Dislocation motion in semiconducting crystals is governed by the lattice resistance proper causing kink-mode motion [Nadgomyi_88]. In general, the stress-temperature dependence of dislocation velocity, v, in the kink-mode of motion can be expressed as

$$v = A\tau^m \exp\left(-\frac{U}{kT}\right), \tag{1.20}$$

where A is a numerical constant, m is a numerical exponent, U is the activation energy for dislocation motion, τ is the applied (or, effective) stress, and the other terms have their usual meaning[Alexander_68, Haasen_68]. As shown by Equation (1.20), the dislocation velocity varies with the stress to a power m and exponentially with temperature.

There are some quantitative results of measured dislocation velocities reported by various authors for GaAs and InAs crystals. The activation energies for dislocation motion were found to be 0.80 - 1.5 eV in GaAs [Nadgornyi_88, Erofeeve_94] and 1.0 - 1.2 eV in InAs (at $\tau = 10\text{MPa}$) [Nadgornyi_88]. Although the difference in dislocation motion between strained and unstrained layers have been noticed [Waters_90, Waters_91], no further investigation was reported.

It has been found that relaxation behaviour of strained layers can be effected by an external force[Antonelli_89_A, Antonelli_89_B]. The first investigation of relaxation behaviour of strained layers under high hydrostatic pressure was reported for $Si_{1-x}Ge$ in 1996 [Zaumseil_96], which showed that a modification of the point defect spectrum,

especially the relieved formation of vacancies, under high pressure was responsible for the enhanced relaxation

1.7 A definition of relaxation

Two different concepts of relaxation have been introduced in this thesis. One is the local relaxation of a strained-layer structure, which represents the structures with elongated misfit dislocations (these dislocations usually cannot be found by the cathodoluminenscence observation on scanning electron microscope but can be found by the observation on transmission electron microscope) generated by glide of the threading dislocations but without massive formation of misfit dislocations. This kind of structure is still treated as coherent. The other is the global relaxation which describes the structures that have been relaxed by the massive formation of misfit dislocations. This kind of structure is incoherent.

1.8 Summary

In this introductory chapter, the concept of strained-layer structure was introduced first and several device applications of $In_{1-x}Ga_xAs$ heteroepitaxial films were then discussed. The fundamental feature of strained layers which makes the difference from the normal, or lattice-matched, structures and the materials challenge arising from it in the synthesis and application of such structures were presented. The strain relaxation through the formation of misfit dislocations at the film/substrate interface was described and the need to understand the mechanisms of strain relaxation was emphasised. The thermodynamic aspects of the strain relaxation process have been extensively studied and several models have been proposed. It has been shown that the introduction of misfit dislocations is energetically favourable in a strained-layer structure if the strained-layer thickness is larger than a critical value. However, dislocation free, fully coherent strained layers of thicknesses larger than that predicted by the models have been readily grown demonstrating the weakness of the theoretical models. The stability,

or metastability, of a strained layer, no matter whether or not its thickness has exceeded the critical thickness, is key to and always a concern for the development of reliable devices based on such a structure. Although some phenomena have been observed showing the difference in dislocation motion between strained and unstrained layers, the underlying mechanisms still remain unclear.

In this thesis, we present a study of dislocations in $In_{1-x}Ga_xAs/GaAs$ heterostructures. The relaxation of strained-layer structures is investigated by observations of misfit dislocations in as-grown structures using transmission electron microscope (TEM) and cathodoluminescence (CL) on scanning electron microscope (SEM). The stability of strained-layer structures are assessed with respect to dislocation activities stimulated by thermal and/or mechanical means within the range of strained-layer thicknesses from sub- to super-critical thickness.

1.9 Outline of the thesis

Chapter 2 describes the methodology employed in this research including a modification to the standard process of TEM film specimen preparation using the epilayer lift-off (ELO) technique and the investigation into the possible impact of this technique on the dislocation configurations.

From Chapter 3 to Chapter 5, the relaxation of $In_{1-x}Ga_xAs/GaAs$ heterostructures by the introduction of misfit dislocations is considered.

In Chapter 3 the development of misfit dislocations through the transformation of threading dislocations and the disagreement of the experimental results with the M-B model are investigated. Two different processes of relaxation, local and global relaxation, are identified. Even though the critical thickness is not reached, threading dislocations have been found to be transformed into including a misfit segment, but this only results in local relaxation of the structure. After the onset of misfit dislocations has been found to occur through glide of threading dislocations at the interfaces, the

development of misfit dislocations are found to be unsynchronous with the change of the excess stress as the strained-layer thicknesses increase. This implies that the global relaxation of the structure is dominated by some other mechanisms, not the M-B model.

In Chapter 4, formation of misfit dislocations in different structures during thermal processing and mechanical tests is investigated. These structures have been thought to be thermodynamically stable or metastable according to the theoretical models. All these structures show the trend to be relaxed by the introduction of misfit dislocations during thermal processing and bending tests. The formation of misfit dislocations is found to be sensitive to temperature and applied stress. The misfit dislocations of not only 60° type but also edge type are found in thermal processed specimens.

In Chapter 5, some novel experimental results are presented showing the strained-layer structures, which have been relaxed by the formation of 60° dislocations, are relaxed further by the introduction of the edge-type misfit dislocations during thermal processing. A mechanism of vacancy-producing jogs protruding on the pre-existed 60° dislocations and moving away towards the specific directions leaving dislocation dipoles behind is proposed.

Chapter 6 is dedicated to motion of dislocations, not misfit dislocations, in the $In_{1-x}Ga_xAs/GaAs$ heterostructures. as well as some different behaviours of dislocations and misfit dislocations. By observing dislocations moving away from indentations during thermal processing and bending tests, the differences in dislocation motion between unstrained and strained-layer structures are confirmed. It is obvious that the misfit stress associated with lattice mismatch plays a key role in inhibition of dislocation motion in strained-layer structures and the duality of misfit stress is therefore proposed to give an explanation. It might be important for investigation of the mechanisms of misfit dislocation development to find it is dislocations, not misfit dislocations, that generate on (or, propagate away from) the pre-existing sources of dislocations.

Finally, in Chapter 7, the conclusions are made for this research and some suggestions for further research are presented.

Chapter 2 : Methodology

2.1 Heteroepitaxial GaAs/$In_xGa_{1-x}As$ /GaAs specimens

The bulk specimens of $In_xGa_{1-x}As$/GaAs heterostructures used in this research consisted of a GaAs substrate, a 50 nm AlAs layer, two 200 nm GaAs layers, and a compressive strained $In_xGa_{1-x}As$ layer between two GaAs layers as illustrated in Fig. 2.1.

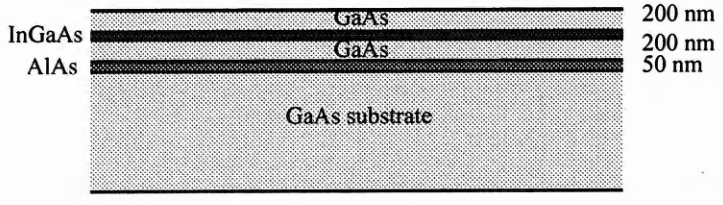

Fig. 2.1. Schematic illustration of GaAs/$In_xGa_{1-x}As$/GaAs specimens

The compositions, strained-layer thicknesses and lattice mismatches between $In_xGa_{1-x}As$ and GaAs are listed in Table 2.1. The lattice parameters of $In_xGa_{1-x}As$ layers are estimated by the Vegard's law which states that the lattice parameter varies linearly with x. To cover strained-layer thicknesses from sub- to super-critical thickness, three different strained-layer thicknesses were chosen for each kind of strained-layer structure specimen. These three thicknesses fall into three different regions respectively, i.e., $h < h_c$, $h_c < h < H_c$, and $h > H_c$, delimited by the critical thickness curves of the M-B model for each indium concentration, x, as shown in Fig. 2.2 .

The inclusion of an AlAs layer in the structure had the aim of preparing film specimens by the epilayer lift-off technique for observation on a transmission electron microscope. The lattice parameters of GaAs (0.565325 nm) [Stringfellow_93] and AlAs (0.56612) [Rhan_96] are very close (0.14% difference) and so the inclusion of an AlAs layer in the structure does not introduce significant strain.

Table 2.1 Specifications of the $In_xGa_{1-x}As/GaAs$ specimens

Number	x	Misfit (%)	Thickness of $In_xGa_{1-x}As$ layer (nm)
1	0.15	1.075	6
2	0.15	1.075	15
3	0.15	1.075	25
4	0.2	1.433	4
5	0.2	1.433	10
6	0.2	1.433	20
7	0	0	0

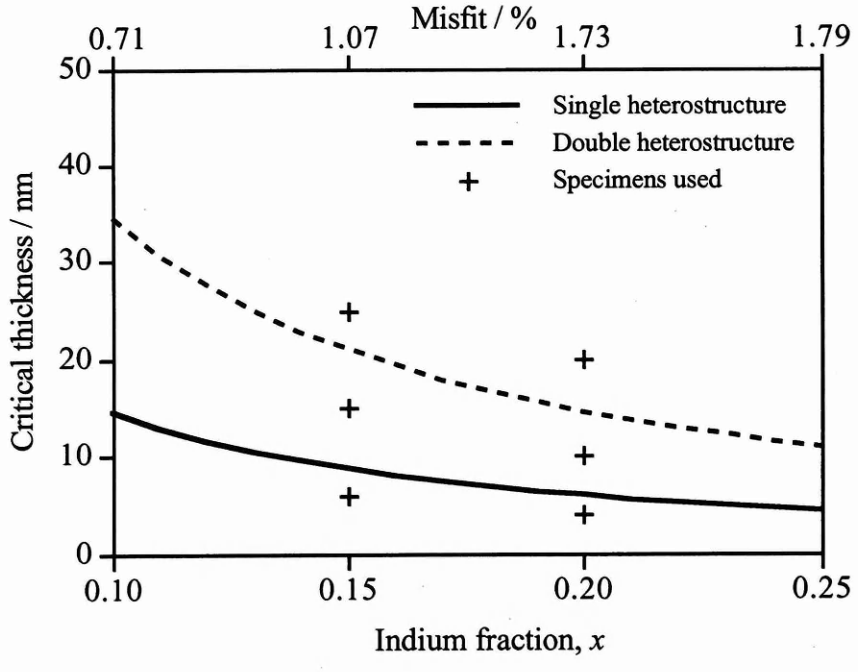

Fig. 2.2. The critical thickness curves predicted by the Matthews-Blakeslee's model for $GaAs/In_xGa_{1-x}As/GaAs$ heterostructures

All specimens were grown by molecular beam epitaxy (MBE). Details of the MBE process for fabrication of the structures are described in Appendix A. The pieces of specimen used for experiments were produced by cleaving the bulk specimens along <110> directions.

Nominal thicknesses were determined by growth rate calibration of the MBE equipment, which had been determined by RHEED (Reflection High-Energy Electron Diffraction) oscillations and X-ray diffraction measurements. The thicknesses of strained layers were also confirmed by cross-sectional measurement in the TEM. Details of the measurement results and the technique is described in Appendix B.

2.2 Cathodoluminensce in the SEM

Many of the secondary electrons which are produced by the incident beam do not escape from the target material, but diffuse through the specimen and are captured. This capture is a process of electron-hole recombination and accompanied by the emission of a photon at optical or near optical frequencies. This effect is known as cathodoluminescence (CL) [Grundy_76, Williams_96]. The cathodoluminescence converts the energy of the electrons (cathode rays) to produce light (luminescence). Many materials emit light under electron bombardment, and if this is detected, an image in the cathodoluminescence mode can be displayed. Any alteration in the energy gap due to local changes of crystal structure, such as dislocations, will lead to a change in emission and dislocations can therefore be investigated by observing their cathodoluminescence images. CL observation allows dislocations beneath the surface of a bulk specimen (up to a depth of approximately 1 μm) to be imaged. The structure can thus be examined non-destructively. Furthermore, CL allows sub-micron features (notably dislocations) to be examined on a low magnification, large area image (of the order of 1 mm). It is particularly suited to low magnification imaging of dislocations in semiconductors as these materials often exhibit cathodoluminescence, and their dislocation density is generally low. CL is being increasingly used to study the nature

and distribution of defects in semiconductor materials and devices such as GaAs, and is capable of providing detailed and important information about these defects [Goodhew_88].

CL is one of the working modes of some scanning electron microscopes (SEMs). If the light emitted from the samples is used to modulate the CRT intensity, information on the distribution of the light-emitting regions can be obtained. This image mode is very useful for studying light-emitting semiconductors [Loretto_94].

The CL observation was carried out with a Germanium Detector on a JEOL JSM-820 scanning electron microscope. Because low temperature can make the CL image more intensive [Goodhew_88], a cold stage was used to cool the specimens to below 100 K.

2.3 Epilayer lift-off (ELO) technique and TEM specimen preparation

2.3.1 ELO technique and TEM observation

The epitaxial lift-off (ELO) technique was first reported by Konagai *et al* in 1978 to graft GaAs solar cells onto an Al plate [Konagai_78, Demeester_93], and has been used to prepare film specimens for observation on transmission electron microscope (TEM) [Breen_89 , Breen_90, Paine_90, Howard_91, Zuo_93]. This technique makes use of the selective removal of an AlAs layer between the specimen film and the substrate. Chemical etching of the AlAs in 10% hydrofluoric acid solution at 0 °C results in a selectivity of 10^8 compared with GaAs [Demeester_93].

The standard ELO technique for preparing TEM film specimens is: first, the surface of specimen is cleaned and covered with black wax, the black wax provides a sufficiently rigid carrier for the thin film; then, the specimen is put into 10% hydrofluoric acid solution for 5 - 15 hours to allow AlAs to be etched away and the film to be floated off; after that, the film specimen is taken out, washed with distilled water,

and stuck the film onto a grid; finally, the TEM film specimen is obtained by dissolving the black wax with trichloroethylene.

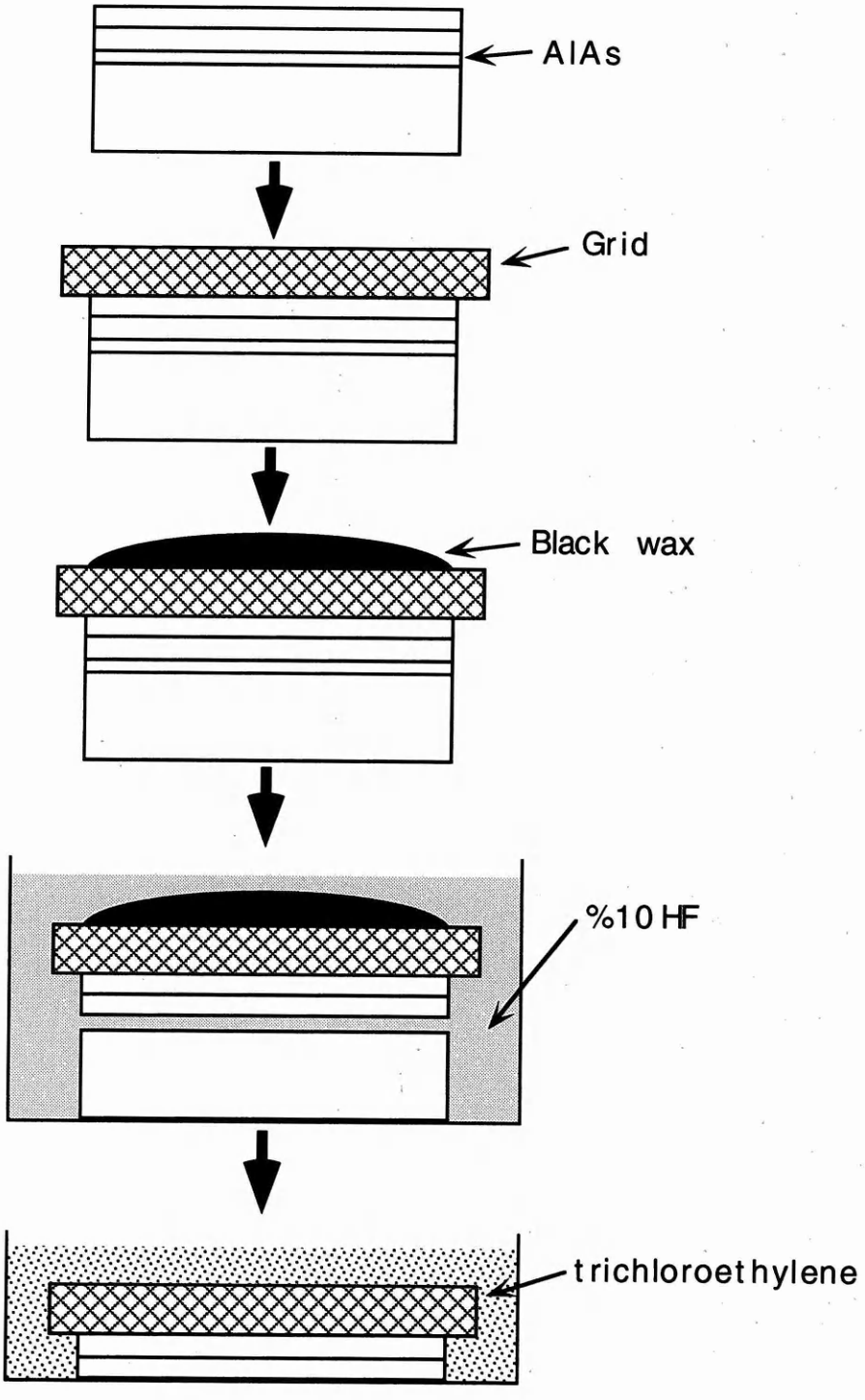

Fig. 2.3. The modified epilayer lift-off technique used for preparation of TEM specimens

A modification has been made to this process in this research, as illustrated in Fig.2.3. Before the surface of specimen is covered with black wax, a copper grid (200 or 400 mesh) is first stuck onto the surface using a Loctite 454 cyanoacrylate adhesive. The film specimen is finally obtained by floating off the film together with a copper grid from the substrate and dissolving the black wax with trichloroethylene. Gluing a grid onto the specimen surface before the film is separated from the substrate makes handling easier and, more importantly, a higher quality of TEM film specimen can be achieved in this way.

TEM observation was carried out on a JEOL 2000FX transmission electron microscope operated at 200 kV. A TEM image of film specimen prepared by the modified ELO technique is shown in Fig. 2.4, and misfit dislocations in a specimen ($GaAs/In_xGa_{1-x}As$(25 nm)/GaAs) are revealed by the TEM image as shown in Fig. 2.5.

Fig. 2.4. TEM bright field image of an ELO film specimen on a 400 mesh copper grid. Bar = 20 μm.

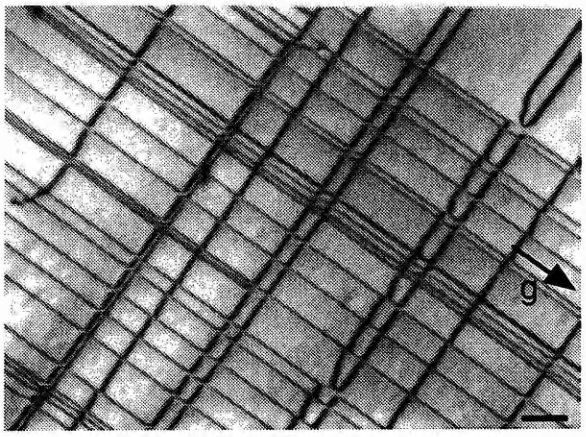

Fig. 2.5. TEM bright field plan-view image of misfit dislocations in a GaAs/$In_xGa_{1-x}As$(25 nm)/GaAs film specimen prepared using the modified ELO technique. **g** = [220], bar = 200 nm.

2.3.2 Suitability of the ELO technique for TEM specimen preparation of strained-layer structures

A major concern for the TEM film specimen preparation is the extent to which dislocations can be introduced, or the configuration of dislocations can be changed during the process of preparation. The ELO technique has been inferred to be reliable by comparing the specimens prepared by this technique with that prepared by standard chemical etching method [Zuo_93]. Using the modified ELO technique, the conclusion can now be drawn directly by comparing the images of dislocations in a specimen before and after the specimen film has been separated from the substrate.

Fig. 2.6 is the CL images obtained at the same observation area from the same specimen before and after the ELO process. It can be seen that no dislocations were introduced, nor was the dislocation configuration changed during the preparation of TEM specimens by the ELO technique.

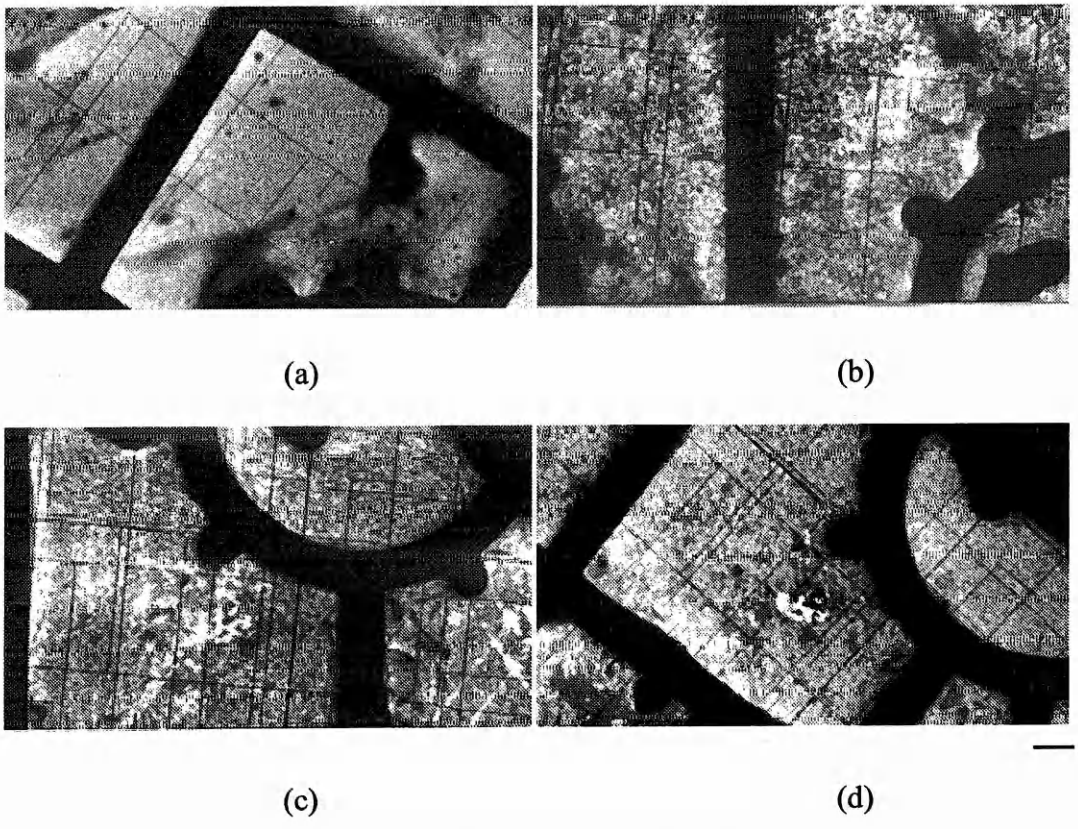

(a) (b)

(c) (d)

Fig. 2.6. CL images of misfit dislocations before and after ELO in GaAs/$In_{0.15}Ga_{0.85}As$/GaAs heterostructures. (a) and (c) are the images taken from the bulk specimens. (b) and (d) are the images taken at the same observation areas as microphotopgraphed in (a) and (b) respectively after the bulk specimens have been made into TEM film specimens by the modified ELO technique. Bar = 10 μm.

2.4 Measurement of dislocation density

The dislocation density ρ is defined as the total length of dislocation line per unit volume of crystal, normally quoted in units of mm^{-2} [HullD_92]. Thus for a volume of V containing dislocation line length l, the dislocation density ρ is

$$\rho = l / V \tag{2.1}$$

To be more accurate, the dislocation density for a specimen is determined by averaging dislocation lengths measured on several photographs taken at different observation areas.

2.5 Determination of the Burgers vector

The Burgers vector defines the displacement caused by, therefore characterising the nature of, a dislocation in crystal [HullD_92]. The determination of Burgers vector in TEM is based on the kinetic theory of electron diffraction contrast [Loretto_94, Grundy_76, Williams_96, Heimendahl_80, Beeston_73]. The contrast arises in an electron image only if the electron intensity varies significantly from one region of a specimen to another and will be a function of the diffraction conditions.

For a film of thickness t and unit intensity incident beam, the amplitude of the diffracted beam is expressed as

$$\phi_g = \int_0^t \exp[-2\pi i(sz + \mathbf{g}\cdot\mathbf{R}(b, x, y, z)]dz, \tag{2.2}$$

where $\mathbf{g}$ is the reciprocal lattice (or diffraction) vector, s is the deviation parameter and i is the angle of incidence. The displacement vector $\mathbf{R}$ is a continuous function of z in the crystal in terms of the Burgers vector $\mathbf{b}$. For a whole dislocation $\mathbf{g}\cdot\mathbf{b}$ is an integer and for the special case of $\mathbf{g}\cdot\mathbf{b} = 0$ no contrast occurs and the displacement vector, or here the Burgers vector, lies in the reflecting planes. The invisibility criterion, $\mathbf{g}\cdot\mathbf{b} = 0$, forms the basis for the most common method used to determine $\mathbf{b}$ for dislocations. If two sets of planes (for which the diffracting vectors are $\mathbf{g}_1$ and $\mathbf{g}_2$) are found with two-beam condition for which a dislocation is invisible then the direction of $\mathbf{b}$ is then given by $\mathbf{g}_1 \times \mathbf{g}_2$.

In the case of a screw dislocation of Burgers vector $\mathbf{b}$ in an elastically isotropic medium, the displacements are particularly simple. The only displacements lie along $\mathbf{b}$ and it is only the magnitude of this displacement that varies from one column of atoms

to another. It is clear that if $\mathbf{g} \cdot \mathbf{b} = 0$ the equation (2.2) reduces to that of a perfect crystal and the screw dislocation will be invisible, i.e. it will show no contrast. For all other values of $\mathbf{g} \cdot \mathbf{b}$ the intensities will be changed near to the dislocation where the term $\mathbf{g} \cdot \mathbf{b}$ leads to significant changes in transmitted intensity. For an edge dislocation with a line direction $\mathbf{u}$ in an elastically isotropic medium the displacements are more complex and both $\mathbf{g} \cdot \mathbf{b}$ and $\mathbf{g} \cdot \mathbf{b} \times \mathbf{u}$ have to be zero for the dislocation to be invisible. For mixed dislocations, all planes are distorted to some extent and these dislocations never go completely out of contrast. It is therefore necessary to be able to identify the condition $\mathbf{g} \cdot \mathbf{b} = 0$ even when contrast is observed.

2.6 Indentation made by microhardness tester

To investigate dislocation motion, the movable dislocations should be specially introduced into the specimen by some external operation. Locked as-grown dislocations are usually motionless up to the highest stresses when intensive multiplication begins. The methods of introducing fresh dislocations should be, at least, reproducible; besides, the fresh dislocations should meet a number of special requirements. First, fresh dislocations must be arranged separately to avoid being influenced by each other. Second, dislocations must be introduced into the proper slip plane. Finally, the dislocations must correspond to the specified conditions under which the dislocation motion is investigated [Nadgornyi_88, HullD_92].

Various methods are used to introduce fresh dislocations into specimens, such as scratching, laser-inducing and indenting [Nadgornyi_88]. In this research, a Leitz Miniload Hardness Tester was used to make indentations. By fixing the load (P = 15 g) and loading time (5 seconds), the same indentations could be made on the surface of specimens.

Fig. 2.7 is the SEM and CL images of an indentation made on the surface of a specimen. The indentation is in the form of prism with the side length of about 5 μm.

The tips of indentations are made towards the edges of specimens, thus, the sides of indentations are approximately at 45° to the edges of specimens, that is, to the <110> directions. Fig. 2.8 is TEM image of a indentation made on the surface of a $In_{0.15}Ga_{0.85}As/GaAs$ heterostrctures specimen. A lot of dislocations can be seen around the indentation, that is the reason why the outline of indentation is blurred when observed by CL imaging.

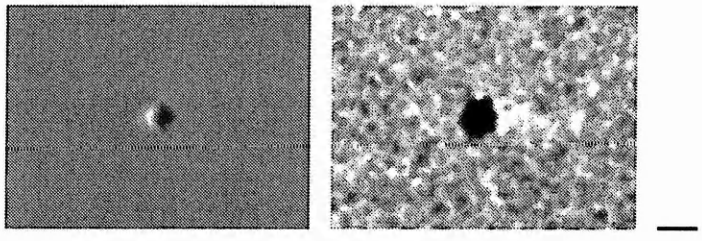

(a) (b)

Fig. 2.7. An indentation made by Miniload Hardness Tester. (a) SEM image. (b) CL image. Bar = 10 μm.

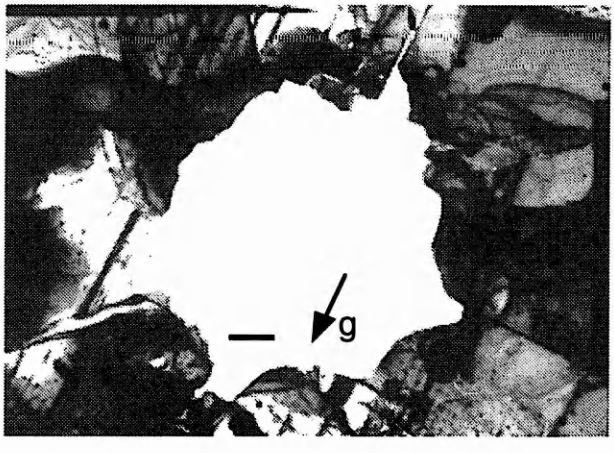

Fig. 2.8. TEM plan-view image of an indentation made on the surface of an $GaAs/In_{0.15}Ga_{0.85}As/GaAs$ specimen by Miniload Hardness Tester. g = [220], bar = 2 μm.

2.7 Assessment of dislocation motion

Generally, dislocation motion is quantitatively described by the evaluation of the dislocation velocity v which depends upon the nature of materials, the stress and the temperature [Hull.D_92]. From the earlier discrete models of dislocations there are two limiting quantities: the maximum velocity of a dislocation which is equal in magnitude to the speed of sound, and the maximum lattice resistance, known as the Peierls stress. In terms of these models the dislocation motion was free from resistance at $v << c_s$ and the resistance is large only at $v \cong c_s$. It was not until the early 1960s when exact experimental studies had been made that the dislocation mobility concept was quantitatively defined. It has since been found that the processes of dislocation motion are considerably more sophisticated than previously thought. It has been revealed that the dislocation velocity v changes with the shear stress within a large range from 10^{-9} to 10^3 m s^{-1} and is very sensitive to stress or temperature changes. It was proposed that at high velocities dislocation motion is governed by interaction with phonons, but at low velocities (the case of ionic crystals) the motion depends upon the thermal activation to surmount obstacles. The velocity of dislocations can be expressed in terms of an Arrhenius law in the thermally activated region as

$$v = v_0 \exp(-E / kT) \tag{2.3}$$

where E is the activation energy. [Nadgomyi_88, Kovacs_73]

In principle, dislocation velocity can be determined by measuring the distance of dislocation motion in a specimen subjected to thermal and/or mechanical tests. By repeating the experiment for different conditions, the velocity can be determined as a function of the factor investigated [Hull.D_92]. Typically, dislocations in semiconducting materials, such as GaAs, are studied by etching low-index planes [Abrahamns_65]. CL observation provides a method to enable dislocations in III-V

semiconductor materials to be investigated without destruction of specimens [Esquivel_73].

It was found in this research that the dislocation motion in the specimens investigated is not a simple function of time. Fig. 2.9 shows the experimental observation of dislocation motion in GaAs/$In_xGa_{1-x}As$/GaAs during a bending test with different durations at the targeted temperature, 673 K. Under the same conditions of ramping temperature and loading, the distance of dislocation motion did not change significantly when the nominal duration changed from 1s to 30s. These nominal durations are the times for which the specimens were held at the target temperature, as determined by a thermocouple mounted on the specimen. Under these experimental conditions it is difficult to identify at which precise moments dislocation motion started and finished. As a meaningful measurement of the duration of dislocation motion was therefore not available, a strict determination of dislocation velocity was not possible. Instead, in this thesis dislocation motion during thermal or mechanical tests has been assessed by measuring the distance moved within the same nominal timescale.

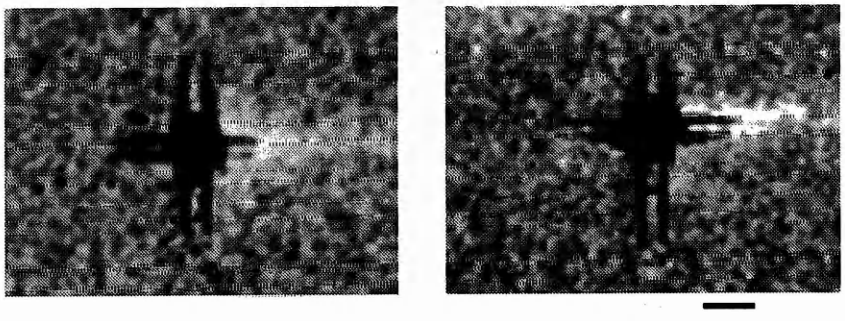

(a) (b)

Fig. 2.9. Dislocation motion in GaAs/$In_xGa_{1-x}As$/GaAs during a bending test at 673 K with different duration of (a) 1 second and (b) 30 seconds respectively. Bar = 10 μm.

2.8 Thermal processing

Thermal processing was designed to investigate the temperature dependence of dislocation behaviour in $In_xGa_{1-x}As/GaAs$ heterostructures. These experiments were carried out on a Carbolite furnace in a N_2 ambient. Temperature was measured near to the specimen by a K-type thermocouple. Fig. 2.10 schematically illustrates the thermal processing apparatus.

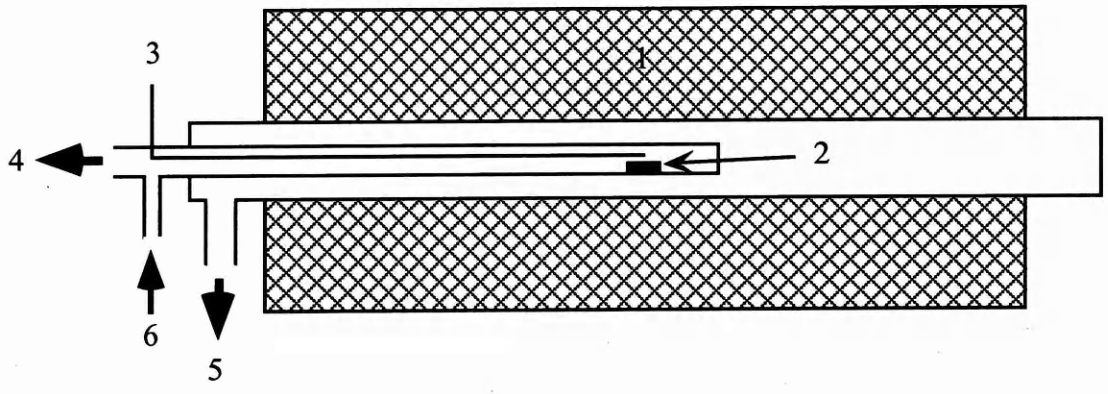

Fig. 2.10. Schematic layout of the thermal processing apparatus.

1. Carbolite furnace
2. Specimens
3. K-type thermocouple
4. High-vacuum system
5. Vacuum system
6. N_2

The procedure of thermal processing was controlled by a programmable furnace controller. After several preparative experiments, the procedure of thermal processing was fixed to be: ramp temperature at the rate of 6 K / minute, keep the temperature at the expected point for 5 minutes, and cool at the rate of 9 K / minute.

2.9 Bending tests

Dynamic dislocation characteristics are determined in most cases by measuring the distances that dislocations move under applied stress [Nadgornyi_88]. Three-point and four-point bending are widely used methods of loading. Three-point bending permits one to obtain stress-dependent running distance in one test [Paufler_87, Esquivel_73, Kishino_76, Kuesters_86].

The effects of applied stress on the formation of misfit dislocations were also investigated by bending tests in this research.

For bending tests, the duration of the applied stress, loading, and temperature should be considered. A rig was designed to carry out three-point bending tests as shown in Fig. 2.11.

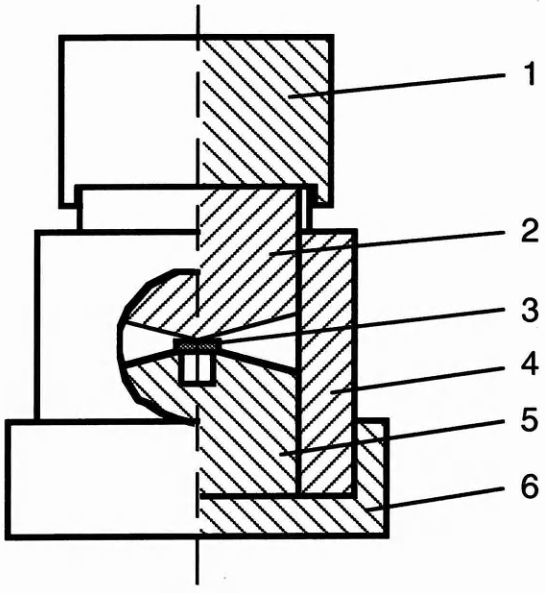

Fig. 2.11. Bending test rig. 1: Loading of mass B

2: Loading of mass A with guide way

3: Specimen

4: Guiding sleeve

5: Fulcrum bearing

6: Pedestal

The design of the guiding sleeve and the loading A with guide way can keep the force caused by load A and B to be applied on the centre between the two fulcrums on the fulcrum bearing and towards the direction perpendicular to the surface of the specimen. The distance between the two fulcrums is 3 mm.

Simple theory of elastic bending states [Hearn_77] that

$$\frac{M}{I}=\frac{\sigma}{y}, \tag{2.4}$$

where M is the applied bending moment at a transverse section, I is the second moment of area of the beam cross-section about the neutral axis, σ is the stress at distance y from the neutral axis of the beam cross-section. For the rectangular beam cross-section shown in Fig. 2.12, the second moment of area I is defined as

$$I = \int y^2 dA = \frac{BD^3}{12}, \tag{2.5}$$

where D is the thickness of the specimens (0.5 mm) and B is the breadth of specimen (1 mm).

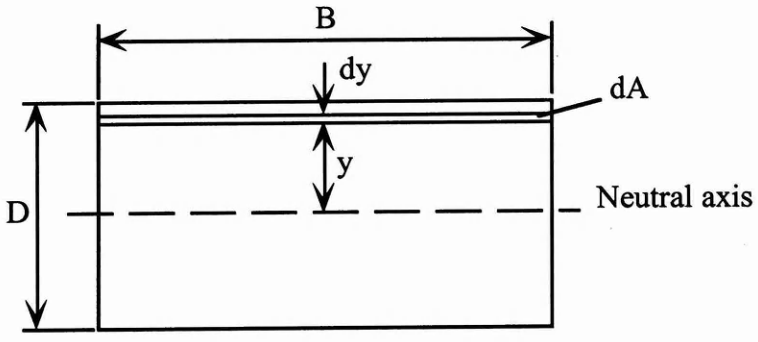

Fig. 2.12. A bending specimen.

When a load is applied, the specimen is undergoing a static three-point bending on the rig causing the bottom of the specimen to be subjected to tension and the top to compression, as illustrated in Fig. 2.12. A tensile or compressive stress can thus be applied on the strained layer and the interfaces depending on their positions during bending. The stress caused by a loading of W at a distance y from the neutral axis of the specimen is

$$\sigma = \frac{M}{I} y$$

$$= \frac{3WLy}{BD^3} \text{ (Pa)}, \tag{2.6}$$

where $M = (W/2) \times (L/2)$ L is the distance between the two fulcrums (2.7 mm). Take $y = D/2$, then the stress caused by bending at top or bottom surface of specimen is

$$\sigma = \frac{3}{2} \frac{WL}{BD^2} \text{ (Pa)}. \tag{2.7}$$

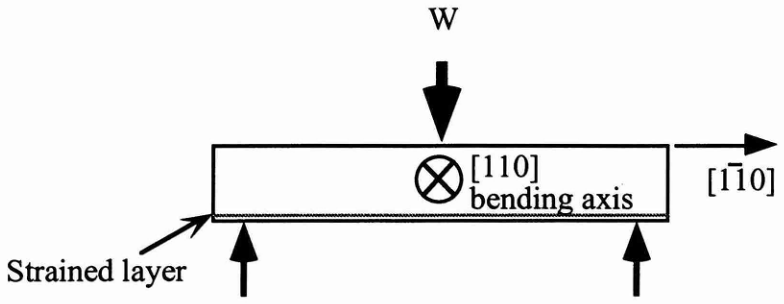

Fig. 2.13. Tensile stress caused by three-point bending on a strained layer.

The bending tests were carried out with a fixed load (0.292 Kg) which produced a maximum stress of 7.25 MPa. The bending axis is the direction around which bending will occur. A [110] bending means, as illustrated in Fig. 1.13, the axis of the bending is along the direction of [110]. Two different kinds of bending test, [110] and [100] bending, were carried out. Bending tests were carried out within a Carbolite furnace. The duration of applied stress is not a factor considered in this research, so it was fixed to be 1 second for all bending tests.

A four-point bending test was also considered, with the specimen designed to be stuck onto a high carbon steel bar as shown in Fig. 2.14. However, this kind of bending test was unsuccessful because a suitable adhesive could not be found.

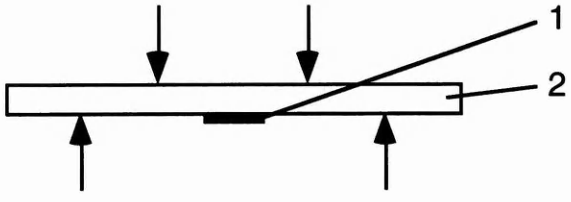

Fig. 2.14. Considered four-point bending test. 1: Specimen. 2: Steel strip.

Chapter 3 : Generation of misfit dislocations on threading dislocations

For lattice-mismatched epitaxial layers, a minimum thickness, the critical thickness, exists for the introduction of misfit dislocations into the structures causing the breakdown of the coherency between the substrate and epilayer. The critical thickness is defined by theoretical models as the thickness at which misfit dislocations can be thermodynamically expected to emerge in a strained-layer structure. Transformation of the threading dislocations, their bowing and elongating to form misfit dislocations under the effects of misfit stress in strained-layer structures, has been taken by the M-B model as a basic mechanism for the critical thickness.

Few misfit dislocations have been revealed at their earliest stage of formation. The misfit dislocations described in the literature either have fully developed well beyond their onset, or do not show clearly the processes of their development from the transformation of threading dislocations.

By TEM observation, this chapter will examine specimens within the span of strained-layer thicknesses from sub- to super-critical thickness. Threading dislocations will be revealed to give a clear image showing how they are transformed to form misfit dislocations with increasing strained-layer thickness. The strained-layer thicknesses representing the different stages of misfit dislocation development will be compared with the critical thickness given by the M-B model.

3.1 Different dislocation geometries in different structures

3.1.1 Threading dislocations in GaAs

For GaAs/$In_xGa_{1-x}As$/GaAs, when x = 0, i.e., continuous GaAs, the dislocations observed have the geometry as shown in Fig. 3.1. All of these dislocations are threading dislocations, straight from the bottom to the top of the film. This is the original configuration of threading dislocations before they are subjected to anything causing them to change.

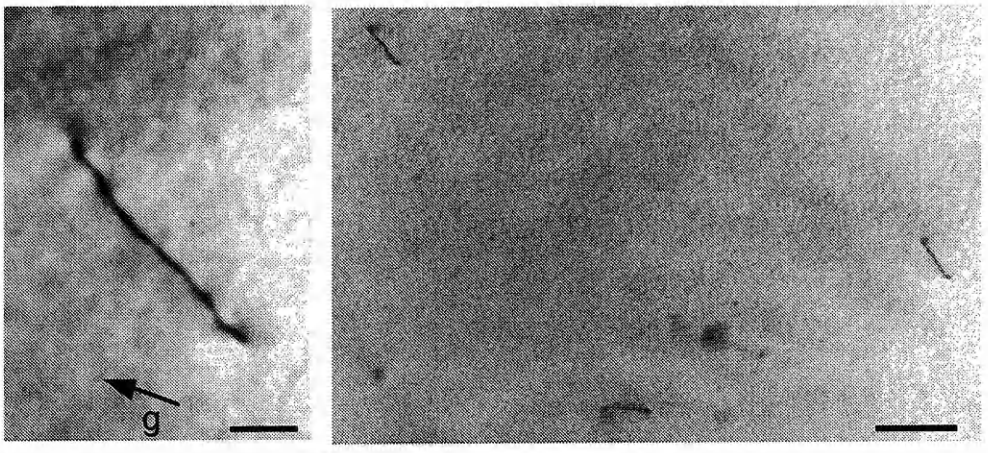

(a) (b)

Fig. 3.1. Threading dislocations in GaAs films. **g** = [220]. Bar = (a) 50 nm, (b) 500 nm.

3.1.2 Onset of misfit dislocations through the transformation of threading dislocations

Fig. 3.2 shows the geometry of dislocations observed in the specimens of x = 0.15 and the strained-layer thickness h = 6 nm (less than h_c = 8.6 nm). The inclusion of a strained layer in the structure brought some changes to threading dislocations. Threading dislocations were divided into two segments by a short dislocation segment as shown in Fig. 3.2(a). This dislocation segment is lying in [110] direction. It connects the two threading segments which reach the top and bottom surfaces respectively. The only explanation is that this segment is a misfit dislocation with 60° character and

formed by dislocation gliding into the interface on (111) slip plane [Matthews_79]. It is a general, not individual, geometry for this kind of specimen that the threading dislocations have been transformed into including a misfit segment, as shown in Fig. 3.2(b).

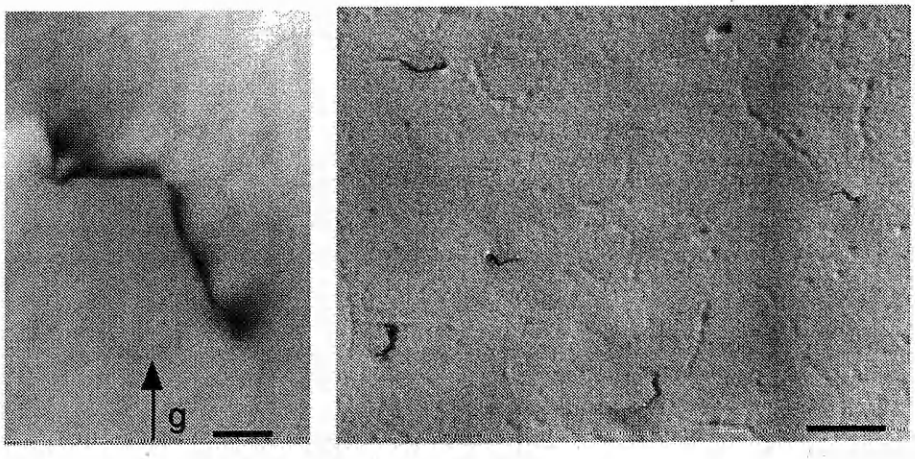

(a) (b)

Fig. 3.2. Threading dislocations with a misfit segment in a specimen of GaAs/$In_{0.15}Ga_{0.85}As$/GaAs, h = 6 nm: (a) **g** = [220], bar = 50 nm; (b) bar = 500 nm.

The dislocation density of these specimens is at the level of 1×10^5 / cm^2.

For the specimens of x = 0.2 and the strained-layer thickness h = 4 nm (less than h_c = 5.8 nm), the threading dislocations were also found to include a misfit segment as shown in Fig. 3.3.

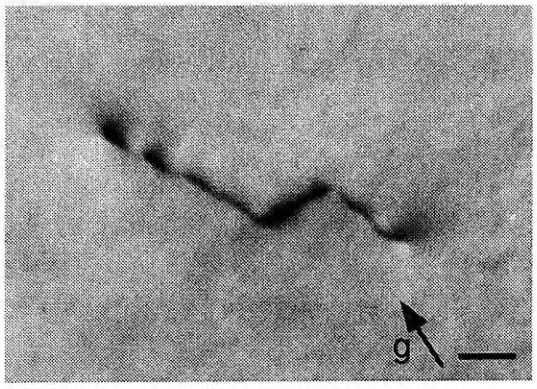

Fig. 3.3. A threading dislocation with misfit segment in a specimen of GaAs/$In_{0.2}Ga_{0.8}As$/GaAs. h = 4 nm. **g** = [220], bar = 50 nm.

3.1.3 Misfit dislocation elongation

As the thickness of the strained layer increases, when h = 15 nm for the specimens of x = 0.15, misfit dislocations are substantially elongated at the interface. Here h lies between h_c (8.6 nm) and H_c (20.9 n m). Most of this kind of dislocation have the configuration as shown in Fig. 3.4. The significant change of these dislocations compared with those in the specimens of h = 6 nm is that the misfit segment is longer. Of the two threading segments of them, one is shorter and curved while the other drags a long tail to get to surface. Compared with the threading dislocations in GaAs films, it can be inferred that the tail is the threading segment coming from the substrate. As growth of the strained layer progressed, this threading dislocation glided into the interface forming a misfit dislocation. When the growth of the strained layer was completed, the threading segment turned back at the other interface and crossed the capping layer, reaching the surface. The different configuration of threading segment A and B indicates their different experience of growth. Before the growth of a strained layer, the threading segment A was not affected by any misfit stress, so it continued to grow in as a smooth line. However, the growth in of segment B was under the effect of stress from beginning to end. Its curved configuration is the reflection of the effects of misfit stress on its growth as a function of the distance from the interface to surface.

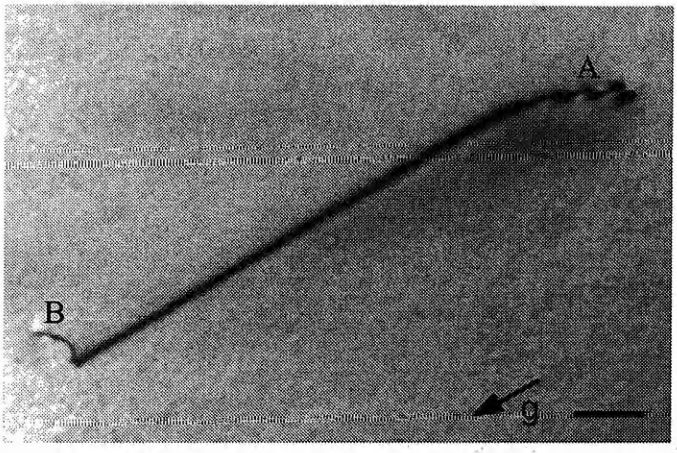

Fig. 3.4. An elongated misfit dislocation in GaAs/$In_{0.15}Ga_{0.85}As$/GaAs, h = 15 nm. **g** = [220], bar = 200 nm.

A few dislocations in this kind of specimen appear in the form shown in Fig. 3.5(a). One of its two threading segments as shown in Fig. 3.5(b) first turned back when a capping layer was grown and glided a short distance forming a new misfit dislocation segment at the other interface of the structure before reaching the surface. (The layer sandwiched between two misfit dislocation lines is the strained layer). The other coming from the substrate is straight and shorter as shown in Fig. 3.5(c).

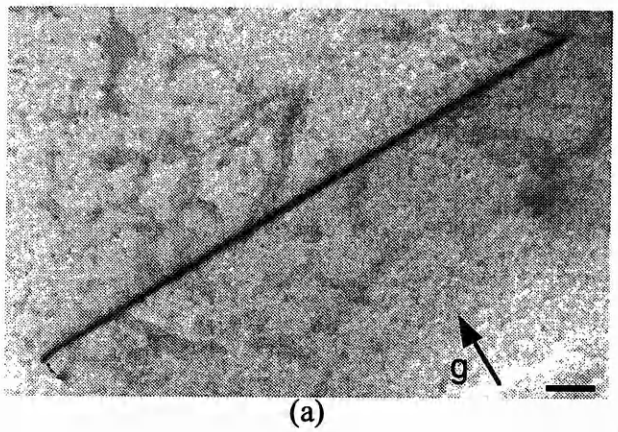

(a)

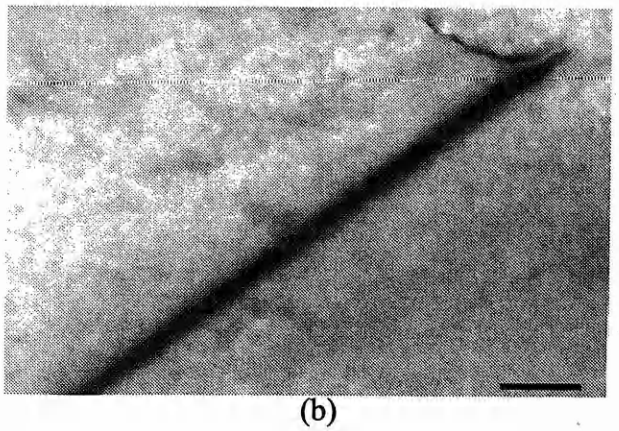

(b)

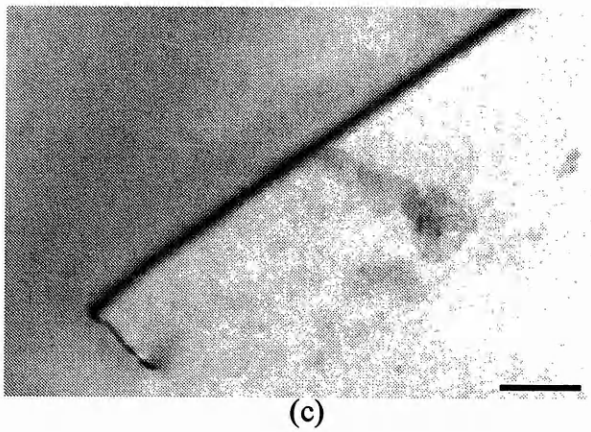

(c)

Fig. 3.5. (a) An elongated misfit dislocation in GaAs/$In_{0.15}Ga_{0.85}As$/GaAs, h = 15 nm. **g** = [220], bar = 200 nm. (b) One of its threading segments crossed the strained layer, generated another misfit segment at the other interface of the structure, and then reached the surface. Bar = 100 nm. (c) The threading segment coming from the substrate. Bar = 100 nm.

There is only a little change in the dislocation density (4×10^5 / cm^2) compared with that in the specimens of h = 6 nm.

Fig. 3.6 is an elongated misfit dislocation in GaAs/$In_{0..2}Ga_{0.8}As$/GaAs when the strained-layer thickness h = 10 nm, which also lies between h_c (5.8 nm) and H_c (14.5 n m).

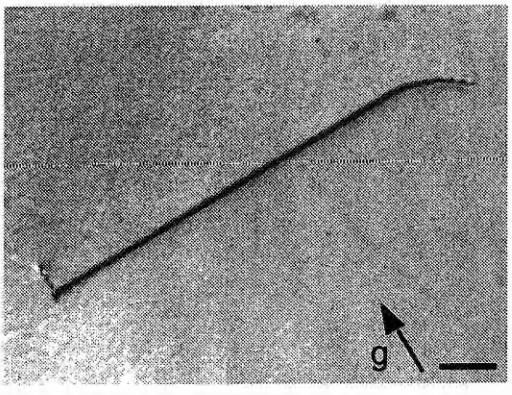

Fig. 3.6. An elongated misfit dislocation in GaAs/$In_{0.2}Ga_{0.8}As$/GaAs, h = 10 nm. **g** = [220], bar = 200 nm.

3.1.4 Misfit dislocation network

The network of misfit dislocations was observed when the thickness of the strained layer increased further. Fig. 3.7 shows the misfit dislocations in GaAs/$In_{0.15}Ga_{0.85}As$/GaAs, when its strained-layer thickness = 25 nm, which exceeds H_c (20.9 n m). It can be seen that dislocations have propagated all over the structure. The dislocation density has increased significantly to 5×10^8 / cm^2 and is several thousand times higher than that in the specimens of h = 6 nm and h = 15 nm.

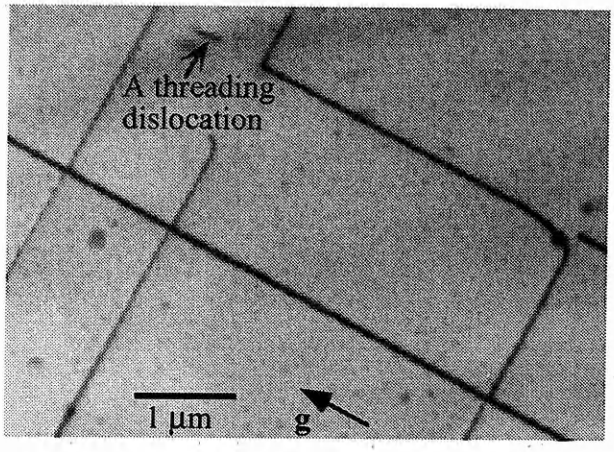

Fig. 3.7. Misfit dislocation network in GaAs/$In_{0.15}Ga_{0.85}As$/GaAs, h = 25 nm. **g** = [220]. A threading dislocation is arrowed.

It is noteworthy that a threading dislocation can still been seen remaining as a straight line, not being transformed to include any misfit segment.

Similarly, as shown in Fig. 3.8, the misfit dislocation network was also observed in the specimens of x = 0.2 with the strained-layer thicknesses h = 20 nm, which exceeds H_c (14.5 n m).

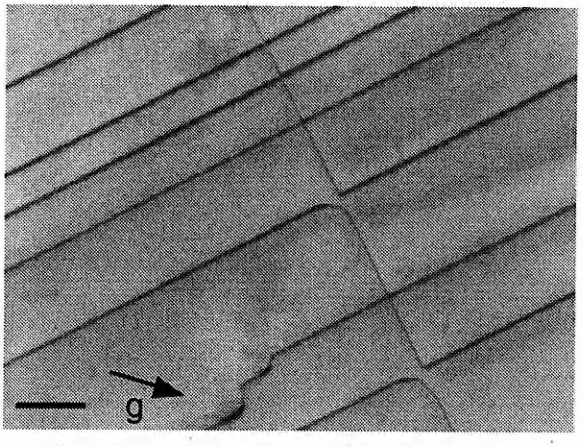

Fig. 3.8. Misfit dislocation network in GaAs/$In_{0.2}Ga_{0.8}As$/GaAs, h = 20 nm. **g** = [040], bar = 500 nm.

3.2 Development of misfit dislocations through transformation of threading dislocations and local relaxation

It is apparent from the experimental observations above that threading dislocations play a role in the introduction of misfit dislocations into a strained-layer structure. There is indeed a process of threading dislocations being transformed to generate misfit dislocations as a strained-layer structure is being build up. The different length of misfit dislocations generated on the threading dislocations reflects the dependence of this process on the thickness of strained layers.

When the interface between a strained layer and its substrate is set up, the threading dislocations will cross the interface as growth progresses. The misfit stresses will take effect on threading dislocations as soon as they enter the strained layer. The stress due to misfit strain resolved onto a threading dislocation is τ_ε,

$$\tau_\varepsilon = \frac{2G(1+\nu)}{(1-\nu)}\varepsilon S, \tag{3.1}$$

where S is an angular factor.

A number of factors which resist dislocation motion along the interface have been considered [Matthews_70, Zuo_93]. The most important resisting force considered is the line tension. It will be discussed in section 3.3.2.

During the motion of a threading dislocation a surface step is created. The force resisting the creation of a surface step is $F_s = \tau_s b S'$ (S' is an angular factor). τ_s is the surface tension stress suggested to be $Gb/8$ [Matthews_76] and is smaller than the misfit stress within the range of the misfit considered here.

Dislocation motion may also be retarded by point defects or solute atoms which segregate to the dislocation [Jesser_90_A, Jesser_90_B]. It has been pointed out [Zuo_93] that as the threading dislocations are grown in during MBE deposition, it is

likely that the dislocation cores will be decorated. Decorated dislocations would require an extra stress to overcome pinning. This decoration pins threading dislocations and acts as a static friction force. As soon as the threading dislocation starts to move, it breaks away from the decoration, and this force disappears. Because of random amounts of dislocation decoration, it can be expected that there would be differences in the force required to overcoming pinning for different threading dislocations. This can explain the observation, shown in Fig. 3.7 that a threading dislocation remains unchanged when the misfit dislocation network has formed.

Another factor which now becomes very important is the Peierls-Nabarro stress. When a dislocation starts to move, a stress due to the discrete nature of the lattice will be in action. This describes the maximum resistance of the lattice to dislocation motion. This is the minimum stress required to move a lattice dislocation rigidly and irreversibly. Therefore the shear stress required to make a dislocation glide is τ_p [HullD_92, Kovacs_73, Wang_96],

$$\tau_p = \frac{2G}{(1-\nu)} \exp\left(\frac{-2\pi w}{b}\right), \tag{3.3}$$

where w is a constant given by $w = d/2(1-\nu)$, d is the interplanar spacing of crystal. Comparing with the misfit stress,

$$\frac{\tau_\varepsilon}{\tau_p} = (1+\nu)\varepsilon S \exp\left(\frac{2\pi w}{b}\right). \tag{3.4}$$

For misfit dislocations in the fcc and diamond cubic lattice, the Burgers vector is of the type $\frac{a}{2}\langle 110\rangle$, and d is at the same order of a (lattice parameter), so $2\pi w / b$ can be approximated to be 9. This makes $\tau_\varepsilon / \tau_p \gg 1$ at the magnitude of ε concerned here.

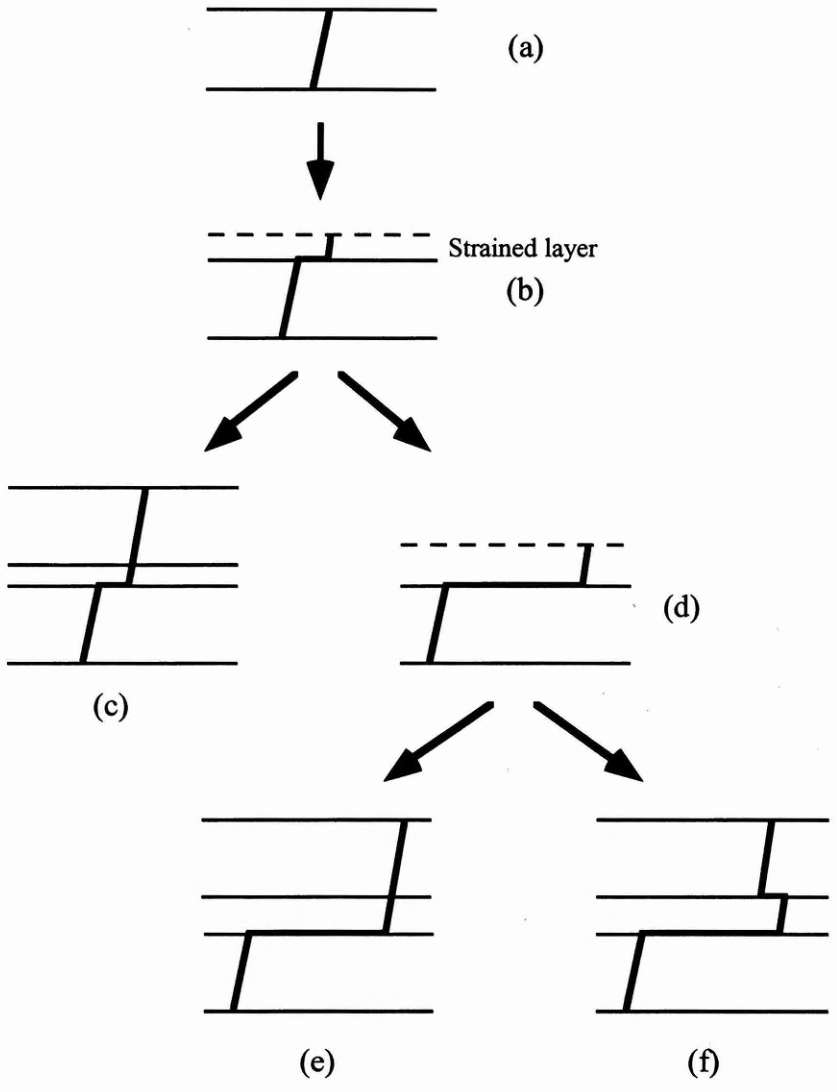

Fig. 3.9. Development of misfit dislocation through the transformation of a threading dislocation. (a) A threading dislocation. (b) A misfit segment generated by glide of a threading dislocation at the interface. (c) The final configuration of a threading dislocation with a misfit segment. (d) The misfit segment becomes longer when the thickness of strained layer increases. (e) A misfit dislocation line in the structure after a capping layer has been grown. (f) Two misfit segments are produced at both interfaces when a capping layer is grown.

Summing up the considerations above, provided that it is not pinned for any reason, a threading dislocation is ready to glide along the interface as soon as it grows

into a strained layer. This process can be illustrated by Fig. 3.9. For a threading dislocation as shown in Fig. 3.9(a), when it grows into a strained layer it will be subjected to a force due to misfit stress. This force will cause the threading dislocation to glide along the interface trailing a misfit dislocation at the interface and dividing the threading dislocation into two segments separated by this misfit segment, as shown by Fig. 3.9(b). If the growth of the strained layer stops now and the growth of a capping layer follows, the threading dislocation will go straight to the surface as shown in Fig. 3.9(c). As the growth of the strained layer progresses, the top segment of the threading dislocation glides away further and the misfit dislocation becomes longer as shown in Fig. 3.9(d). If the growth of a capping layer now follows, the threading dislocation may go straight to the surface as shown in Fig. 3.9(e). Alternatively, it may turn back first to form a new misfit segment at the other interface then reaching the surface as shown in Fig. 3.9(f). But this second glide of the threading dislocation at the other interface is very limited because all of the dislocation lines observed in the specimens with misfit dislocation network (Fig. 3.7 and Fig. 3.8) do not appear in pairs.

Although the misfit dislocations have been generated by glide of the threading dislocations and have also been elongated with the increase of the strained-layer thickness, they only occur at very limited areas with respect to the whole structure. Up to these stages, the relaxation resulting thereby can only be thought to be local. No experimental evidence has been obtained to show how misfit dislocations develop to form a misfit dislocation network resulting in a global relaxation of the structure, but it is clear that these two relaxations do not have the same significance to the structure.

3.3 Disagreement of experimental results with the M-B model

The TEM observations have confirmed the mechanism of formation of misfit dislocations from threading dislocations as a means of relieving stress in strained-layer structures. The strained-layer thicknesses at which misfit dislocations are found to generate from threading dislocations agree quite well with the prediction given by the

M-B model if, when considering the transient state of growth, the value of h_c is used instead of H_c for a double heterostructure. However, the fact that misfit dislocation segments were formed at a smaller strained-layer thickness, h_c', than predicted by the Matthews-Blakeslee model is not negligible. The formation of misfit dislocation segments on threading dislocations is not a chance occurrence and happened to all of the specimens examined where the strained-layer thicknesses were smaller than h_c.

3.3.1 The critical thickness

The transformation of threading dislocations in a strained-layer structure was taken by the M-B model as a criterion to determine the critical thickness for the relaxation of the structures. According to the model, any motion of threading dislocations at the interface resulting in the introduction of misfit dislocations means the break of the force balance on threading dislocations and is the indication that the critical thickness has been reached.

Table 3.1 shows the critical thicknesses, h_c and H_c, given by the M-B model for different $In_xGa_{1-x}As/GaAs$ structures and the thicknesses, h_e, of strained layers at which the onset of misfit dislocations through the transformation of threading dislocations have been observed experimentally.

The results of TEM cross-sectional measurement of strained-layer thicknesses, h_m, are also showed in Table 3.1. Theses results verify the nominal thicknesses of the specimens. The measurements, even taking the upper limits of error, ensure that, as designed, the smallest thicknesses of specimens for both $x = 0.15$ and 0.2 are less than the critical thickness given by the M-B model for single layer system, i.e., $h_m = 4.6 + 0.5$ nm $< h_c = 5.8$ nm for $x = 0.2$ and $h_m = 6.4 + 0.5$ nm $< h_c = 8.6$ nm for $x = 0.15$.

Table 3.1. The critical thicknesses, h_c and H_c, given by the M-B model for $In_xGa_{1-x}As/GaAs$ heterostructures, the thicknesses, h_e, at which the onset of misfit dislocations have been found in the structures, and the results of TEM cross-sectional measurement of strained-layer thicknesses, h_m,.

Structure	h_c or H_c (nm)	h_e (nm)	h_m (nm)
$In_{0.15}Ga_{0.85}As/GaAs$	8.6		
$GaAs/In_{0.15}Ga_{0.85}As/GaAs$	20.9	6	6.4 ± 0.5
$In_{0.2}Ga_{0.8}As/GaAs$	5.8		
$GaAs/In_{0.2}Ga_{0.8}As/GaAs$	14.5	4	4.6 ± 0.5

The accuracy of specimen composition is also a matter for concern. According to the manufacturer [Wang_99] the accuracy for x is ± 5%. Therefore the composition ranges are x = 0.1425 to 0.1575 for the specimens of x = 0.15 and x = 0.19 to 0.21 for the specimens of x = 0.2. Thus, even at the extremes of the error limits for both strained-layer thickness and composition, the smallest specimen thicknesses for both x = 0.15 and 0.2 are less than h_c.

According to the M-B model, misfit dislocations can be expected to emerge only when the thickness of the strained layer in $GaAs/In_{0.15}Ga_{0.85}As/GaAs$ reaches 20.9 nm. If we consider the process of growth in which the structure is build up layer by layer, an interface between GaAs and $In_{0.15}Ga_{0.85}As$ will be set up first and the critical thickness for this structure, h_c = 8.6 nm, should be considered. However, the onset of misfit dislocations has been found to be when the thickness of strained layer in $GaAs/In_{0.15}Ga_{0.85}As/GaAs$ is only 6 nm. It is not only below the critical thickness, H_c = 14.5, predicted by the M-B model for $GaAs/In_{0.15}Ga_{0.85}As/GaAs$, but also smaller than

that, h_c = 8.6 nm, for $In_{0.15}Ga_{0.85}As/GaAs$. Similarly, for $GaAs/In_{0.2}Ga_{0.8}As/GaAs$, the onset of misfit dislocation has been found to be when the thickness of strained layer is 4 nm which is smaller than the critical thicknesses given by the M-B model for $GaAs/In_{0.2}Ga_{0.8}As/GaAs$ and $In_{0.2}Ga_{0.8}As/GaAs$ respectively. Thus, for both of the structures examined, the onset of misfit dislocations have been found to be when their strained-layer thicknesses are below the critical values predicted by the M-B model.

3.3.2 Line tension and its effects on development of misfit dislocations

The line tension of a dislocation was considered by the M-B model as the most important force resisting the driving force due to misfit strain for the introduction of misfit dislocations.

Consider the curved dislocation in Fig. 3.10. The line tension T will produce forces tending to straighten the line. The direction of the net force is perpendicular to the dislocation and towards the centre of curvature. The line will remain curved if there is a shear stress, τ_0, which produces a force on the dislocation line in the opposite sense. The line will be in equilibrium in this curved position when

$$T = \tau_0 b \frac{dl}{d\theta}. \tag{3.4}$$

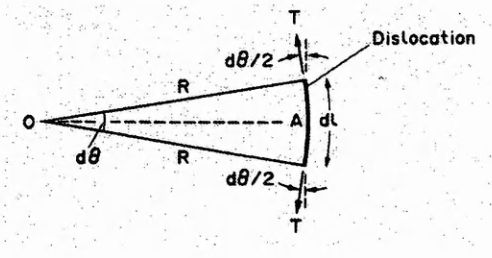

Fig. 3.10. Curved element of dislocation under line tension T [HullD_92]

For the threading dislocations observed, such as those in GaAs films, it can be assumed that $d\theta$ <<1. So the line tension is much greater than τ_0 when τ_0 tends to curve the dislocation line, and can be considered to be large enough to keep a short segment of dislocation straight. On the other hand, if the line tension is a force resisting

the motion of a dislocation, it must act in the direction parallel to the motion of the dislocation. The force which now takes effect is therefore the resolution of the line tension in the direction of the dislocation motion, $2T\sin(d\theta/2)$. Thus it is too small to play a role with a very small $d\theta$ at the starting stage of the motion of a dislocation.

Actually, from the observation above, the transformation of threading dislocations in a strained layer structure cannot be described as a process of bowing. When a threading dislocation grows, passing the interface and entering the strained layer, as shown in Fig. 3.9(b), its part in the strained layer becomes as a movable segment. Thus, a weak point exists for a threading dislocation at the intersection of its line and interface after it has entered a strained layer. Under the effects of misfit stress, this weak point will be broken and the segment located in the strained layer will move away from its original position along the interface trailing a misfit segment behind. In this way, a threading dislocation is divided into two parts. Because the movement is a glide, the easiest movement for a dislocation, it should occur before any other possible dislocation movements which the bowing of a dislocation may involve. The different configurations appearing in two threading segments divided by a misfit dislocation shown in Fig. 3.4, 3.5, and 3.6 are evidence that these two threading segments developed differently as growth progressed. The sequence of their formation can be assumed, according to TEM observations, to be that a threading dislocation from the substrate first met the first interface between GaAs and $In_xGa_{1-x}As$ and entered the strained layer; then it glided on the interface forming the misfit segment while it was passing through the strained layer, and met the second interface, when growth of the strained layer was completed; and finally, it turned back and crossed the capping layer reaching the surface. Therefore, there is no opportunity for a threading dislocation first to be formed straight crossing all the structure, from substrate to strained layer until reaching the surface of capping layer, and then to be bowed to form misfit dislocation at interfaces. The top end of the threading dislocation, if one takes two threading segments

as a whole, is readily shifted when the top part of it enters a strained layer and glides along the interface.

If misfit dislocations were formed in the way proposed by the M-B model, they would be present in pairs, that is, they would form at both of the interfaces synchronously. In fact, all of the misfit dislocations observed above are not in pairs.

So, as a factor to be considered for the formation of misfit dislocations, the line tension may affect the elongation process, keeping the dislocations shorter (the $d\theta$ now becomes larger), but cannot play a role as a barrier to prevent the threading dislocations from gliding.

The M-B model is expected to predict accurately the critical thickness for strains of up to approx. 1% [Hull.R_96]. However, as a result of analytic approximations in the M-B theory, the predicted critical thicknesses are double-valued at low strains and non-existent at higher strains [Downes_97]. Where two values are yielded, the lower value is considered unphysical as it is of the order of one Burgers vector.

3.3.3 A gap between local and global relaxation

The theoretical models give the thermodynamic equilibrium conditions for the formation of misfit dislocations in a strained-layer structure. According to the M-B model the critical thickness is an equilibrium point which marks the force balance for the formation of misfit dislocations on threading dislocations, i.e., the balance between the driving force caused by misfit stress and the resistance force caused by line tension, will be broken. The balance will turn out to be the dominant of driving force for the formation of misfit dislocations. In practice, the observed onset of misfit dislocations can be taken as the sign, according to the model, that not only has the thermodynamic equilibrium been broken, becoming the dominant part of the driving force (the critical thickness has been reached), but also the kinetic barriers for the process have been overcome. That means the driving force, or the excess stress $\tau_{ex} = \tau_{\varepsilon} - \tau_{l} > 0$ (τ_{l} is

the line tension stress) has had the significance of both thermodynamic and kinetic for the formation of misfit dislocations. The excess stress represents the net stress driving misfit dislocation elongation as defined by equation (1.18) [Downes_97, Dodson_87] and is only a function of the strained-layer thickness. When the onset of misfit dislocations through the transformation of threading dislocations has been initiated, it is the start point of the excess stress. Then one can expect that the development of misfit dislocations will be in proportion to the increase of the excess stress with the increase of strained-layer thickness. The increase of the excess stress would cause the misfit dislocations to develop proportionally if it was the dominating mechanism for the process.

The increase of the excess stress is shown in Fig. 3.11, calculated according to equation (1.18). The excess stress B is calculated according to the M-B model for $In_{0.15}Ga_{0.85}As/GaAs$, and A is the same calculation but the start point is shifted towards to a lower strained-layer thickness at which the misfit segment has been found experimentally on threading dislocations. That is, the excess stress A takes the strained-layer thickness of 6 nm as its starting point because the onset of misfit dislocations has been observed, while the excess stress B keeps the original prediction of the M-B model starting from the strained-layer thickness of 8.6 nm.

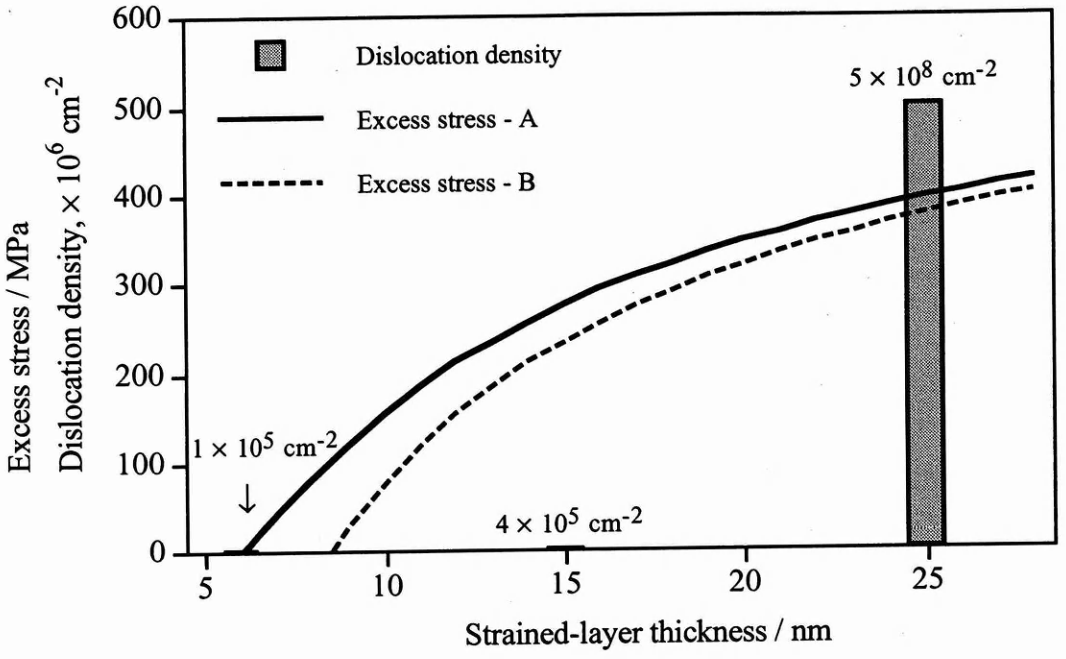

Fig. 3.11. The excess stress for $GaAs/In_{0.15}Ga_{0.85}As/GaAs$ and the changes of the misfit dislocation density after the onset of misfit dislocations have been experimentally observed in these structures.

When the onset of misfit dislocations has been found in $GaAs/In_{0.15}Ga_{0.85}As/GaAs$, its strained-layer thickness is 6 nm and the density of misfit dislocations is at the level of 1×10^5 cm^{-2}. The increase of the strained-layer thickness to 15 nm caused the misfit dislocations to become longer but this elongation did not change the dislocation density significantly (4×10^5 cm^{-2}). However, when the strained-layer thickness reached 25 nm, there was a sudden increase in dislocation density to 5×10^8 cm^{-2}, several thousand times higher. Therefore, there is a jump in the misfit dislocation density between the onset and the massive formation of misfit dislocations. This means that, after their generation through the transformation of threading dislocations, the development of misfit dislocations did not correspond to the increase of the excess stress implied by the model, as shown in Fig. 3.11.

The appearance of this jump indicates that the barriers responsible for the introduction of misfit dislocations through the transformation of threading dislocations,

and for the massive formation of misfit dislocations, are different. Although the misfit dislocations generated by glide of the threading dislocations have elongated with the increase of the strained-layer thickness, this elongation is not synchronous with the increase of the excess stress and is very limited, compared with the network of misfit dislocations which can be regarded as a global relaxation, resulting only in a local relaxation.

3.4 Conclusions

Four kinds of dislocation geometries have been found in GaAs/$In_xGa_{1-x}As$/GaAs for x = 0, 0.15, and 0.2:

(a) Straight threading dislocations in GaAs (i.e., x = 0);

(b) Threading dislocations with misfit segments when the strained-layer thicknesses h are below the critical thickness h_c predicted by the M-B model;

(c) Elongated misfit dislocations when $h_c < h < H_c$; and

(d) Misfit dislocation network when $h > H_c$.

The TEM observations of misfit dislocations in GaAs/$In_xGa_{1-x}As$/ GaAs prove that there is a transformation of threading dislocations into misfit dislocations in strained-layer structures. After entering the interface, the threading segments in a strained layer move away along the interface under the effects of misfit stress trailing a misfit segment behind and dividing the original threading dislocations into two parts. The misfit segments will be elongated with increasing strained-layer thickness. The possibility of a threading dislocation gliding back at the other interface to form one more misfit dislocation exists when the growth of a capping layer is followed, but both the probability and the extension of this second-glide are very limited.

The misfit dislocations generated through the transformation of threading dislocations are actually the behaviour of individual dislocations, therefore, only contribute to the local relaxation of the structures. With increasing strained-layer thickness, a sudden increase of dislocation density has been identified between the onset of 60° misfit dislocations through the transformation of threading dislocations and the formation of a 60° misfit dislocation network, which distinguishes the local relaxation from the global relaxation of a strained-layer structure. It remains unclear how misfit dislocations were massively introduced resulting in the global relaxation. However, the misfit dislocations did not develop in proportion to the increase of strained-layer thickness after the kinetic barriers for their generation and elongation through the transformation of threading dislocations had been overcome, indicating that the development of these dislocations lags the driving force. This implies that some other mechanism, rather than the M-B model, is dominating the global relaxation of strained-layer structures.

Chapter 4 : Formation of misfit dislocations during thermal processing and bending tests

The structures considered in this chapter are those in which the interfaces between strained layers and substrates are built up in a state of global coherence. As analysed in Chapter 3, the structure is accurately described as coherent only when it is considered globally, not locally. This coherence includes two types in relation to the M-B model. In one type of structure the strained-layer thickness is below the critical thickness (h_c or H_c). This kind of structure has been thought to be thermodynamically stable according to the theoretical models [Lourenco_94], this means this kind of structure is thermodynamically unable to form misfit dislocations. In the other type of structure the strained-layer thickness has exceeded the critical thickness but misfit dislocations are not introduced (globally) during fabrication. For these structures, although the conditions of thermodynamics have been met (critical thickness has been reached) according to the M-B model, misfit dislocations could not be formed because of kinetic reasons. Therefore, these structures have been considered to be metastable.

4.1 Formation of misfit dislocations at elevated temperatures

The investigation of strained-layer structures during post-grown thermal processing by measuring the normalised strain [Lourenco_94] indicated that the relaxation of the structure is strongly dependent on temperature, with significant changes occurring at high temperature. It is therefore supposed that the formation of misfit dislocations could provide the visual evidence showing the changes which happened to the structures.

4.1.1 CL imaging

The introduction of misfit dislocations into GaAs/$In_xGa_{1-x}As$/GaAs strained-layer structures by thermal processing is shown in Fig. 4.1 for $x = 0.15$, $h = 6$ and 15 nm, and Fig. 4.2 for $x = 0.2$, $h = 4$ nm.

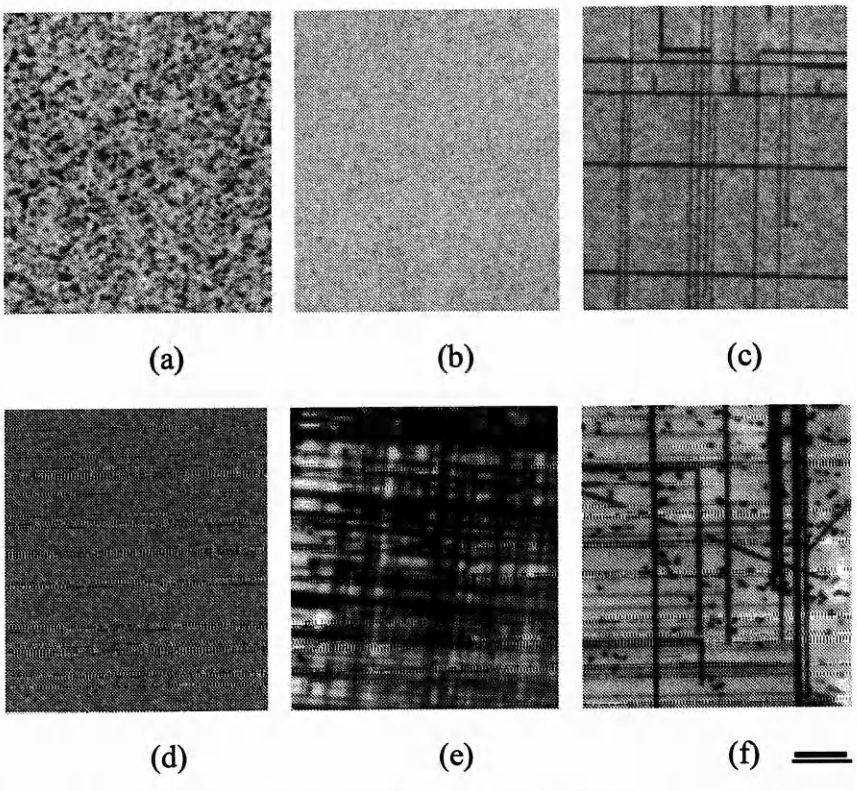

Fig. 4.1. CL images of GaAs/$In_{0.15}Ga_{0.85}As$/GaAs before and after thermal processing. (a) The as-grown specimen of h = 6 nm. (b) The as-grown specimen of h = 15 nm. (c) Misfit dislocations in the as-grown specimen of

h = 25 nm. (d) The specimen of h = 15 nm after thermal processing at 1170 K for 300 seconds. The specimens of h = (e) 15 nm and (f) 6 nm after thermal processing at 1220 K for 300 seconds. Bar = 10 μm.

Fig. 4.1(a) and (b) are CL images of the x = 0.15 specimens of which the strained-layer thicknesses are h = 6 and 15 nm respectively. Although some transformed threading dislocations and elongated misfit dislocations exist as shown in Chapter 3, no identifiable dislocations can be found by CL imaging when a larger area was viewed at lower magnification. This indicates that these structures are globally coherent in their as-grown state. For comparison, Fig. 4.1(c) shows a CL image of misfit dislocations in an as-grown specimen of x = 0.15 with the strained-layer thickness h = 25 nm. Misfit dislocations formed during MBE are revealed very clearly by CL imaging, indicating that the interfacial structure has lost coherence.

Thermal processing at 1170 K caused no changes in the specimen of GaAs/$In_{0.15}Ga_{0.85}As$/GaAs with the strained-layer thickness h = 15 nm, as shown in Fig. 4.1(d). But, when temperature was 50 K higher, i.e., thermal processing at 1220 K for 300 seconds, a lot of misfit dislocations can be seen to be formed not only in the specimen of h = 15 nm, as shown in Fig. 4.1(e), but also in the specimen of h = 6 nm, Fig. 4.1(f).

The black spots in Fig. 4.1(f) indicate that there is some surface damage of the specimen after thermal processing at higher temperature. Because the TEM images of these specimens, as shown below, do not show any difference in the background from that of as-grown specimens, this damage should be limited to within the area of spots and does not affect the whole structure of the specimens significantly.

Misfit dislocations were also introduced into GaAs/$In_2Ga_{0.8}As$/GaAs specimens with the strained-layer thickness of 4 nm by thermal processing. Fig. 4.2(a) is the CL image of an as-grown specimen of GaAs/$In_{0.2}Ga_{0.8}As$/GaAs with the strained-layer thickness of 4 nm. No dislocations could be introduced into this kind of structure until

temperature reached to 1350K. Fig 4.2(b) shows the CL image of misfit dislocations formed in a specimen of this kind during thermal processing at 1350 K for 300 seconds.

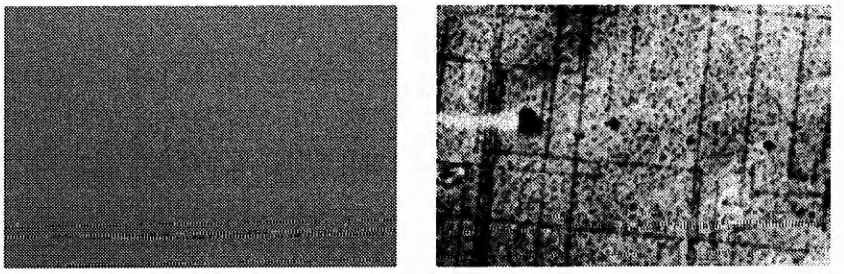

(a) (b)

Fig. 4.2. CL imaging of GaAs/$In_{0.2}Ga_{0.8}As$(h = 4 nm)/GaAs before and after thermal processing. (a) As-grown state. (b) After thermal processing at 1350 K for 300 seconds. Bar = 10 μm.

The misfit dislocations formed during thermal processing do not show any particular difference in their geometries from those seen in as-grown structures when viewed by CL imaging, except that their density is obviously higher.

4.1.2 TEM imaging

Fig. 4.3 shows TEM plan-view images of misfit dislocations formed in GaAs/$In_{0.15}Ga_{0.85}As$/GaAs (h = 15 nm) during thermal processing at 1220 K. (a) is the bright field image and (b) is the dark field image. The dislocation lines in Fig. 4.3(a) looked rather hazy when viewed in bright field. This haziness is resulted from the fact that these lines are actually present in pairs, which can be revealed clearly by dark field imaging as shown in Fig. 4.3(b).

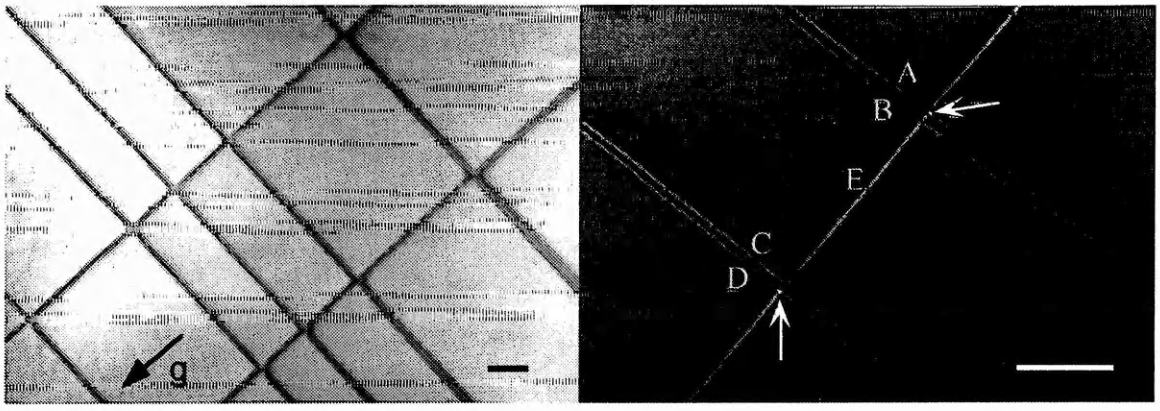

(a) (b)

Fig. 4.3. TEM plan-view images of misfit dislocations formed in GaAs/$In_{0.15}Ga_{0.85}As$ (h = 15 nm)/GaAs during thermal processing at 1220 K for 300 seconds. (a) Bright field image. **g** = [220], bar = 200 nm. (b) [220] dark field image. Bar = 100 nm.

The question now arises whether both lines of every pair are located at the same interface or separately at two different interfaces. According to the M-B model, misfit dislocations would elongate from bowing of threading dislocations and form pairs of misfit dislocations at both of the interfaces. But it has been seen in Chapter 3 that none of the misfit dislocations in the as-grown structures are present in pairs. Measurement of the distance between the two lines of a dislocation pair in Fig. 4.3 agrees, although approximately, with the strained-layer thickness of the specimen. Two different configurations can be seen in TEM plan-view images when a dislocation pair crosses a dislocation line. One line of a dislocation pair, *B* or *C* in Fig. 4.3(b), passes another dislocation line *E* straight away while the other, dislocation line *A* or *D*, produces a tip as arrowed, because of dislocation reactions, at the crossing point when it passes the same dislocation line. This means that the dislocation lines *A* and *D* meet the dislocation line *E* but the dislocation lines *B* and *D* do not. The dislocation line *E* is definitely located at only one interface. So, the two lines of every dislocation pair are located at different interfaces. That is, in Fig. 4.3(b), the dislocation lines *A* and *D* are located at the interface in which the dislocation line *E* is also located, and the dislocation lines *B*

and *C* at the other. The dislocation lines *A* and *B* should be located at the same (111) slip plane which has different indexing from that of another slip plane in which the dislocations *C* and *D* are located.

This configuration of misfit dislocations might be evidence that the M-B model does work for the formation of misfit dislocations, but the evidence is for the post-growth thermal processing not for the process of the structure fabrication. However, once again, misfit dislocations are proved not to be produced only by one mechanism. Together with the misfit dislocations present in pairs, there are some other misfit dislocations which are present in single lines, not in pairs, as the dislocation line *E* in Fig. 4.3(b). It is concluded therefore that the dislocation *E* was not produced by the same way which produced the dislocation pairs.

Though no misfit dislocations can be found by CL imaging, a few dislocations are found by TEM imaging in GaAs/$In_{0.15}Ga_{0.85}As$/GaAs (h = 15 nm) after thermal processing at 1170 K, as shown in Fig. 4.4. These dislocations are single lines scattering over the specimen and are not very long, so they could not form a dislocation network. A unusual geometry can be seen in one of the ends of the dislocation shown in Fig. 4.4. Between a 60° dislocation line and one of its threading segments, there is a misfit segment which, as will be discussed in Chapter 5, is the edge type.

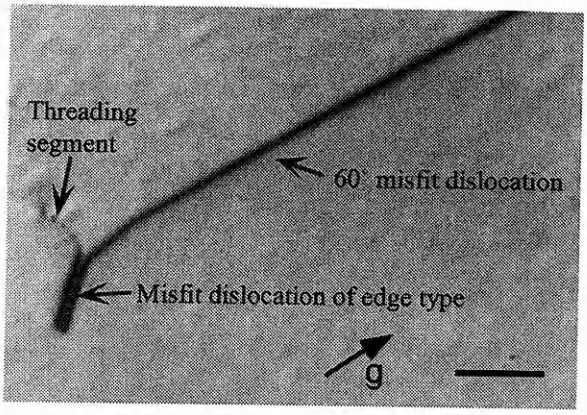

Fig. 4.4. TEM plane-view images of misfit dislocations formed in GaAs/$In_{0.15}Ga_{0.85}As$(h = 15 nm)/GaAs during thermal processing at 1170 K for 300 seconds. **g** = [220], bar = 200 nm.

Fig. 4.5 shows the misfit dislocations in a specimen of GaAs/$In_{0.15}Ga_{0.85}As$/GaAs with the strained-layer thickness h = 6 nm after thermal processing at 1170 K for 300 seconds. It is not easy to identify if the short misfit segment on a threading dislocation in Fig. 4.5(a) was caused by thermal processing or produced during structure fabrication. But, it is definite that thermal processing at a temperature of 50 K higher, 1220 K for 300 seconds produced many misfit dislocations in a specimen of the same kind, as shown in Fig. 4.5(b). These misfit dislocations do not appear in pairs.

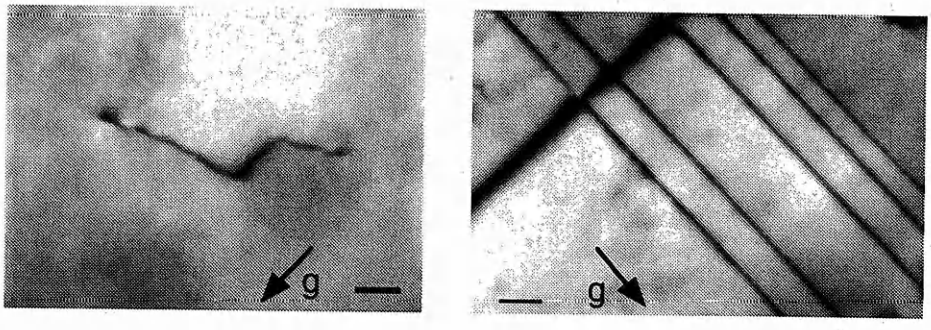

Fig. 4.5 Misfit dislocations in the specimens of GaAs/$In_{0.15}Ga_{0.85}As$/GaAs with the strained-layer thickness h = 6 nm after thermal processing at (a) 1170 K and (b) 1220 K for 300 seconds. **g** = [220], bar = (a) 50 nm, (b) 200 nm.

4.1.3 Misfit dislocations of edge type

Misfit dislocations of edge type are also found in GaAs/$In_{0.15}Ga_{0.85}As$/GaAs (h = 15 nm) after thermal processing at 1220 K for 300 seconds as shown in Fig. 4.6. The spacing of the dislocation pairs is wider when viewed by [400] reflection, as shown in (b), than that when viewed by [220] reflection in (a). This suggests the dislocation pair is located at a (001) plane, that is, one of the two interfaces. The dislocation shown in (a) was invisible when viewed by (c) [040] and (d) [131] reflection. Using $\mathbf{b} = \mathbf{g}_1 \times \mathbf{g}_2$ if $\mathbf{g} \cdot \mathbf{b} = 0$, it can be determined that the Burgers vector of the dislocation is in the direction of [022] and the dislocation is pure edge type.

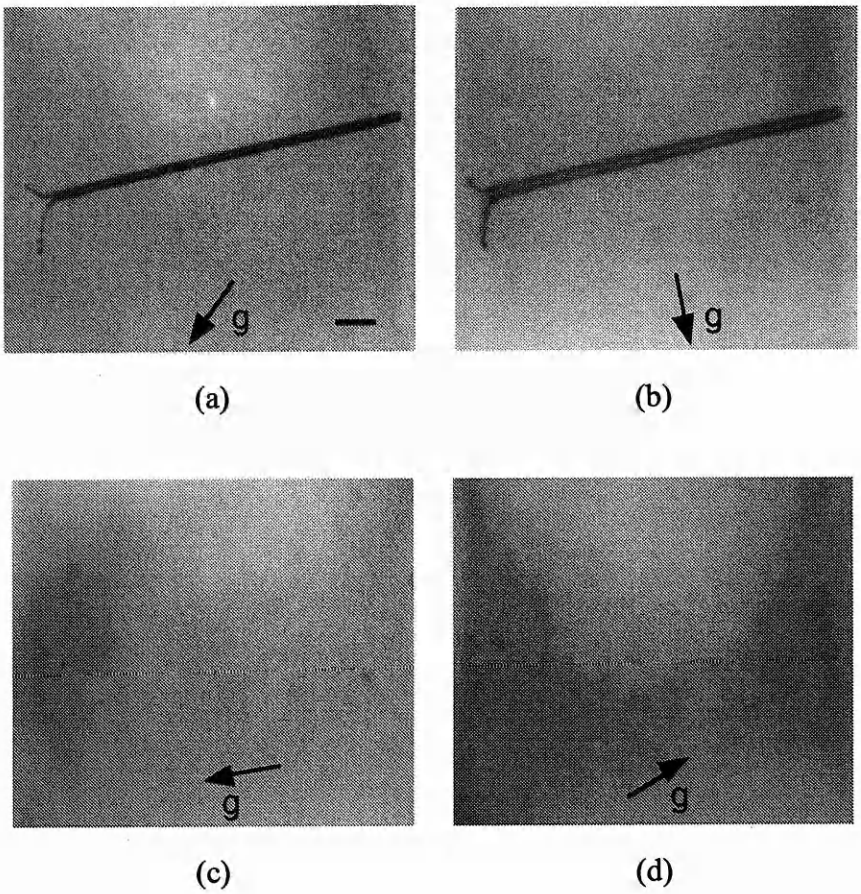

Fig. 4.6. TEM plan-view images of a misfit dislocation formed in GaAs/$In_{0.15}Ga_{0.85}As$(h = 15 nm)/GaAs during thermal processing at 1220 K for 300 seconds viewed by different Bragg reflections. (a) $\mathbf{g} = [2\bar{2}0]$, (b) $\mathbf{g}$ = [400], (c) $\mathbf{g}$ = [040], (d) $\mathbf{g}$ = [131]. Bar = 200 nm.

The length of the dislocations generated during thermal processing is related to temperature. Fig. 4.7 represents the dislocations formed in a specimen of the same kind as Fig. 4.6 but at the temperature of 50 K lower, 1170 K. The dislocations are also the edge type, the same as that shown in Fig. 4.6, but are much shorter.

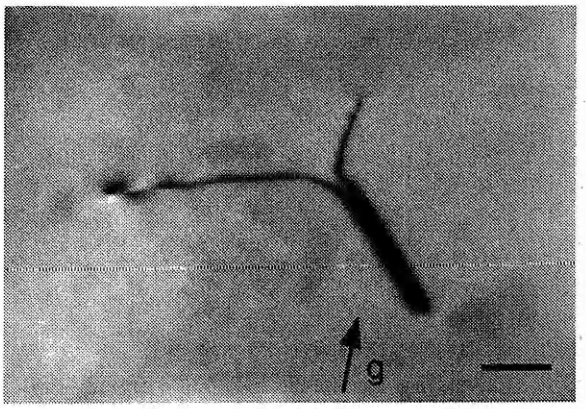

Fig. 4.7. TEM plan-view image of a misfit dislocation formed in GaAs/$In_{0.15}Ga_{0.85}As$(h = 15 nm)/GaAs during thermal processing at 1170 K for 300 seconds. **g** = [220], bar = 100 nm.

It is very noticeable that the development of these dislocations during thermal processing, although it occurred on a threading dislocation, did not result in the formation of 60° misfit dislocations, but edge ones. According to the M-B model, for the introduction of edge misfit dislocations, the critical thickness should be H_c (Edge) = 1.05 H_c (60°) as given by Equation (1.8). Thus, besides the difference in mechanisms of generation (glide or climb), the thermodynamic condition should also be favourable first for the formation of 60° dislocations. The dislocation did not adopt the easiest way to form a 60° dislocation by glide, but took the most difficult way of climb to form an edge one. This fact indicates that the formation of 60° dislocations by glide is not the only mechanism of the relaxation of a strained-layer structure.

The mechanism which produces edge misfit dislocations was very active in relaxing the structure during thermal processing at high temperatures resulting in the formation of edge misfit dislocations with various geometries as shown in Fig. 4.8. The

dislocation A was generated on a 60° dislocation B. The dislocation B should be generated first during thermal processing and then the dislocation A generated on it. The dislocation C was generated on a threading dislocation D. The generation of the dislocation E has been more complex and has led to an unusual geometry. It might be a dislocation group formed by movement of several dislocations. Dislocations F and G are very special. They have formed a closed circle without any segment threading to the surfaces. They should result from the directional expansion of dislocation loops under the effects of misfit stress.

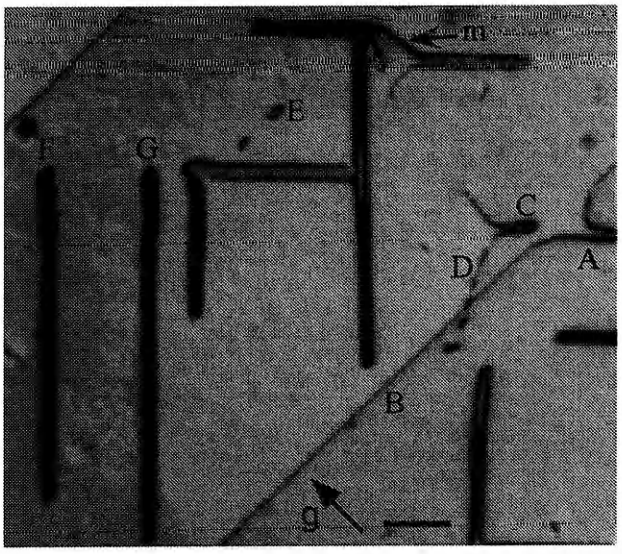

Fig. 4.8. TEM plan-view images of 60° and edge misfit dislocations formed in GaAs/$In_{0.15}Ga_{0.85}As$(h = 15 nm)/GaAs during thermal processing at 1220 K for 300 seconds. **g** = [220], bar = 200 nm.

Dislocation in Fig. 4.4 and dislocation segment m in Fig 4.8 provide a clue to understand the mechanisms of formation of edge-type dislocation pair shown in Fig. 4.6 and 4.7. It is easy to understand that dislocation pair A in Fig. 4.8 was generated by climbing at an interface from 60° dislocation B because dislocation B is definitely located at one interface. However, threading dislocations are present from bottom to top of specimen and it has been shown that dislocation pair in Fig. 4.6 is located at only one interface. It seems impossible for a threading dislocation to climb along an interface at

the intersection point of this threading dislocation and interface to form a dislocation pair like the one shown in Fig. 4.6. As suggested by the dislocation shown in Fig. 4.4 and dislocation *m* in Fig. 4.8, firstly, a 60° dislocation segment was generated by glide of threading dislocation along an interface, but it is difficult to identify whether or not this generation occurred during MBE growth or thermal processing, then, this 60° dislocation segment, or a part of this segment, climbed along the interface forming an edge-type dislocation pair.

4.2 Formation of misfit dislocations under an applied stress

Misfit stress is a decisive factor in strained-layer structures. Any change of the stress state inside the structure caused by external stress, i.e., an applied stress, will affect the equilibrium set up between strained layer and substrate. This can be expected to affect the misfit dislocations.

4.2.1 CL imaging

Fig. 4.9 is a set of successive CL images of a GaAs/$In_{0.15}Ga_{0.85}As$/GaAs (h = 15 nm) specimen after [110] bending by a tensile stress of 7.25 MPa at 670, 690, and 710 K respectively. It shows the process of dislocation multiplication from a very few short dislocations in (a) to longer ones in (b) and finally intensive increase of both length and amount in (c). Dislocations *A*, *B*, *C*, and *D* in (a) were not elongated further when the temperature increased by 20 K as shown in (b) although some new and longer dislocations appeared. Fig. 4.10 is CL images of specimens with the same composition but different strained-layer thickness (h = 6 nm) after the same bending at 570, 670, and 690 K and shows the similar process of misfit dislocation development.

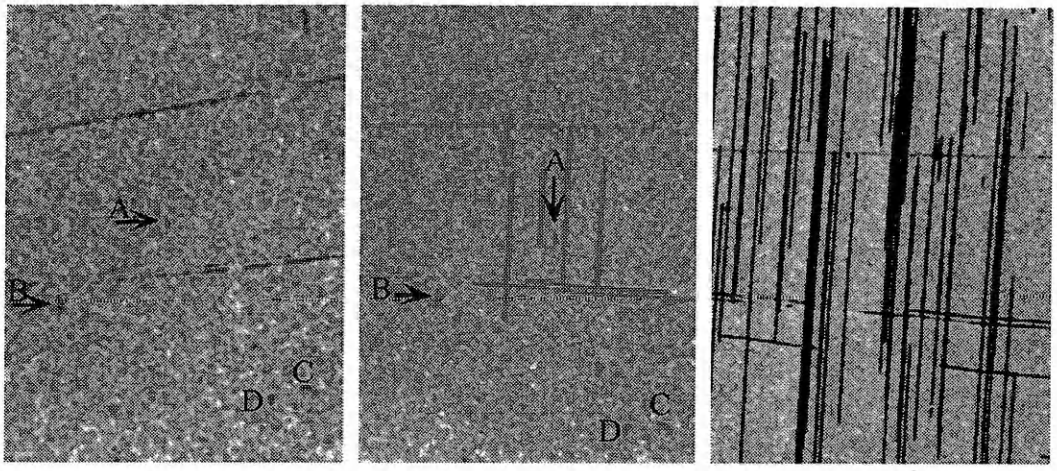

(a) (b) (c)

Fig. 4.9. Successive CL images of a GaAs/$In_{0.15}Ga_{0.85}As$(h = 15 nm)/GaAs specimen after [110] bending by an tensile stress of 7.25 MPa at (a) 670, (b) 690, and (c) 710 K. Bar = 100 μm.

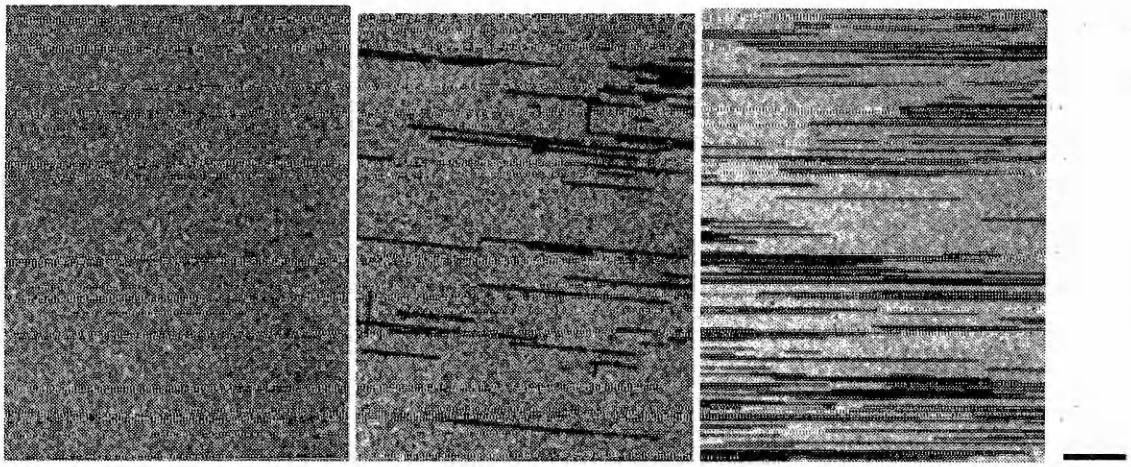

(a) (b) (c)

Fig. 4.10. CL images of GaAs/$In_{0.15}Ga_{0.85}As$(h = 6 nm)/GaAs specimens after [110] bending by an tensile stress of MPa at (a) 620, (b) 670, and (c) 690 K. Bar = 100 μm.

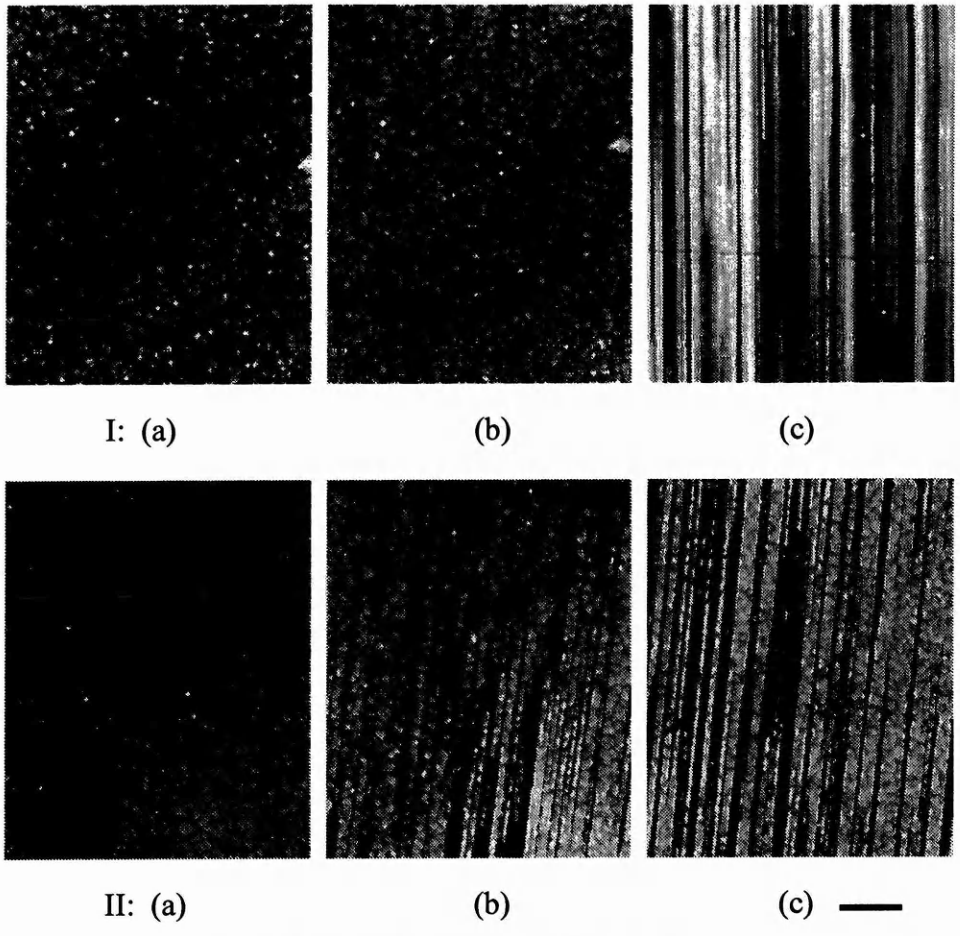

Fig. 4.11. CL images of dislocations after [110] bending by an tensile stress of 7.25 MPa in GaAs/$In_{0.2}Ga_{0.8}As$/GaAs at (a) 690, (b) 710, and (c) 730 K for specimens I: h = 10 nm and II: h = 4 nm. Bar = 100 μm.

Dislocations are also seen in the specimens of x = 0.2 with the strained-layer thickness h = 10 and 4 nm after [110] bending test at 710 and 730 K, as shown in Fig. 4.11.

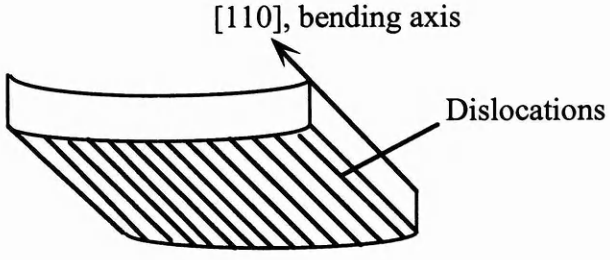

Fig. 4.12. The relation of the bending axis and the line directions of dislocations formed during [110] bending.

The relationship of the line directions of these dislocations to the bending axis can be determined by comparing these lines with the sides of the specimens. During [110] bending tests, the long sides of the specimens which were in the direction of $[1\bar{1}0]$ were perpendicular to the bending axis. All of the misfit dislocations shown above can be determined by CL imaging to be perpendicular to the long sides of the specimens. Therefore, as schematically illustrated in Fig. 4.12, all dislocation lines formed during [110] bending are parallel to the bending axis, i.e., along the direction of [110]. No dislocations can be found to be present in other directions not parallel to the bending axis.

4.2.2 TEM imaging

TEM revealed that the dislocations caused by bending tests have the character of misfit dislocations. As shown in Fig. 4.13, they are straight lines with specific line directions of <110>. These remain the same for all bending-tested specimens with different compositions or different strained-layer thicknesses.

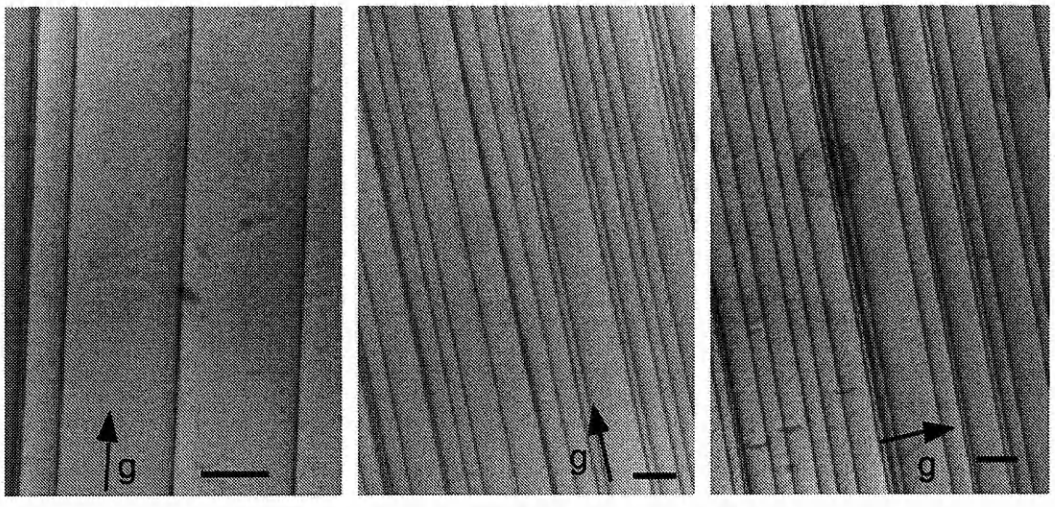

(a) (b) (c)

Fig. 4.13. TEM plan-view images of dislocations caused by bending tests in (a) GaAs/$In_{0.15}Ga_{0.85}As$(h = 6 nm)/GaAs, (b) GaAs/$In_{0.15}Ga_{0.85}As$(h = 15 nm)/GaAs , and (c) GaAs/$In_{0.2}Ga_{0.8}As$(h = 4 nm)/GaAs. **g** = [220], bar = 500 nm.

Very few threading segments of misfit dislocations can be found in these TEM images. This implies that the dislocation lines formed during bending tests are quite long. The reason that these dislocations could run a long way is that they only moved along (001) interfaces, or, the intersections of {111} slip planes and (001) interfaces, which are parallel to the surfaces. Otherwise, they would terminate by reaching the surfaces. Therefore these dislocations are only active within the specific crystal planes — the interfaces being two dimensional.

Unlike in the specimens which were thermally processed, edge dislocations are not found in the bending test specimens.

4.2.3 Different dislocation configurations under [110] and [100] bending

It has been shown that the formation of misfit dislocations under an applied tensile stress is related to the bending axis, that is, the direction of applied stress. The sensitivity of the misfit dislocation line directions to the bending axis can be well demonstrated by a [100] bending test, i.e., the bending axis is at 45° to [110] direction. It can be seen in Fig. 4.14 that, rather than forming in [100] directions as shown in Fig. 4.13, dislocations caused by [100] bending in GaAs/$In_xGa_{1-x}As$/GaAs appeared in the directions of [110] and [$1\bar{1}0$] forming a network consisting of many orthogonal dislocations as seen generally in an as-grown incoherent structure. The relationship of the line directions of dislocations and the banding axis in [100] bending tests is shown in Fig. 4.15. This is further evidence that the formation of misfit dislocations during bending tests is affected by the applied stress together with misfit stress.

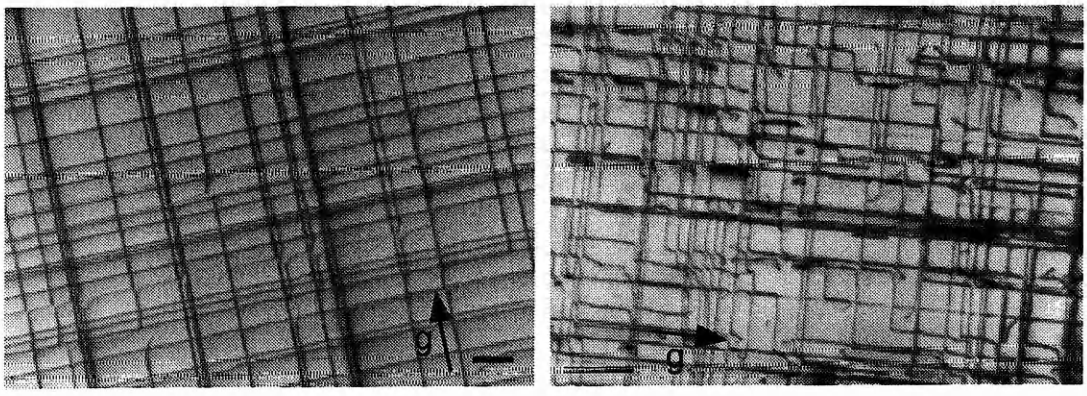

(a) (b)

Fig. 4.14. TEM plan-view images of dislocations caused by [100] bending in (a) GaAs/$In_{0.15}Ga_{0.85}As$(h = 15 nm)/GaAs, (b) GaAs/$In_{0.2}Ga_{0.8}As$(h = 4 nm)/GaAs. **g** = [220], bar = 500 nm.

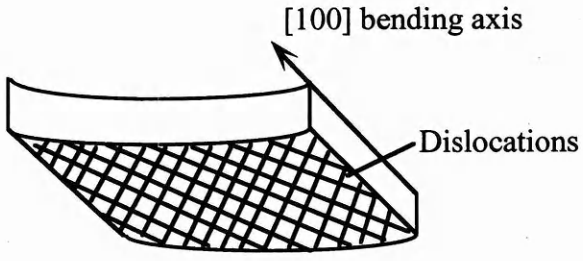

Fig. 4.15. The relation of the bending axis and line directions of dislocations in [100] bending.

Similar to [110] bending, the fact that the dislocations are long straight lines and there are few threading dislocations indicates they are present only in the interfacial planes and therefore are two-dimensional.

4.2.4 Regions of dislocation and non-dislocation

The effects of an applied tensile stress on the formation of misfit dislocations in a compressive strained layer can be well manifested by a CL image of misfit dislocations formed by [100] bending as shown in Fig. 4.16. The specimen was a piece of GaAs/$In_{0.15}Ga_{0.85}As$/GaAs with strained-layer thickness h = 15 nm. It can be seen from the CL image that, after the bending test, there is a clear boundary in the specimen dividing the regions of dislocation and non-dislocation. This boundary is precisely the

position where one of the two outer loading lines of the 3-point bending was located. The area between two outer loading lines (outer span of the 3-point bending) is the region of the specimen where the tensile stress was applied by 3-point bending and beyond that the stress had no effect. A sketch illustrating the regions of dislocation and non-dislocation in a specimen produced during [100] bending is shown in Fig. 4.17.

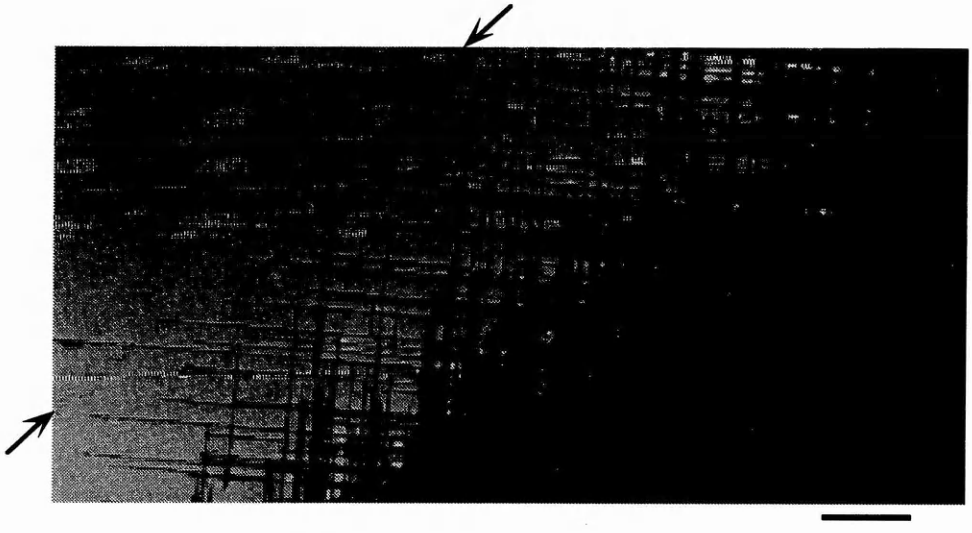

Fig. 4.16. CL image of dislocations showing regions of dislocation and non-dislocation caused by [100] bending at 710 K in GaAs/$In_{0.15}Ga_{0.85}As$(h = 15 nm)/GaAs. Two arrows mark the linear position where one of the outer loading lines of [100] bending located at. Bar = 50 μm.

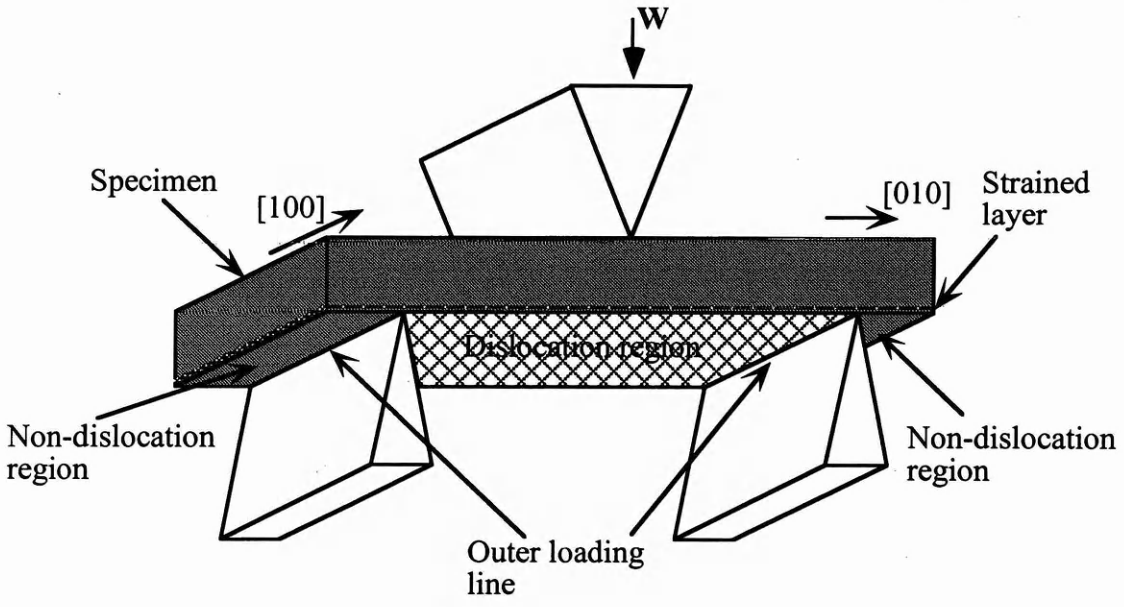

Fig. 4.17. A sketch illustrating the regions of dislocation and non-dislocation in a strained-layer structure caused by [100] 3-point bending.

It can be seen from Fig. 4.16 that the density of misfit dislocations caused by the bending test is a function of the distance away from the outer loading line. The further away, the higher density. This is simply because that the bending moment is a function of the distance away from the fulcrum [Hearn_77].

4.3 Temperature dependence of formation of misfit dislocations

Post-growth thermal processing introduced misfit dislocations into the strained-layer structures which were originally coherent. No matter the strained-layer thickness h can be characterised as $h_c < h < H_c$ (h = 15 nm for GaAs/$In_{0.15}Ga_{0.85}As$/GaAs) or $h < h_c$, (h = 6 nm for GaAs/$In_{0.15}Ga_{0.85}As$/GaAs and h = 4 nm for GaAs/$In_{0.2}Ga_{0.8}As$/GaAs), the relaxation of the structures eventually occurred by the formation of misfit dislocations at high temperatures. For the specimens of the same kind, the densities of misfit dislocations (as shown in Fig. 4.1(d), (e), and (f)) and the length of the individual dislocations, as shown in Fig. 4.6 and Fig. 4.7, are both temperature related.

4.3.1 Thermal expansion coefficients

For strained-layer-structures, the difference in thermal expansion coefficients between the substrate and the strained layer may cause additional stress as temperature rises.

The lattice parameter of GaAs is 0.565325 nm at 300 K [Stringfellow_93]. Thermal expansion coefficients of GaAs [Adachi_96] are changed with temperature and are 6.89 (10^{-6} K^{-1}) at 800 K which was the temperature of fabrication of the InGaAs/GaAs heterostructures and 7.64 (10^{-6} K^{-1}) at 1300 K which was the highest temperature for the thermal processing experiments.

The lattice parameter for $In_xGa_{1-x}As$ can be derived from the parameters of GaAs and InAs (0.60583 nm [Stringfellow_93]) by Vegard's law and is 0.5714 nm for x = 0.15 and 0.57343 nm for x = 0.2. The thermal expansion coefficients for $In_xGa_{1-x}As$ can be calculated according to [Takahashi_93]

$$\alpha(x) = 5.20 + 0.83(1 - x)\ (10^{-6}\ K^{-1}), \tag{4.1}$$

which gives the thermal coefficients of $In_xGa_{1-x}As$ 5.906 (10^{-6} K^{-1}) for x = 0.15 and 5.864 (10^{-6} K^{-1}) for x = 0.2.

The thermal expansion coefficients of both $In_{0.15}Ga_{0.85}As$ and $In_{0.2}Ga_{0.8}As$ are smaller than that of GaAs. This means that, as a compressive strained layer of $In_xGa_{1-x}As$ based on GaAs, the lattice mismatch between $In_{0.15}Ga_{0.85}As$ or $In_{0.2}Ga_{0.8}As$ and GaAs will decrease with the rise of temperature. Calculations of the lattice parameters alternated by rising temperature from 300 to 1300 K verifies that the misfit between $In_xGa_{1-x}As$ and GaAs changes from 0.01075 at 300 K to 0.00902 at 1300 K for $In_{0.15}Ga_{0.85}As$/GaAs and from 0.0143 to 0.0126 for $In_{0.2}Ga_{0.8}As$/GaAs within the same range of temperature. That is, misfit between $In_xGa_{1-x}As$ and GaAs will decrease 16% for x = 0.15 and 13% for x = 0.2 when temperature rises from 300 K to 1300 K.

Therefore, thermal processing at higher temperatures causes not an increase, but a decrease of misfit for $In_xGa_{1-x}As/GaAs$ heterostructures. The driving force for the formation of misfit dislocations during thermal processing was therefore reduced by the high temperature.

4.3.2 Temperature dependence

The formation of misfit dislocations is visual evidence of loss of coherence of the interfacial structure in a strained-layer structure. The misfit is accommodated by a mixture of misfit dislocations and elastic strain in a strained-layer structure. Thus the misfit f is accommodated by the elastic strain ε and the plastic strain (misfit dislocations) δ [Fitzgerald_91],

$$f = \frac{a_s - a_o}{a_s} = \varepsilon + \delta$$

where a_S and a_O are the lattice parameters of the substrate and overlayer respectively. (The effects of temperature on misfit is ignored in the following discussion although, as discussed above, misfit f is actually a function of temperature for the strained-layer structures when the substrate and overlayer do not have the same thermal expansion coefficients.) Because misfit dislocations exist at the interface, δ is non-zero and can be estimated from the misfit dislocation spacing S,

$$\delta = b_e / S, \tag{4.2}$$

where b_e is the interface-plane component of the Burgers vector in the direction of spacing S.

Therefore, δ is actually a measurement of the relaxation caused by the formation of misfit dislocations. By writing equation (4.1) in another form, the deduction of the elastic strain in a strained-layer structure due to the formation of misfit dislocations is $\varepsilon = f - \delta$. Fig. 4.18 shows the changes of the elastic strain (normalisation of misfit

strain) caused by the formation of misfit dislocations in the specimens of GaAs/$In_{0.15}Ga_{0.85}As$/GaAs during thermal processing and bending tests.

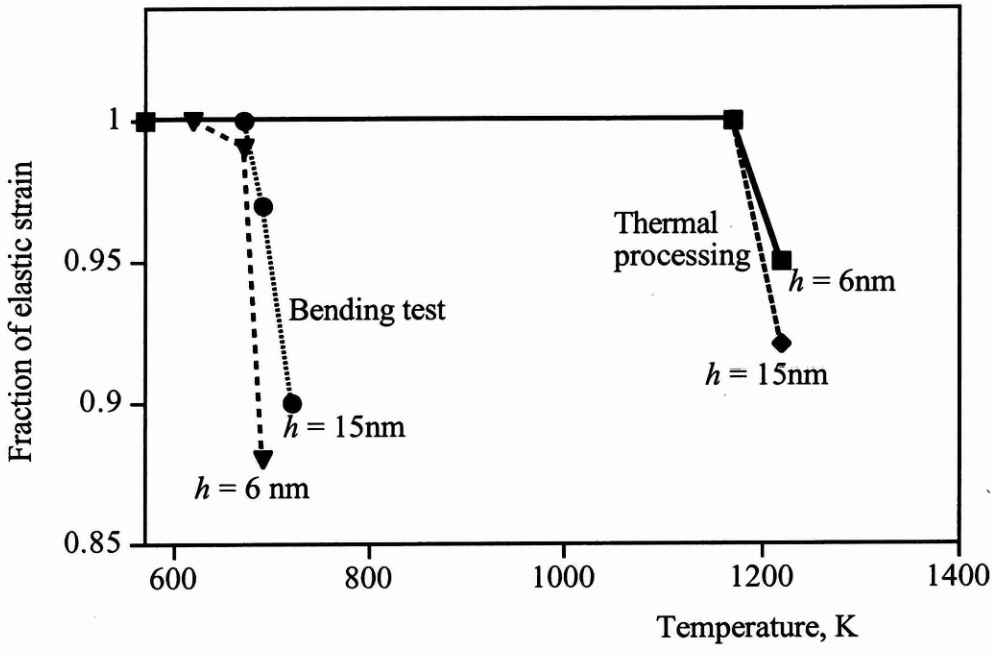

Fig. 4.18. Deduction of the elastic strain caused by the formation of misfit dislocations in GaAs/$In_{0.15}Ga_{0.85}As$/GaAs during thermal processing and bending test.

It can been seen in Fig. 4.18 that, for both h = 6 nm and h = 15 nm, the formation of misfit dislocations begins at almost the same temperatures for both thermal processing and bending tests. The relaxation achieved by the formation of misfit dislocations is almost the same in each case. The amounts of relaxation are 5 ~ 8 % for thermal processing and 10 ~ 12 % for the bending tests. This implies that they are both dependent on misfit stress which is the key factor for the behaviour of misfit dislocations and is only a function of indium content.

Fig. 4.18 suggests that there is a critical temperature for the formation of misfit dislocations. A difference of 50 or 40 K in temperature (from 1170 to 1220 K for thermal processing and 670 to 710 K for bending tests) causes a change from an absence of misfit dislocations to their massive formation. This critical temperature may

indicate the point at which the thermodynamics and kinetics have both become favourable for the formation of misfit dislocations and the process can thus proceed straight away.

The experimental results shown above can be taken as evidence that, as discussed in Chapter 3, although misfit dislocations had been generated from the transformation of threading dislocations, the structure was not at the critical thermodynamic or kinetic point for the relaxation of the whole structure. Otherwise, misfit dislocations would be introduced substantially, as seen here, without any standstill after the start of their formation. Even if the massive formation could not occur immediately following the increase of strained-layer thickness after the transformation of threading dislocations had begun, at least, misfit dislocations should develop in proportion to the increase of the driving force showing a significant difference in dislocation density if this mechanism had worked. The massive formation of misfit dislocations in as-grown GaAs/$In_xGa_{1-x}As$/GaAs is an indication that the thermodynamic and kinetic point for this process has been reached, but the structures are now well past the strained-layer thickness at which the transformation of threading dislocations occurred. Therefore, these two processes, the massive formation of misfit dislocations and the generation of misfit dislocations on threading dislocations, are dominated by separate mechanisms.

High temperature undoubtedly changes the critical conditions at which misfit dislocations are introduced into a strained-layer structure. For GaAs/$In_{0.15}Ga_{0.85}As$/GaAs with the strained-layer thickness h = 25 nm, the massive formation of misfit dislocations occurred during MBE growth at 870 K. This event could not occur for the same heterostructures with smaller strained-layer thickness h = 6 nm and h = 15 nm during MBE, but is observed to occur at a higher temperature (1220 K) during post-growth thermal processing. Therefore, the critical thickness for the formation of misfit dislocations is not only the function of strained-layer thickness, but also a function of temperature.

4.3.3 Thermal stability of interface

The discussion in *4.3.2* is premised by the assumption that the interface of pseudomorphic GaAs/$In_xGa_{1-x}As$/GaAs structures is not destroyed, or even significantly changed, by high temperature treatment. However, interdiffusion in semiconductor heterostructures has been considered to be able to occur under both growth conditions and during subsequent processing [References in Gillin_94]. If interdiffusion occurs, it changes the compositions of the layers adjacent to the interface, and one can expect the disappearance of the interface eventually because of the full intermix as the final stage of interdiffusion.

The melting point of InGaAs can be calculated by interpolation between the melting point of GaAs (1513 K) and InAs (1215 K) [Brenchley_97] and is 1468 K for $In_{0.15}Ga_{0.85}As$ and 1453 K for $In_{0.2}Ga_{0.8}As$. The temperature of thermal processing has reached high enough, 0.83 T_m for 1220 K and 0.93 T_m for 1350 K, for interdiffusion to occur [References in Gillin_94].

Although it is difficult to give direct evidence of interdiffusion during thermal processing, the formation of misfit dislocations demonstrates that the misfit stress due to lattice mismatch between strained layer and substrate is still efficacious at a high temperature to drive the formation of misfit dislocations. If interdiffusion had occurred, it would result in intermix between $In_xGa_{1-x}As$ and GaAs. This would lead to a decrease in the composition gradient across the interface and consequently eliminate the lattice mismatch. In this case, the formation of misfit dislocations would become impossible owing to the loss of the driving force. The formation of misfit dislocations does occur during thermal processing, and appears at a higher density compared to that in as-grown structures. This indicates that, even though the occurrence of interdiffusion can not be ruled out, it is not serious enough to destroy or significantly change the pseudomorphic $In_xGa_{1-x}As$/GaAs interfaces.

4.4 Applied stress dependence of the formation of misfit dislocations

Fig. 4.18 also indicates that the applied stress is another factor which has a significant effect on the formation of misfit dislocations. Even below the fabrication temperature (670 - 710 K), massive formation of misfit dislocations can be caused by an applied stress in structures such as GaAs/$In_{0.15}Ga_{0.85}As$/GaAs (h = 6 and 15 nm) and GaAs/$In_{0..2}Ga_{0.8}As$/GaAs (h = 4 nm), which were originally coherent in the as-grown state.

4.4.1 Distribution of misfit stress in strained-layer structures

The relaxation of a strained-layer structure is strongly dependent on the local stress field, and it is thus important to understand the stress distribution of the epitaxial system [Pichaud_98].

The equilibrium stress state of a strained-layer system can be obtained by balancing the forces and moments. The complexity of the expression for the stress in the strained layer and the substrate depends on the approximation used. Assuming that ν is the same for the film and the substrate, the stress distribution for a structure as shown in Fig. 4.19, at which the origin of the x axis is taken at half the thickness of the substrate, is [Chu_85, Pichaud_98]

$$\sigma_s(x) = \pm\frac{G_f\varepsilon}{1-\nu}\left(\frac{h}{t}+6\frac{h}{t^2}x\right) \text{ for } x\in\left[-\frac{t}{2},\frac{t}{2}\right], \tag{4.3}$$

$$\sigma_f(x) = \mp\frac{G_f\varepsilon}{1-\nu}\left[1-6\frac{G_f}{G_s}\frac{h}{t^2}\left(x-\frac{h+t}{2}\right)\right] \text{ for } x\in\left[\frac{t}{2},\frac{t}{2}+h\right], \tag{4.4}$$

where t and h are the thickness of the substrate and film respectively, and s stands for substrate and f for film.

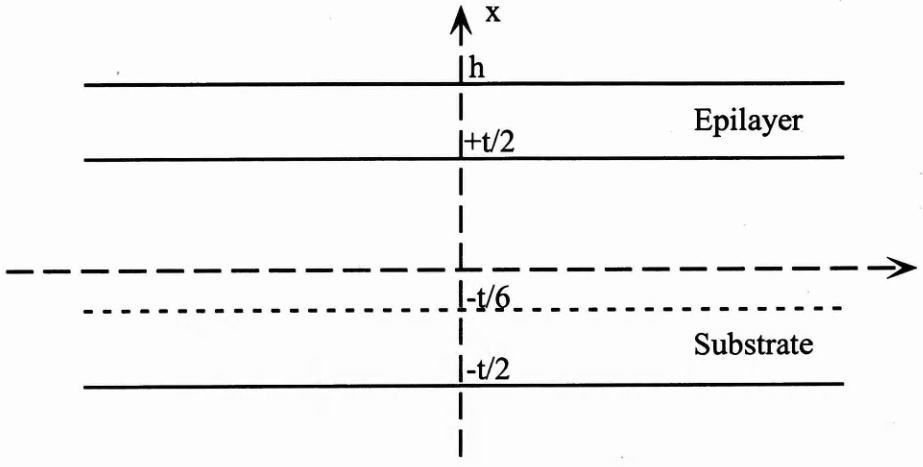

Fig. 4.19. Coordinate of neutral plane in a strained-layer structure.

As there is a strained layer, the surface of the substrate adjacent to strained layer is subjected to tension or compression depending on the nature of the strained layer, and the opposite surface (free surface) to compression or tension. Therefore there must be a region within the substrate cross-section at which the stress changes sign, i.e. where the stress is zero, and this is termed the neutral plane. The co-ordinate of the neutral plane in the structure shown in Fig. 4.19 is $-t/6$ [Pichaud_98].

Consider a strained-layer structure with a substrate of t = 0.4 mm and a strained layer of h = 15 nm. Calculation gives a stress of 0.07 MPa for the surface of substrate at t = +0.2 mm and 0.035 MPa at t = -0.2 mm. The stress within the strained layer is almost uniform, 470 MPa. The stress distribution corresponding to such a structure is shown in Fig. 4.20.

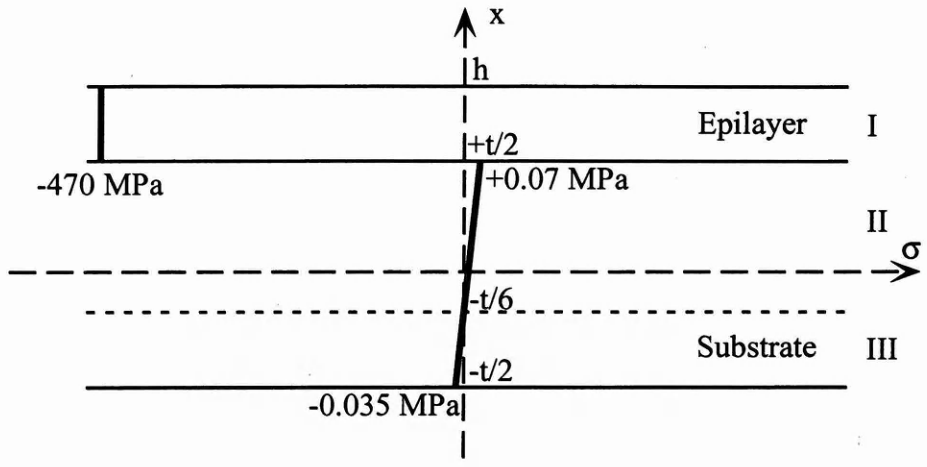

Fig. 4.20. Stress distribution in a strained-layer structure with the thickness of substrate t = 0.4 mm and strained layer h = 15 nm.

There are three regions which differ from each other in the level and sign of stresses. Region I is the strained layer, where the stress is compressive for the structures investigated, and the stress level is the highest. Region II and region III belong to the substrate and are separated by the neutral plane where the stresses change sign from tensile in region II to the compressive in region III. The level of stress in the substrate is much lower than that in the strained layer.

This distribution suggests that the misfit stress in a strained-layer structure is mainly concentrated within the strained layer and the substrate can be considered to remain unaffected as long as there is sufficient thickness, as generally recognised [Pichaud_98].

There is a GaAs capping layer in the strained-layer structures investigated. Because the capping layer is thick enough (ten times thicker than strained layer) and the interface between capping layer and the strained layer is intrinsically the same as that between the substrate (GaAs) and the strained layer, the joining of such a capping layer with the strained layer produces a stress distribution similar to that described above. Therefore, the discussion of distribution of stress is applicable to the both interfaces in the structures.

The equilibrium stress state within a strained-layer structure is determined by the stress distribution. The activity of misfit dislocations is thus under the control of the stress distribution. An applied stress of 7.25 MPa is not very high compared with the stress within the strained layer, 470 MPa, but it can be sufficient enough to make some changes in the distribution of the local stress field near the interface because the maximum stress at the side of substrate is only 0.07 MPa. It remains unclear how an applied stress changes the stress distribution. However, it is clear that the changes brought by such an applied stress produce impacts on the stability of interfaces.

4.4.2 Mechanical stability of interface

In a structure subjected to homogeneous deformation, crystal lattices become unstable [Born_88]. Under an applied stress, formation and multiplication of misfit dislocations occurs in a strained-layer structure as a consequence of both deformation and relaxation.

The atoms at the interface of a strained-layer structure are subjected to the two competing periodicities of the two crystals [Merwe_91B]. A strained-layer structure is thus subjected to an unusual loading condition, that of constant biaxial deformation [Dodson_87]. For a compressive strained-layer structure the lattices of the strained layer are constrained by the lattices of substrate as illustrated in Fig. 4.21. Normally, the stress due to lattice mismatch applied to the lattices of substrate, $\sigma_{\varepsilon\text{-}s}$, is quite small as analysed above. In other words, the restraint of the lattices of strained-layer upon the lattices of substrate is very weak.

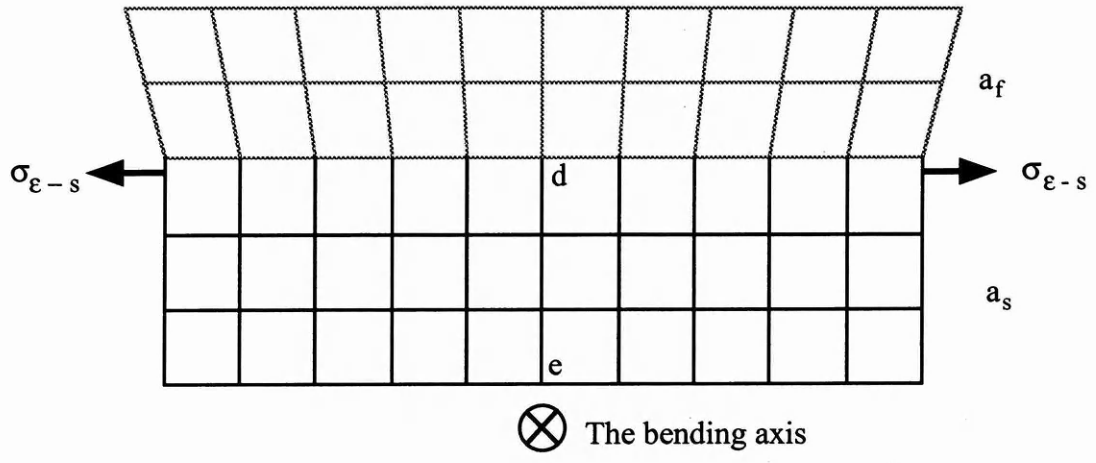

Fig. 4.21. A sketch illustrating the lattices in a compressive strained-layer structure. a_f is the lattice parameter of strained layer and a_s the substrate, and $a_f > a_s$. $\sigma_{\varepsilon-s}$ is the stress due to misfit applied on the lattices of substrate.

An applied stress has different effects on the both sides of an interface. Firstly, it has different impacts when it causes the expansion of the interface. This expansion helps the lattices of the strained layer to expand to recover their normal state on the one hand, but also causes additional strains on the lattices of the substrate on the other hand. Secondly, comparing the ratios of the applied stress to the misfit stresses within the strained layer and the substrate, it can be found that the latter (7.25 / 0.07) is higher than the former (7.25 / 470) by four orders of magnitude for this system.

The plastic behaviour of crystalline materials is temperature dependent [Ralls_76, Felbeck_84]. It was found that [Nadgornyi_88] dislocation velocity in GaAs at 670 - 770 K is higher than that at 470 K by about 10^5 times under an applied stress of 10 MPa. This indicates that dislocation activities in GaAs are highly temperature activated. For GaAs/$In_xGa_{1-x}As$/GaAs, an applied stress of several MPa helps the recovery of lattices of $In_xGa_{1-x}As$ from being strained, but with very limited efficiency because the misfit stress constraining the lattices is much higher. However, for the substrate GaAs, such an applied stress at the temperatures above 670 K can be great enough to cause deformation of the crystal. This deformation produces dislocations [Kuesters_86] and stimulates dislocation activities which take microdefects existing even in dislocation-

free materials as dislocation sources [Dodson_87]. In this case, the mechanisms of deformation through generation and motion of dislocations will operate [Born_88, HullD-92].

When the mechanisms of deformation through generation and motion of dislocations operate, the force exerted by the misfit stress on dislocations [HullD-92, Matthews_76, Sutton_95] plays an important role in both generation and motion of dislocations. Consider the lattice shown in Fig. 4.21. It is undergoing a [110] bending moment and the bending axis is on the side of substrate along the direction perpendicular to the plane of paper, as marked on the figure — this being a direct analogy to three point bending of a simple beam (see Fig. 2.13). During bending of this kind, the applied stress acting on the lattice is in the same directions as $\sigma_{\varepsilon\text{-}s}$ and forces the lattice to expand in these directions. If deformation of the lattice occurs, the resulting dislocations should have the extra atom planes with their normal parallel to the expansion direction, that is, parallel to the direction of applied stress. Their locations should be the same as the *d-e* plane in Fig. 4.21. If such planes include the directions of slip, dislocations will propagate along these directions on these planes. However, a strained-layer system has its own dislocation motion requirements for relaxation of its structure. For a strained-layer system with fcc or diamond structure, misfit stress together with the orientation of (001) interfaces makes the <110> directions on (001) the most energetically favourable slip system [Matthews_79, Jain_94]. Misfit stress will act on dislocations and limit them to activate only in the slip system <110>/(001). Dislocations produced in this way adopt the form of misfit dislocations. This makes the activity directions of dislocations generated during a bending test change from a region of plane in an unstrained structure to a region of line in a strained-layer system, that is, the intersections of <110> and (001). Therefore, driven by the applied stress together with the misfit stress, dislocations appear as straight lines in which the line directions are parallel to the bending [110] axis in GaAs/$In_xGa_{1-x}As$/GaAs subjected to a [110] bending, as seen in Fig. 4.9, 4.10, 4.11, and 4.13. They are two-dimensionally

distributed within special planes, interfaces, in the specimens. These dislocations thus result from both the relaxation of the strained-layer structure and the deformation of crystal.

For the [100] bending, because [100] is not the slip direction, the effective stress is the resolution of the applied stress on the slip directions, that is, [110] and [$1\bar{1}0$]. This makes the dislocations formed in GaAs/$In_xGa_{1-x}As$/GaAs during [100] bending become a network of orthogonal dislocation lines located along both [110] and [$1\bar{1}0$], as seen in Fig. 4.14 and 4.16.

4.5 Misfit dislocation generation and multiplication

The successive CL images of dislocations formed in the bending test specimens of GaAs/$In_{0.15}Ga_{0.85}As$/GaAs (h = 15 nm), as shown in Fig. 4.9 and 4.10, suggest that these dislocations generated and propagated individually and separately. The dislocations which appeared after a bending test, such as those marked in Fig. 4.9 (a), did not elongate further in the bending test afterwards, as can be seen in Fig. 4.9 (b). The numerous dislocations formed can be identified as separated lines parallel to each other. A rather high density has been achieved without their meeting each other, as shown in Fig. 4.9, 4.10, 4.11, and 4.13. No links can be found among these dislocations. This means that a high density of misfit dislocations, or the multiplication of misfit dislocations, does not result from, or is not even related to, any possible interaction among them. Also, the density and the distribution of dislocations formed in bending tests suggests that these dislocations are not generated from the pre-existing threading dislocations because of the lower density and random distribution of threading dislocations.

The examination of the configuration of dislocations around indentations reveals that pre-existing dislocation sources are unrelated to the generation of misfit dislocations. Fig. 4.22 shows the dislocations generated around an indentation in a

specimen of GaAs/$In_{0.15}Ga_{0.85}As$/GaAs (h = 15 nm) after thermal processing at 1220 K. Although misfit dislocations have been generated all over the specimen as shown in Fig. 4.1 and 4.3, the dislocations generated around the indentation are not misfit dislocations.

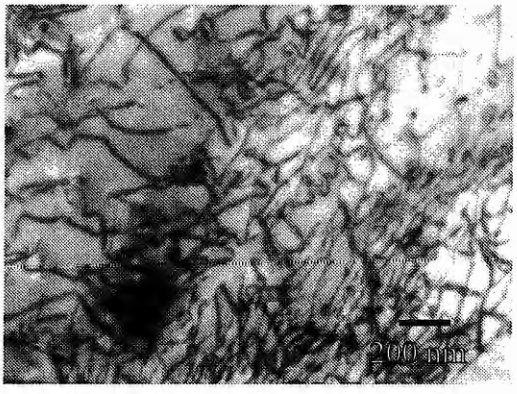

Fig. 4.22. Dislocations around an indentation in GaAs/$In_{0.15}Ga_{0.85}As$(h = 15 nm)/GaAs after thermal processing at 1220 K.

Under an applied stress of 7.25 MPa at 670 K, numerous misfit dislocations were generated in GaAs/$In_{0.15}Ga_{0.85}As$/GaAs (h = 15 nm) as shown in Fig. 4.10(b). However, Fig. 4.23 shows that the main part of the dislocations generated from the indentation are not misfit dislocations, although some misfit dislocations, as one labelled on Fig. 4.23, exist beside them.

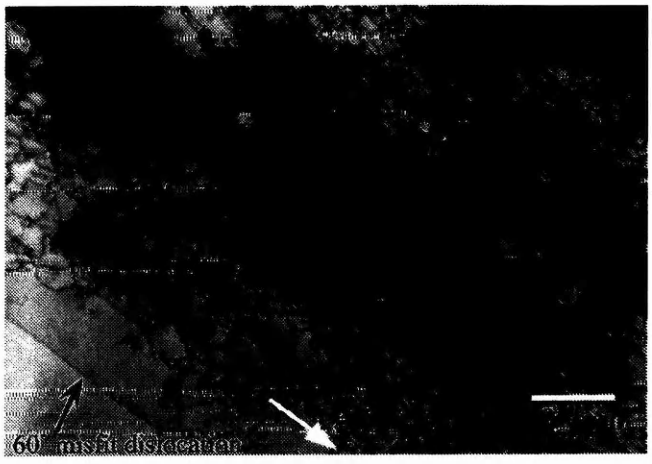

Fig. 4.23. Dislocations and misfit dislocations in GaAs/$In_{0.15}Ga_{0.85}As$(h = 15 nm)/GaAs generated by an applied stress of 7.25 MPa at 670 K.

It can therefore be inferred that the misfit dislocations generated during thermal processing and bending tests were produced by the mechanism of homogeneous nucleation [HullD-92]. Their generation did not rely on the pre-existing dislocation sources. Multiplication of misfit dislocations resulted from the self propagation of individual dislocations and was not produced by dislocation interactions as proposed by Hagen and Strunk [Hagen_78, Strunk_79].

4.6 Conclusions

For the structures which have not been relaxed by the massive formation of 60° dislocations, no matter whether they are thermodynamically stable or metastable as classified by the theoretical models, all tend to relax. They relax by the introduction of misfit dislocations provided that the requirements of thermodynamics and kinetics are satisfied, as happens in the thermal processing and bending tests.

Higher temperature reduces the strained-layer thickness required for the formation of misfit dislocations. The thermodynamic equilibrium set up during the fabrication of a strained-layer structure will be lost when the structure is subjected to a post-growth treatment at high temperatures. But the interface in a strained-layer structure is thermal

stable and will not be lost by interdiffusion thereby maintaining the driving force due to lattice mismatch for the formation of misfit dislocations. Relaxation can occur in strained-layer structures with the same composition, i.e. with the same misfit stress, but different strained-layer thicknesses depending on temperature. Thus, the critical condition of strained-layer thickness for relaxation through the formation of misfit dislocations is changed with temperature, and it can be said that the critical thickness itself is a function of temperature.

An applied stress can effectively bring about relaxation in a strained-layer structure. Under an applied stress, misfit dislocations can be produced as the result of both the relaxation of the strained-layer structure and the deformation of the crystal. Because of the addition of the mechanism of mechanical deformation, the strained-layer thicknesses at which relaxation occurs becomes smaller even below the fabrication temperature of the structures.

The generation of misfit dislocations is dominated by homogeneous nucleation, and this makes pre-existing sources of dislocations, such as threading dislocations, a relatively unimportant factor. Extensive formation of misfit dislocations results from the propagation or elongation of individual dislocations. Dislocation interaction does not play an important role in this process.

Chapter 5 : Further relaxation of pre-relaxed structures by thermal processing

The accommodation of misfit between an epitaxial film and its substrate by misfit dislocations has been intensively investigated [Matthews_74, Hull_96 and references cited therein]. In all heteroepitaxial semiconductor systems investigated (diamond or zinc-blende crystal systems), the dominant type of misfit dislocations observed is the so-called 60°, or mixed dislocations [Fitzgerald_91]. Orthogonal arrays of 60° misfit dislocations formed at an interface have been taken as the general configuration of misfit dislocations in these systems, and the investigation of nucleation, propagation and multiplication of misfit dislocations has been based on this kind of dislocation [Matthews_76, Hagen_78, Freund_90].

The stability of intentionally strained semiconductor layers is a matter for concern. The resultant stresses in these structures are of sufficient magnitude for the introduction of dislocations to occur on a problematic scale. In contrast, where strained layers are to be used as buffer layers, complete relaxation is desired [Fitzgerald_91]. In any case it is important to predict with reliability the level of dislocation introduction and consequent strain relaxation in strained-layer devices. This requires understanding not only of nucleation, propagation and multiplication but also of the transformation of pre-existing 60° dislocations under the effects of misfit stresses.

This chapter considers the latter process by investigating the changes of pre-existing 60° misfit dislocations in GaAs/$In_xGa_{1-x}As$/GaAs during thermal processing. This process has been considered by R. Beanland and co-workers [Beanland_97]. They observed the rotation of 60° dislocations into 90° dislocations producing greater misfit relief by the conversion of screw components into edge components.

5.1 Formation of edge-type misfit dislocations in 60° dislocation-relaxed structures

To investigate the behaviour of pre-existing 60° dislocations in as-grown strained-layer structures which have been relaxed by these dislocations, the specimens of such structures were thermally processed at elevated temperatures. Fig. 5.1 is the CL images showing the changes of dislocation configurations caused by thermal processing in a GaAs/$In_{0.15}Ga_{0.85}As$(25 nm)/GaAs specimen. (a) is the original configuration of the 60° misfit dislocation network. There was no change to this configuration when treated at temperatures below 1020K, as shown by (b). When treated at 1040K, many new straight dislocation lines appeared which can be seen in (c). These newly-formed dislocations are all at an angle to the original dislocations. No additional dislocations were formed parallel or perpendicular to the original dislocations, i.e., no new 60° dislocations were found to be formed during thermal processing.

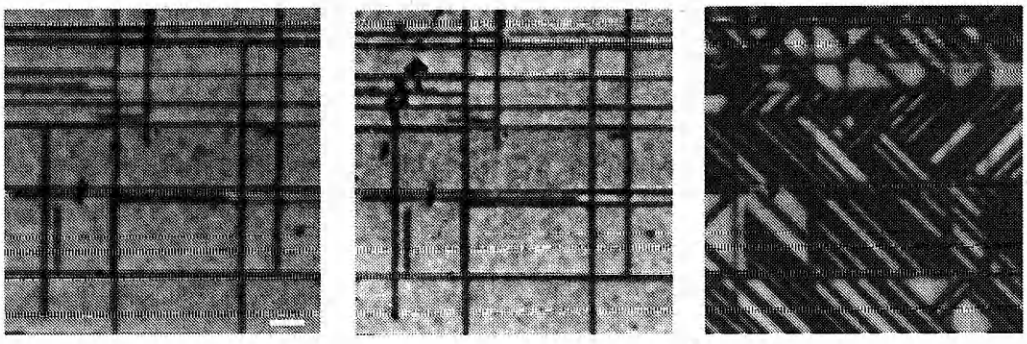

(a) (b) (c)

Fig. 5.1. CL images of changes of misfit dislocations in a specimen of GaAs/$In_{0.15}Ga_{0.85}As$(25 nm)/GaAs: (a) the original configuration, (b) after thermal processing at 1020 K for 300 s, and (c) the dislocation configuration after thermal processing at 1040 K for 300 s. Bar = 10 μm.

A TEM plan-view of the original dislocations in GaAs/$In_{0.15}Ga_{0.85}As$(25 nm)/GaAs is shown in Fig. 5.2. As has been discussed in the previous chapters, these misfit dislocation lines are formed at the interfaces between the $In_{0.15}Ga_{0.85}As$ layer and

GaAs layers along the intersections of {111} slip planes and (001) interfaces, that is, in <110> directions along (001) planes. The Burgers vectors of these dislocations are of type $\frac{a}{2}\langle 101\rangle$ inclined at 45° to (001) and 60° to their line directions. So they are the mixed type, or 60°, misfit dislocations [Matthews_74].

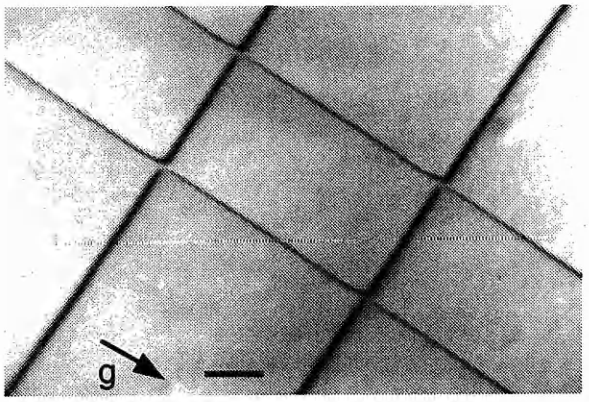

Fig. 5.2. TEM image of misfit dislocations in an as-grown specimen of GaAs/$In_{0.15}Ga_{0.85}As$(25 nm)/GaAs. **g** = [220], bar = 200 nm

Fig. 5.3 shows TEM images of dislocations in GaAs/$In_{0.15}Ga_{0.85}As$(25 nm)/GaAs after thermal processing at 1040 K for 300 seconds. The Bragg reflection responsible for image contrast in Fig 5.3(a) was [220]. The dislocations whose line directions are <110>, such as the dislocation lines *M1* and *M2*, are the 60° dislocation lines pre-existing in the as-grown specimen. The other dislocation lines, such as *P1* and *P3*, are newly-formed dislocations and it is not difficult to find that they are all at 45° to the original dislocations, i.e., they are in the line directions of <100>. All dislocations whose line directions are in [100], such as *P1 and P2*, are invisible in Fig. 5.3(b) when they are viewed using **g** = [400]. From the criterion of $\mathbf{g} \cdot \mathbf{b} = 0$, the invisibility of these dislocations shows that their Burgers vectors must lie in (100) planes and they are therefore edge type dislocations. Similarly, the dislocation line *P3* and all others whose line directions in [010] are also edge type because they are invisible in Fig. 5.3(c) when they are viewed using **g** = [040] showing their Burgers vectors to lie in (010).

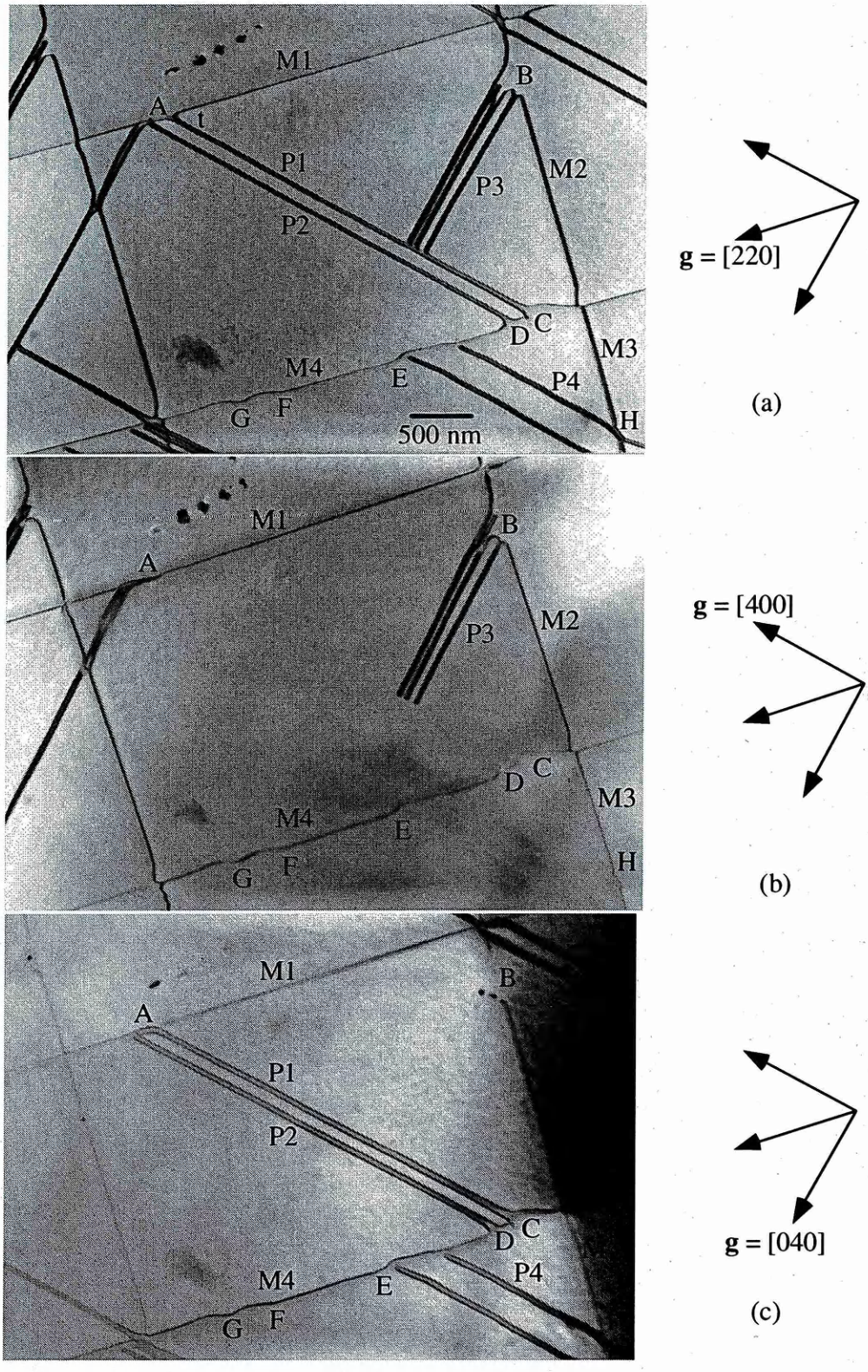

Fig. 5.3. TEM bright filed plan-view images of misfit dislocations under different Bragg reflections in GaAs/$In_{0.15}Ga_{0.85}As$(h = 25 nm)/GaAs after thermal processing at 1040 K for 300 s.

The visibility criterion for a dislocation with Burgers vector **b** and diffraction vector **g** is $\mathbf{g} \cdot \mathbf{b} \neq 0$. This implies that misfit dislocations of 60° type are always visible for **g** = [220] and $[2\bar{2}0]$. For a [220] reflection, the set of misfit dislocations parallel to $[\bar{1}10]$ direction will be in contrast for both pure edge and 60° dislocations, as can be seen in Fig. 5.3(a). For the pure edge-type misfit dislocations with **b** = (a/2) [110] and (a/2) $[1\bar{1}0]$, the invisibility criterion requires the satisfaction of both $\mathbf{g} \cdot \mathbf{b} = 0$ and $\mathbf{g} \cdot (\mathbf{b} \times \mathbf{u}) = 0$, where **u** is the sense of the dislocation [Miller_80]. Fig. 5.3(b) and (c) show that all of the newly-formed dislocations satisfy these requirements.

It can be seen that all of the newly-formed dislocations are in pairs protruding from the original 60° dislocations. They are the prolongation of the original dislocation lines in a different direction, and there is no break on the lines. In Fig. 5.3(a), two pairs of dislocation lines, *P1* and *P2*, come from *C* and *D* respectively on the dislocation line *M4*. They were not coming from, but were hindered by the line *M1* because, as revealed very clearly by Fig. 5.3(b), the line *M4* seems to be broken at *C* and *D*, which means that the dislocation line turned around there while the line *M1* remains continuous at *A*. It can be seen from Fig. 5.3(c) that the pair *P1* has been bent at *A*. The tip *t* in Fig. 5.3(a) must result from dislocation interactions which happened when the pair *P1* met the line *M1*. Three pairs come from the line *M2* and were stopped by the newly-formed dislocation pair *P1*, as can be seen in Fig. 5.3(a) and Fig. 5.3(b). So it is clear that all of the newly-formed dislocations were coming from the pre-existing 60° dislocations. Some of them ended at the pre-existing 60° dislocations, while others ended at other newly-formed dislocations. This indicates that these newly-formed dislocations are located at the interfaces, they are therefore interfacial or misfit dislocations [Matthews_79]. Also, both lines of every pair can be verified to be located at the same interface because they jogged from, and ended at the same dislocation lines. This means that their movement did not cross the strained layer but was only along the interface.

Another feature of the newly-formed dislocations is that all dislocation pairs which originated from the same 60° dislocation line have the same line direction. *M2*

and *M3* can be regarded as one dislocation line, and two groups of edge dislocations, *P3* and *P4* are related to it. *P3* and *P4* have different line directions. It can be seen that *P3* (*P3* can be taken as a group of edge dislocations) is a continuous extension of the line *M2*. When viewed using a different **g** vector which makes *P3* invisible as shown in Fig. 5.3(c), there is a break on the dislocation line *M2* where *P3* originated as marked by *B*. This is an indication that the line *M2* turns towards another direction at *B* forming a dislocation segment of different character from the line *M2* itself. That segment is *P3* . Therefore, *P3* is coming from, not terminating at, line M2. For *P4*, if it was also coming from *M3*(*M2*), there should also be a break at *H* on the line *M3* in Fig. 5.3(b) when it is itself invisible under a different **g** , as *B* on the line *M2* in Fig. 5.3(c). There is no break at the point *H* on the line *M3* but a distortion, as can be seen in Fig. 5.3(b). This distortion of the line *M3* at *H* resulted from dislocation interactions when the pair *P4* passed across the line *M3*, which also proves that the pair *P4* did not come from the line *M3*. Thus, by comparing Fig. 5.3(a) with Fig. 5.3(b) and Fig. 5.3(c), it can be identified that *P3* came from *M2* while *P4* came from another 60° dislocation line not *M3*(*M2*), and all of the newly-formed edge dislocation pairs which came from the same pre-existing 60° dislocation line are in the same line direction.

The changes in dislocation configurations caused by thermal processing at 1040 K for 300 seconds in GaAs/$In_{0.2}Ga_{0.8}As$(20 nm)/GaAs are shown in Fig. 5.4. Similarly, the two-beam **g** assigns the line directions of the newly-formed dislocation pairs to [100] or [010], and that of the original 60° dislocations to [110] or [$\bar{1}10$].

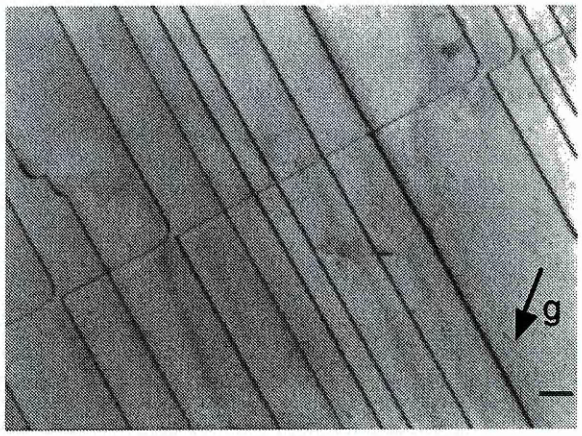

(a)

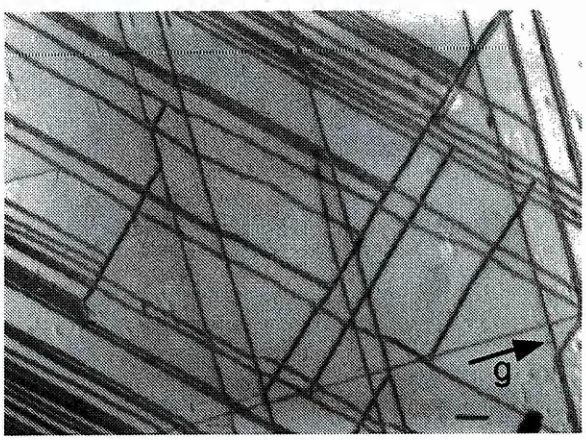

(b)

Fig. 5.4. TEM bright field plan-view images of misfit dislocations in $GaAs/In_{0.2}Ga_{0.8}As$(20 nm)/GaAs before and after thermal processing. (a) The 60° misfit dislocations in as-grown specimen. **g** = [040]. (b) The dislocations in the specimen after thermal processing at 1040 K for 300 s. **g** = [220]. Bar = 500 nm

The changes of dislocation densities due to the introduction of new dislocations are measured to be from 2×10^9 to 7.7×10^9 / cm^2 in Fig. 5.3(a) and from 2.5×10^9 to 2×10^{10} / cm^2 in Fig. 5.4(b) respectively.

5.2 Difference in energy status between 60° and edge misfit dislocations

The energy per unit area arising from a strain ε in a strained layer, E_ε, is

$$E_\varepsilon = 2G\left(\frac{1+\nu}{1-\nu}\right)\varepsilon^2 h, \tag{5.1}$$

where G is the shear modulus, ν is Poisson's ratio, and h is the thickness of strained layer. The self-energy associated with the formation of a square array of dislocations per unit area in a strained layer with a thickness of h is, according to Freund [Freund_90] and Beanland [Beanland_97],

$$E_d = \frac{\rho G b_e^2}{4\pi(1-\nu)}\left[\ln\left(\frac{2\alpha h}{b}\right) - \frac{\cos 2\theta}{2}\right] + \frac{\rho G b_s^2}{4\pi}\ln\left(\frac{2\alpha h}{b}\right), \tag{5.2}$$

where α is the core parameter, b_e is the edge component and b_s is the screw component of the Burgers vector, θ is the angle between the Burgers vector and the normal to the surface, and ρ is the linear misfit dislocation density.

When misfit dislocations are introduced, the total energy of the strained-layer structure is lowered because some of the misfit is accommodated by misfit dislocations. The change of total energy ΔE therefore is,

$$\Delta E = E_\varepsilon - E_d. \tag{5.3}$$

ΔE differs with the different types of misfit dislocations. ΔE caused by 60° dislocations, that is, a/2<101> dislocations with <110> line directions, is

$$\Delta E_m = 2G\left(\frac{1+\nu}{1-\nu}\right)\varepsilon^2 h - \frac{\rho G b^2(2-\nu)}{8\pi(1-\nu)}\ln\left(\frac{2\alpha h}{b}\right). \tag{5.4}$$

And ΔE caused by edge dislocations, a/2<101> dislocations with <010> line directions, is

$$\Delta E_e = 2G\left(\frac{1+\nu}{1-\nu}\right)\varepsilon^2 h - \frac{\rho G b^2}{4\pi(1-\nu)}\ln\left(\frac{2\alpha h}{b}\right). \tag{5.5}$$

The change rate of ΔE with respect to the dislocation linear density ρ for different types of dislocations, $d(\Delta E)/d\rho$, can be obtained by differentiating equation (5.4) and (5.5),

$$\frac{d(\Delta E_m)}{d\rho} = -\frac{Gb^2(2-\nu)}{8\pi(1-\nu)}\ln\left(\frac{2\alpha h}{b}\right), \tag{5.6}$$

and

$$\frac{d(\Delta E_e)}{d\rho} = -\frac{Gb^2}{4\pi(1-\nu)}\ln\left(\frac{2\alpha h}{b}\right). \tag{5.7}$$

It can be seen that, for specific materials, these change rates are only a function of the strained-layer thickness. They are plotted in Fig. 5.5 for GaAs/$In_xGa_{1-x}As$/GaAs heterostructures, (taking $G = 3.3 \times 10^{10}$ Nm^{-2}, $\nu = 0.3$, $b = 0.4$ nm, and $\alpha = 1$), showing the difference between 60° and edge dislocations in reducing the total energy per unit area if they are introduced at an interface. For the same linear density of dislocations, when edge-type dislocations are introduced, the total energy is lowered more, by a factor of (2- ν)/2, than when 60° dislocations are introduced. A strained-layer structure relaxed by 60° dislocations is not as stable as that relaxed by edge dislocations. And the 60° dislocations are not as stable as the edge ones because of their higher energy status in a strained-layer structure. The relaxation of the strained-layer structure due to the formation of the edge-type misfit dislocations is thus a progression towards the energy minimum. Both the formation of new edge dislocations and the transformation of the pre-existing 60° dislocations can therefore be expected in an as-grown strained-layer structure which has been relaxed by 60° misfit dislocations.

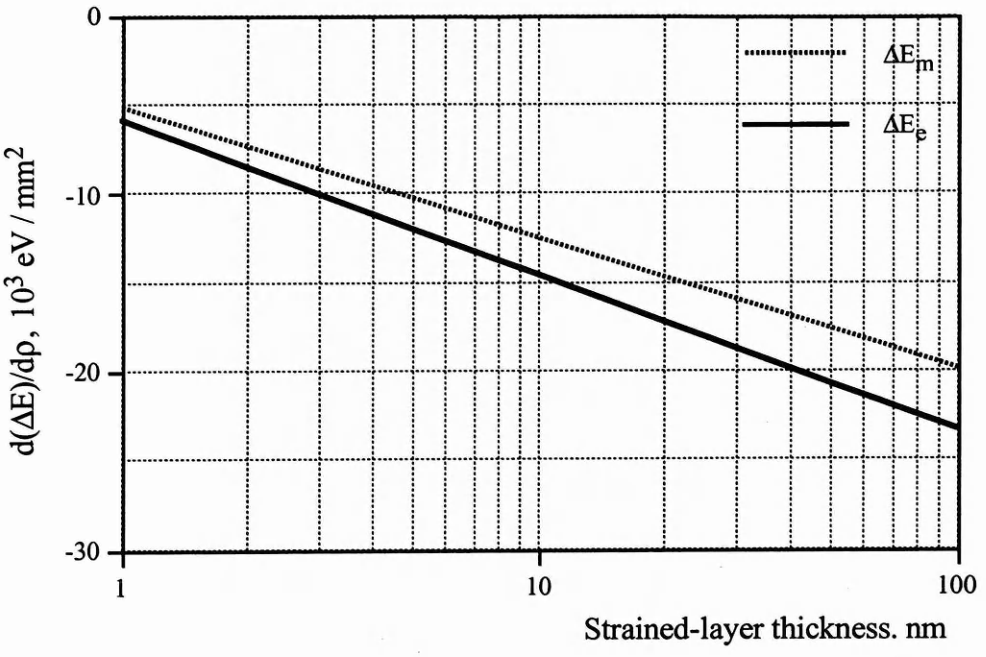

Fig. 5.5. The decrease of total energy in $In_xGa_{1-x}As/GaAs$ heterostructures caused by the introduction of 60° (ΔE_m) and edge dislocations (ΔE_e).

5.3 Effects of the force due to misfit strain on 60° misfit dislocations

The misfit accommodated by misfit dislocations with the geometry shown in Fig. 5.2 is

$$\delta = b / 2d, \tag{5.8}$$

where d is the average distance between dislocation lines in the same interface. Measurements of d ($\approx$ 1000 nm) in $GaAs/In_{0.15}Ga_{0.85}As/GaAs$ shows that $\delta \approx 10^{-4}$. This is just less than one percent of the misfit, 0.01075, between $In_{0.15}Ga_{0.85}As$ and GaAs. So the majority of misfit still remains in the structure. And the principle that the stresses due to misfit strain gives rise to the driving force for introduction, or transformation, of misfit dislocations is still in effect, even though the 60° misfit dislocation network has formed [Drigo_89]. Also the Burgers vectors of the 60° misfit dislocations contain a screw component which does not relieve the misfit strain and only their edge

component contributes to the strain relaxation. The relaxation of the misfit strain by the introduction of these misfit dislocations is therefore an imperfect process.

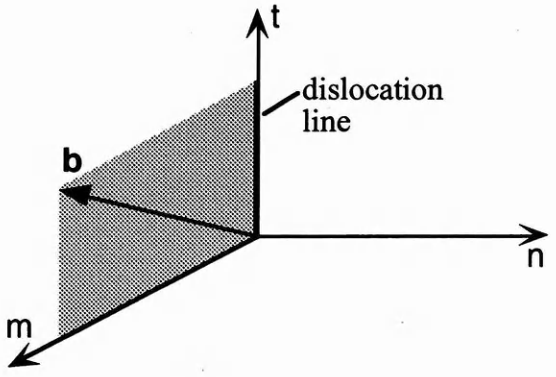

(a)

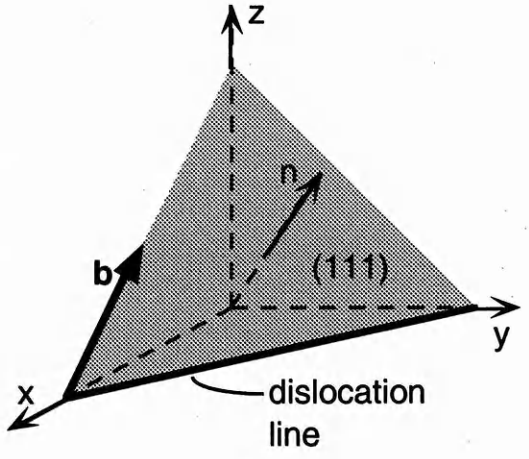

(b)

Fig. 5.6. A 60° dislocation line and its Burgers vector

Consider the coordinates in Fig. 5.6(a). Suppose a 60° dislocation line runs parallel to the *t* axis and its slip plane is perpendicular to the *n* axis. The Burgers vector **b** of the dislocation can be written as

$$\mathbf{b} = b_m\mathbf{i} + b_t\mathbf{k}, \tag{5.9}$$

where b_m and b_t are the edge and screw components of Burgers vector and **i** and **k** are unit vectors in the *m* and *t* directions. Let the misfit stresses placed on the surfaces of the crystal containing the dislocation include six stresses τ_{mm}, τ_{nm}, τ_{tm}, τ_{nn}, τ_{mn},

and τ_{tn}. Assuming that these stresses are constant throughout the crystal. Of the six stresses τ_{nt} and τ_{mt} exert a force on the screw component of the dislocation, τ_{mm} and τ_{mn} exert a force on the edge component. The stresses τ_{nt} and τ_{mn} cause the dislocation to move on the slip plane; the stresses τ_{mt} and τ_{mm} cause it to move perpendicular to the slip plane. The stresses τ_{tt} and τ_{nn} do no work and produce no force on the dislocation. The total force $\boldsymbol{F}$ exerted on a unit length of the dislocation line is

$$\mathbf{F} = -(\tau_{mn}b_m + \tau_{nt}b_t)\mathbf{i} + (\tau_{mm}b_m + \tau_{mt}b_t)\mathbf{j}, \tag{5.10}$$

where $\mathbf{j}$ is the unit vector in the n direction [Hull.D_92, Weertman_92]. It can be seen that one of the components of this force is parallel to the slip plane and the other is normal to it.

Now consider the component of the force normal to the slip plane, that is, the force parallel to n axis, F_n. As n is the normal of slip plane, the direction of n axis can be determined by $\mathbf{n} = \mathbf{t} \times \mathbf{b}$ because $\mathbf{b}$ lies in slip plane. For 60° (a/2<101>/<110>) dislocation lines in a fcc or diamond structure, n is at <111> as shown in Fig. 5.6(b). Because of the nature of misfit stresses which arise from the mismatch between a film and its substrate when they are joined together by the interface, any movement (glide or climb) of the dislocations resulting from misfit stress (resulting in relaxation) must take place at interfaces. On (001) interfaces, where misfit stresses arise from and will be annihilated, F_n causes a force acting on 60° dislocations perpendicular to their line directions, that is, along the <110> directions. This force will cause these dislocations to move away from their slip planes along interfaces when climb processes are active.

5.4 Vacancies as strain relievers and vacancy-producing jogs

When a misfit between a thin film and its substrate exists, vacancies can be created at the interface and the periodic structure at the interface will be made

particularly striking by decorating it with vacancies [Matthews_79]. Fig. 5.7 shows the coherent interfacial structure (a) and the interfacial structure decorated by the creation of vacancies (b) in a compressive strained-layer structure. The number of the vacancies will be appropriate to the periodicity of the interface structure. Under the effects of misfit stresses these vacancies will move along the interface to the most highly distorted sites, of which the most important are certainly dislocations. Their motion is such that they continue to reflect the periodicity of the interfacial structure.

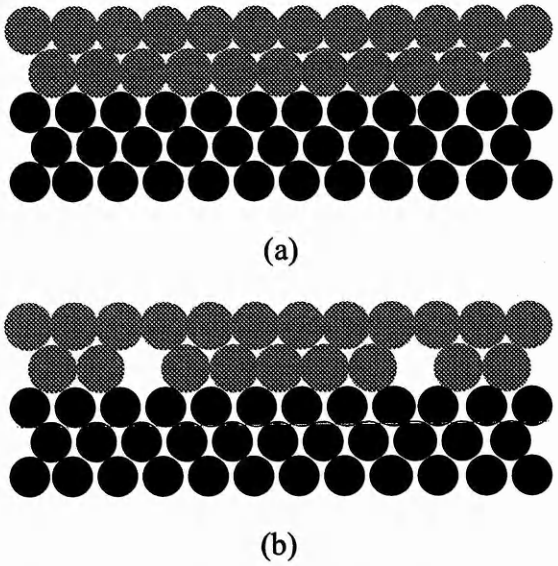

(a)

(b)

Fig. 5.7. The interface structures in a compressive strained-layer system. (a) The interface is coherent. (b) The interfacial structure has been made more striking by decorating with vacancies.

Hopgood [Hopgood_94] pointed out that vacancies in a compressive strained $In_xGa_{1-x}As$ layer can relieve the strain energy. The strain energy per unit volume relieved by a vacancy concentration C_v can be expressed as

$$\Delta E_v = -4G\left(\frac{1+\nu}{1-\nu}\right)\left(\frac{xC_v\Delta d_v\Delta d_{In}}{d_{GaAs}^2}\right), \tag{5.11}$$

where d_{GaAs} is the lattice constant of GaAs, Δd_{In} is the difference between the lattice constants of InAs and GaAs, that is, $\Delta d_{In} = d_{InAs} - d_{GaAs}$, and Δd_v is the difference between the lattice constant of GaAs and the dimension of the vacancy,

$\Delta d_v = d_v - d_{GaAs}$ and it is negative. This is the difference in strain energy per unit volume between $In_xGa_{1-x}As$ on GaAs and $In_xGa_{1-x}As+v$ ($In_xGa_{1-x}As$ which contains vacancies) on GaAs. The negative of ΔE_v indicates that creation of vacancies will decrease the strain energy.

At high temperatures as used in thermal processing, thermal activation assists in the formation and movement of vacancies. The movement of vacancies or small clusters of vacancies will have an impact on the pre-existing dislocations and, because high temperatures make climb active, enable them to move away from their slip planes along the interfaces. The distortion of the dislocation line *M4* in Fig. 5.3(a) can be taken as evidence of this. If nothing had happened to this dislocation line its original shape would be straight, like the line *M1* and other 60° dislocation lines in this figure and all dislocation lines in Fig. 5.2. But it can be seen that this line *M4* has been bowed out at the point *G* and the section *E* - *F*.

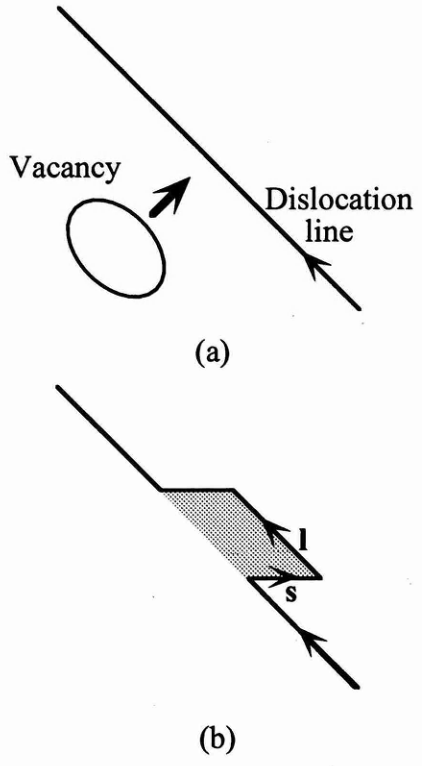

Fig. 5.8. Jog formation. (a) Movement of vacancy or cluster of vacancies produce impact on dislocation line. (b) A jog is formed on dislocation line by motion of vacancies.

The consequence of vacancy movement affecting a dislocation line is illustrated in Fig. 5.8. The vacancy movement causes a short section of dislocation line to move away resulting in a jog emerging from the original dislocation line. If a small segment $\boldsymbol{l}$ of the line undergoes a small displacement $\boldsymbol{s}$, the local change in volume is [HullD_92]

$$dV = \mathbf{b} \cdot \mathbf{l} \times \mathbf{s} = \mathbf{b} \times \mathbf{l} \cdot \mathbf{s}. \tag{5.12}$$

The two sides of the area element $\mathbf{l} \times \mathbf{s}$ are displaced by $\mathbf{b}$ relative to each other during the movement. The slip plane of the element is by definition perpendicular to $\mathbf{b} \times \mathbf{l}$. When either $\mathbf{s}$ is perpendicular to $\mathbf{b} \times \mathbf{l}$ or $\mathbf{b} \times \mathbf{l} = 0$, which means the element is pure screw, dV is zero. Otherwise, volume is not conserved ($dV \neq 0$) and the motion is climb. For a 60° dislocation $\mathbf{b} \times \mathbf{l} \neq 0$, and any movement away from its slip plane will give an $\mathbf{s}$ which cannot be perpendicular to $\mathbf{b} \times \mathbf{l}$. Therefore any movement of 60°

dislocations towards any other than their line directions at (001) will be nonconservative. This is the mechanism of jogs arising from 60° dislocations to hold vacancies in a strained-layer structure. The jog is thus referred to as a vacancy-producing jog. One of the most important processes of its formation is the absorption and emission of vacancies, that is, jogs are sources and sinks for vacancies [Nabarro_67, Kovacs_73]. The jogs will move away from the original 60° dislocation lines under the effects of misfit stresses. A moving jog trails a dislocation dipole and drags a string of vacancies behind [HullD_92, Weertman_92].

Because the jog is merely a segment of the dislocation line itself and has the same Burgers vector as the remainder of the dislocation line [Weertman_92], any dislocation jogging from the pre-existing 60° dislocations must have a Burgers vector of $\frac{a}{2}<101>$, that is, it must be a perfect dislocation. It can not be a screw dislocation at (001) with this Burgers vector. It cannot be a mixed one either, because mixed dislocations with such a Burgers vector can only be formed by glide, not climb. Therefore, it is determined by the nature of 60° dislocations and the driving force, as discussed above, that the dislocations which can be produced by jogging from pre-existing 60° dislocations are only the edge dislocations. For such edge dislocations with the Burgers vectors of $\frac{a}{2}<101>$, their line directions must be <010>. The motion of the jogs after arising from the pre-existing 60° dislocations thus must be along the directions normal to the planes in which their Burgers vectors lie. This is the reason that all of the newly-formed dislocations observed had moved in the same direction, at 45° to the original 60° dislocation lines from which they arise. Any motion deviating from this direction would not be able to go further because of higher Peierls barrier. This may explain why bowing out at the point *G* and the section *E* - *F* on dislocation line *M4* in Fig. 5.3(a) could not develop further to form dislocation dipoles towards other directions.

Henceforth as the jog moves through the lattice, the dislocation dipole trailed by it becomes longer until it is stopped by another dislocation. The dislocation dipole consists of two parallel dislocations of opposite sign that are separated from each other by a short distance due to the nature of vacancies and the forces on the dislocations.

5.5 Stages of relaxation with respect to different misfit dislocations

The experimental results shown above prove that, as pointed out by Goodhew [Goodhew_99, Goodhew_94], relaxation of strained-layer structures never can be complete and strained layers never relax fully to give a strain-free surface. Even for strained-layer structures which have been relaxed by 60° dislocation network, they are still not stable with respect to relaxation through the formation of misfit dislocations, and only have metastability which is temperature dependent. Such structures can still relax further.

The newly-formed edge dislocations are actually the extension of the pre-existing 60° dislocations under the effects of misfit stress and, from this point of view, their formation does not need nucleation. However, nucleation seems to be necessary for the formation of the new 60° dislocations in as-grown structures which have been relaxed by 60° dislocations. This is because all suitable sources for the generation of misfit dislocations have been taken by 60° dislocations during fabrication of the structures, and the experimental evidence shows that no new 60° misfit dislocations were produced by the extension of the pre-existing 60° misfit dislocations. Thus, nucleation becomes a kinetic barrier curbing the formation of new 60° misfit dislocations, while the formation of edge dislocations on the pre-existing 60° dislocations as the extension of these dislocations becomes energetically favourable for further development of relaxation but without the formation of new 60° dislocations.

The newly-formed misfit dislocations are all of edge type, not 60° type. This indicates that the relaxation of misfit strain by 60° dislocations has been thoroughly

completed as soon as the critical point for such a relaxation is reached. Otherwise, either the formation of the new 60° dislocations or the elongation of the pre-existing 60° dislocations, or both, could be expected. When a strained-layer structure has been relaxed by 60° dislocations, no more 60° dislocations can be introduced into the structure afterwards because the conditions for the formation of 60° dislocations have been depleted. At this stage, further relaxation, when it is still required by the structure as discussed above, can only be realised by the misfit dislocations whose mechanism of formation satisfies the current structure. That is misfit dislocations of the edge type working for the another stage of relaxation.

It was pointed out [Goodhew_97] that climb might be involved in some complex misfit dislocation geometries. From the results above, it is clear that the relaxation of strained-layer structures actually involves the mechanisms of both glide and climb, which distinguishes the different stages of relaxation. The first stage is realised by glide, resulting in the formation of 60° misfit dislocations. After that, the structures can be relaxed further by the mechanism of climb as the second stage, resulting in the formation of edge misfit dislocations.

5.6 Conclusions

The behaviour of 60° misfit dislocations in as-grown GaAs/$In_xGa_{1-x}As$/GaAs strained-layer structures during thermal processing shows that there are still misfit stresses remaining in an as-grown strained-layer structure which has been relaxed by the formation of 60° misfit dislocations. These stresses will act as a driving force for the transformation of the pre-existing 60° dislocations towards a lower energy configuration as observed in GaAs/$In_xGa_{1-x}As$ during thermal processing. The vacancy-producing jogs protrude from the pre-existing 60° dislocations. The jogs move away from the original dislocations trailing dislocation dipoles behind at interfaces. The resultant dislocations are of the edge type with the Burgers vectors of $\frac{a}{2}<101>$

perpendicular to their line directions of <010> and form new orthogonal arrays of dislocations at the interfaces with a higher dislocation density. Considering the changes of the dislocation densities together with the differences in lowering strain energy, the strained-layer structure is relaxed much further by the introduction of edge misfit dislocations in this way. It should be mentioned that these newly-formed edge dislocations are still not the most efficient accommodation for misfit which only occurs when their Burgers vectors lie in (001).

The fact that only edge dislocations, not new 60° dislocations, were introduced during thermal processing reflects the different mechanisms for the introduction of misfit dislocations according to the relaxation state. The 60° dislocations are first to be formed because they take the easiest way of formation by glide, and the process of their formation is completed as soon as the real critical conditions (both thermodynamic and kinetic) for such a process has been reached. The driving force due to misfit stresses for the nucleation, propagation and multiplication of 60° dislocations is dissipated and can not have any further effect afterwards on this process. Metastability between misfit stresses and misfit dislocations is now gained. It becomes energetically impossible for the relaxation through the formation of 60° misfit dislocations to take place in a 60° dislocation-relaxed structure. Higher temperature is unable to change this situation but does take effect in another way - by exciting the process of dislocation climb. Under the effects of the remaining misfit stresses the pre-existing 60° misfit dislocations undergo a transformation at high temperature, resulting in the emergence of edge dislocations by climb. More dislocations with higher efficiency in relaxing strain energy are introduced, and a lower strain energy status is therefore gained for the strained-layer structure. Thus, two mechanisms dominate the introduction of two different kinds of dislocations into a strained-layer structure for the different stages of relaxation.

Chapter 6 : Differences in dislocation behaviours between GaAs/$In_xGa_{1-x}As$/GaAs and GaAs

This chapter deals with differences in dislocation behaviour between different structures, i.e. between plain GaAs and strained-layer structures of $In_xGa_{1-x}As$/GaAs.

Firstly, the differences in dislocation motion are investigated. This involves the examination of dislocation motion stimulated by thermal and mechanical means and the comparison of distance of dislocation motion in different structures. The dislocations considered in this section are those which are common to both types of structure. They are not misfit dislocations, as these only relate to strained-layer structures. By examining the same kind of dislocations in different structures, the effects of a strained layer on dislocation motion are investigated.

Secondly, the different configurations of dislocations produced by an applied stress are compared between strained-layer structures and plain GaAs. How the inclusion of a strained layer affects dislocation motion is examined.

Finally, the dislocation behaviours under electron beam irradiation within the TEM are investigated. The differences in these behaviours will distinguish misfit dislocations from other dislocations.

6.1 Dislocation motion

The motion of a dislocation results from forces acting on the dislocation. The forces can be initiated by an external stress, by sources of internal stresses, and by the dislocation self stress [Nadgornyi_88]. The energy which has to be provided for a dislocation to overcome the barriers it encounter during its motion determines the dependence of this motion on temperature and applied stress [HullD_92].

Dislocation motion (velocity) has been well defined as the dependence of stresses and temperature, $v(\sigma,T)$ [Nadgornyi_88]. For a strained-layer structure, an additional stress, misfit stress, arises because of lattice mismatch between the strained-layer and the substrate. It is not surprising that dislocation motion is affected by such an additional stress.

Dislocation motion can be investigated by direct techniques which are common in procedure: producing isolated movable dislocations, moving them in a controlled manner, and tracking their motion. The assessment of dislocation motion for different specimens, as described in Chapter 2, is made by measuring the length of dislocations that have appeared around the indentation after thermal or mechanical testing with reference to the original configuration of indentation shown in Fig. 2.7. In this way, the difference in dislocation motion between strained and unstrained structures is investigated in terms of the distance of dislocation motion under the same experimental conditions.

6.1.1 CL imaging of dislocation motion

CL imaging enables the variation of distance of dislocation motion in different specimens of GaAs/$In_xGa_{1-x}As$/GaAs to be recorded. Thus, dislocation motion can be quantitatively assessed based on CL observations.

6.1.1.1 Dislocation motion activated by elevated temperatures

(a) (b) (c)

Fig. 6.1. Dislocation clusters propagated away from indentations forming dislocation crosses centred by indentation in GaAs/$In_{0.15}Ga_{0.85}As$ (h = 15 nm)/GaAs at elevated temperatures. T = (a) 473, (b) 673, and (c) 873 K. Bar = 10 μm.

When an indentation is made on the surface of a specimen, crystal defects are produced and strain energy due to crystal distortion is stored around the indentation. Dislocations created by indentation can be thermally activated to move at a higher temperature and propagate away from their original position. Fig. 6.1 is a series of CL images showing the response of dislocations in GaAs/$In_{0.15}Ga_{0.85}As$ (h = 15 nm)/GaAs to elevated temperatures. It can be seen from these images that these dislocations appear in lines of dislocation clusters around the indentation.

Fig. 6.2 is the CL images of dislocation clusters moving away from indentations in GaAs at different temperatures.

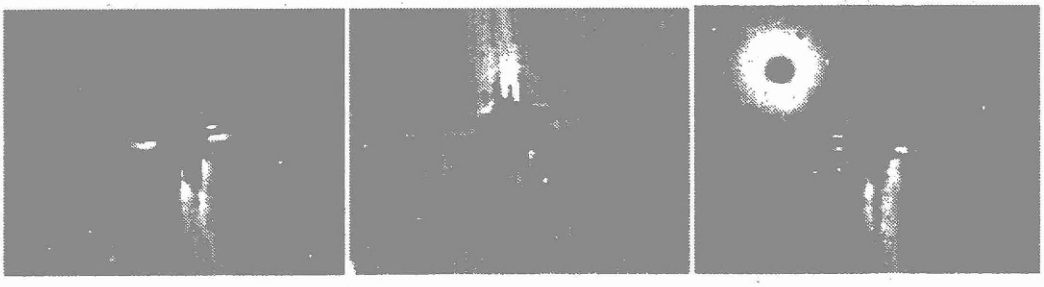

(a) (b) (c)

Fig. 6.2. Dislocation motion in GaAs under elevated temperatures. T = 473 (a), 673 (b), and 873 K (c). Bar = 10 μm.

These images show that the dislocations introduced by indentations are movable. They propagated away from indentations during thermal processing forming straight lines of dislocation clusters, and these lines appear as crosses centred on the indentation. The length of these dislocation lines is the distance of movement of dislocation clusters. The apparent difference in dislocation motion between GaAs/$In_xGa_{1-x}As$ /GaAs and GaAs manifested by CL images is the distance of motion, which will be discussed in 6.2. By measuring the length of dislocation clusters from the CL images, the dislocation motion in these specimens can be quantitatively assessed and a difference in dislocation motion between GaAs/$In_xGa_{1-x}As$ /GaAs and GaAs can thus be inferred.

6.1.1.2 Dislocation motion under an applied stress

During a bending test, the applied stress causes a force to act on dislocations and make them move. Fig. 6.3 and Fig. 6.4 show the CL images of dislocation clusters in GaAs/$In_{0.15}Ga_{0.85}As$ (h = 15 nm)/GaAs and GaAs after bending tests. These tests were carried out at different temperatures with the same load which produced a constant tensile stress, τ = 7.25 MPa, at the underside of the specimen, i.e., at the surface of strained-layer side as shown in Fig. 2.13. Except for the extent of dislocation motion, which will be discussed in 6.2, they have similar features to those seen in the CL images of dislocation motion under thermal processing.

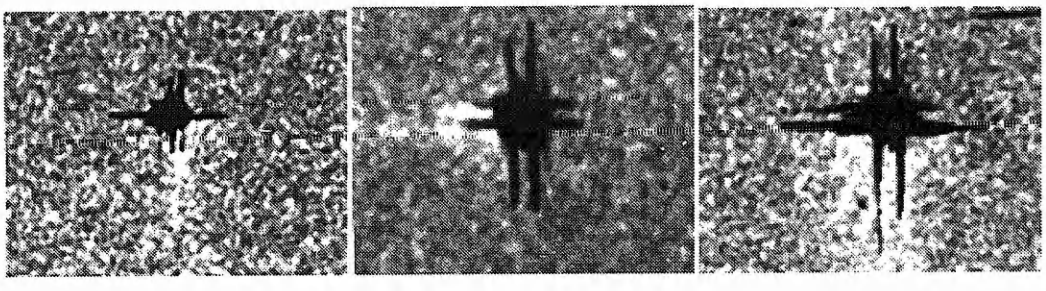

(a) (b) (c)

Fig. 6.3. Dislocation motion in GaAs/$In_{0.15}Ga_{0.85}As$ (h = 15 nm)/GaAs under a constant tensile stress of τ = 7.25 MPa at temperatures T = (a) 473, (b) 673, and (c) 743 K. Bar = 10 μm.

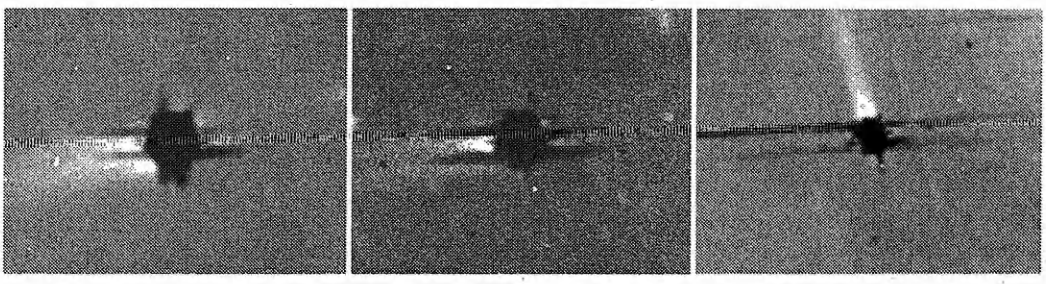

(a) (b) (c)

Fig. 6.4. Dislocation motion in GaAs under a constant tensile stress of τ = 7.25 MPa at temperatures T = (a) 473, (b) 673, and (c) 743 K. Bar = 10 μm.

6.1.2 Direction of dislocation motion

TEM imaging reveals the details of dislocation clusters whose formation was stimulated by thermal processing or bending tests. From TEM images, the directions of dislocation motion can be determined and their configurations can be examined.

Fig. 6.5 and Fig. 6.6 are the TEM plan-view images of dislocations formed during thermal processing or bending test in GaAs, GaAs/$In_{0.15}Ga_{0.85}As$(15 nm)/GaAs, and GaAs/$In_{0.2}Ga_{0.8}As$(10 nm)/GaAs respectively. When observed using a lower magnification, as in CL imaging, all of these dislocations appear clustered in the form of straight lines in a certain direction. Using two-beam conditions in TEM imaging, these lines are assigned the directions of <110>. From this point of view, the two different structures, strained and unstrained, do not show any differences.

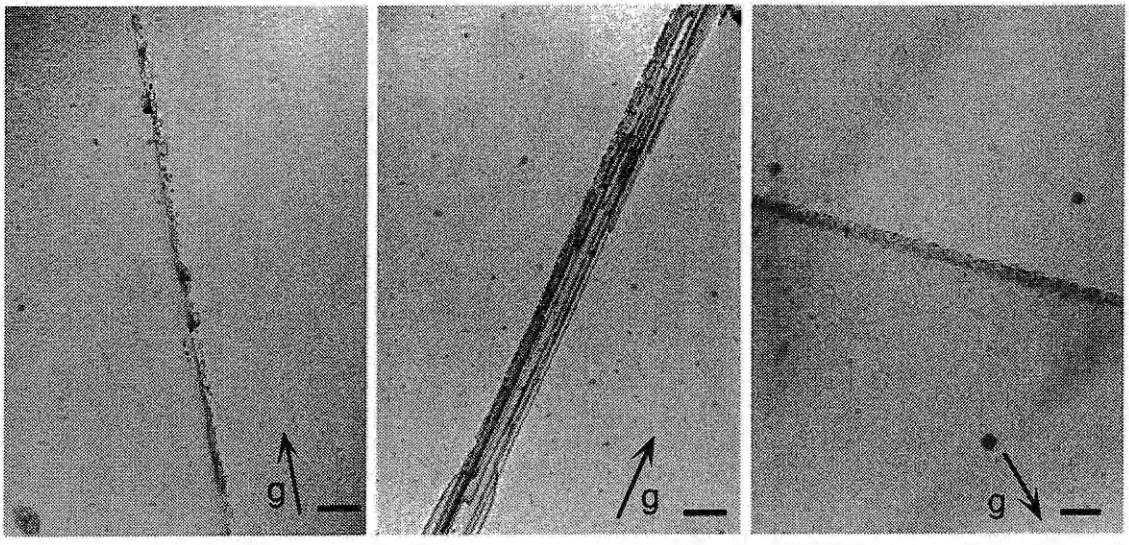

(a) (b) (c)

Fig. 6.5. TEM bright field plan-view images of dislocations formed in (a) GaAs/$In_{0.15}Ga_{0.85}As$(15 nm)/GaAs, (b) GaAs/$In_{0.2}Ga_{0.8}As$(10 nm)/GaAs, and (c) GaAs during thermal processing at 773 K. **g** = (a) [220], (b) [220], (c) [040], bar = 500 nm.

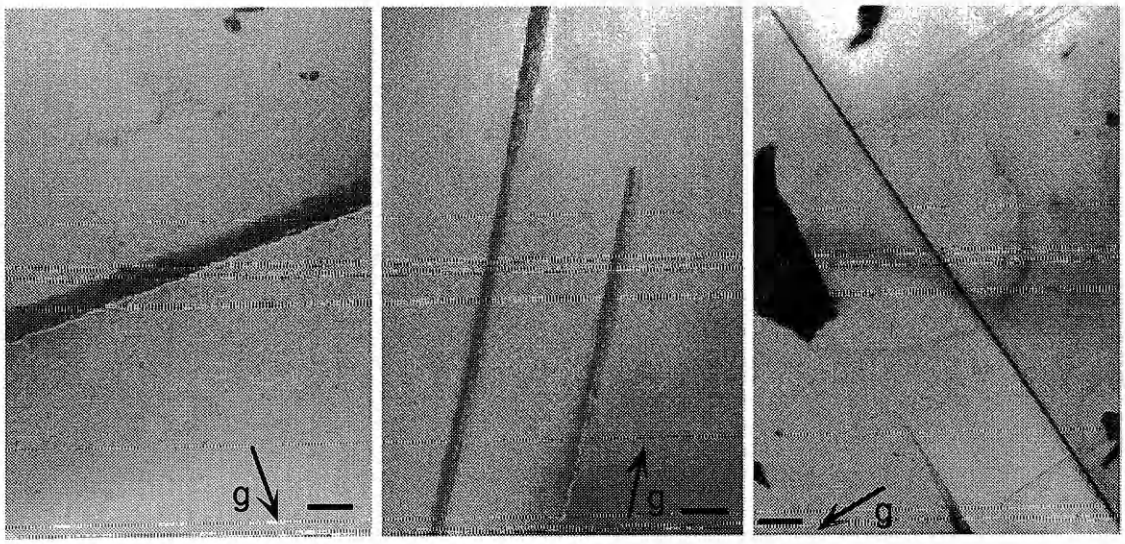

(a) (b) (c)

Fig. 6.6. TEM bright field plan-view images of dislocations formed in (a) GaAs/$In_{0.15}Ga_{0.85}As$ (15 nm)/GaAs, (b) GaAs/$In_{0.2}Ga_{0.8}As$ (10 nm)/GaAs, and (c) GaAs under a constant tensile stress of τ = 7.25 MPa at 673 K. **g** = [220], bar = 500 nm.

The sides of indentations are at approximately 45° to the edges (<110> directions) of the specimens. If dislocations move from one of these sides towards different <110> directions, they can be expected to cross each other. That is the case shown in Fig. 6.6(c). One group of dislocations are in the directions of [110] while the other group in $[1\bar{1}0]$ and they appear to cross each other, although they may be in different planes.

For all specimens subjected to thermal processing or bending tests, no dislocation motion along any other direction was found by TEM observation.

6.1.3 Geometry

Dislocations formed during thermal processing or bending tests appear in lines as shown from CL imaging and can be assigned a line direction when observed in the TEM. They are actually clusters of many irregular dislocation lines and loops. When observed in TEM at a higher magnification, their details can be revealed as shown in Fig. 6.7 for the specimens after thermal processing and Fig. 6.8 after the bending tests. These dislocations cannot be simply classified, or, can not be described by a general character suitable for all of them, no matter whether the structure is strained or unstrained. Some of them are dislocation twins such as that in Fig. 6.7(a) and Fig. 6.8(a) and (b), some are quite straight lines such as Fig. 6.7(b) and Fig. 6.8(c), and others are collections of dislocation loops as shown in Fig. 6.7(c).

Propagation of these dislocations is found to be three-dimensional, such as dislocations in Fig. 6.7(a), 6.7(c), 6.8(a) and 6.8(b). When these dislocations appear as clusters of dislocations, such as Fig. 6.7(b), they do not have the shape and separation of misfit dislocations. Dislocation clusters in Fig. 6.8(c) are straight, but they are present in GaAs, a unstrained structure. So, all these dislocations propagating from indentations during thermal processing or bending tests are not misfit dislocations.

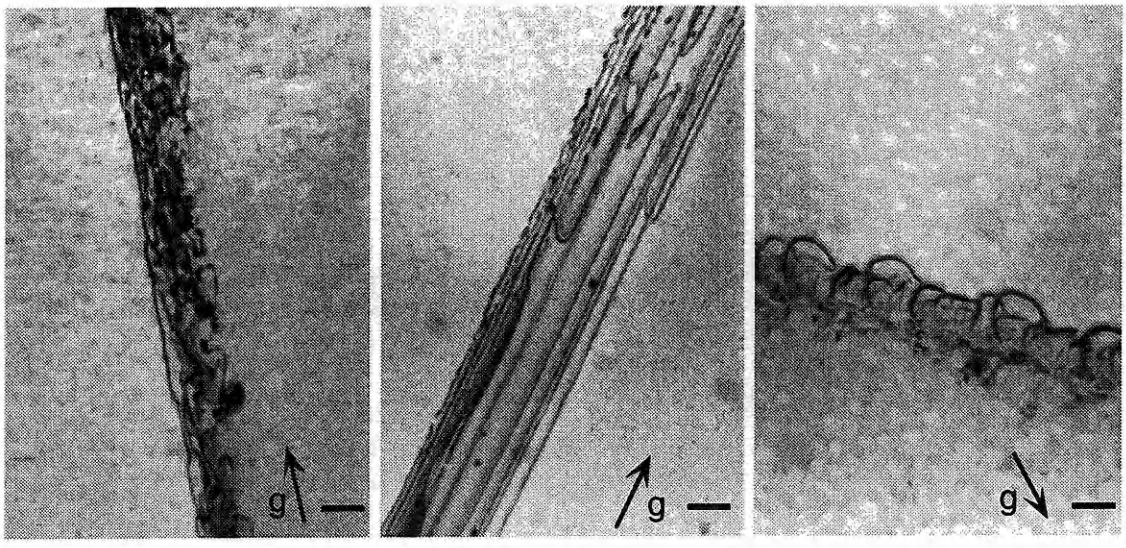

(a) (b) (c)

Fig. 6.7. TEM bright field plan-view images of dislocations formed in (a) GaAs/$In_{0.15}Ga_{0.85}As$ (15 nm)/GaAs, (b) GaAs/$In_{0.2}Ga_{0.8}As$ (10 nm)/GaAs, and (c) GaAs during thermal processing at 673 K. **g** = (a) [220], (b) [220], (c) [040], bar = 200 nm.

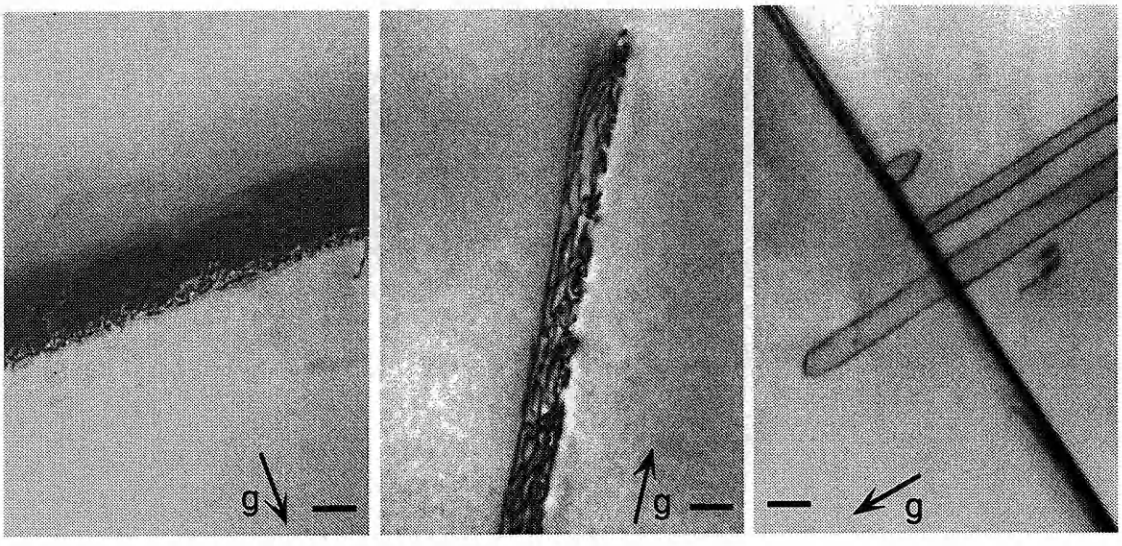

(a) (b) (c)

Fig. 6.8. TEM bright field plan-view images of dislocations formed in (a) GaAs/$In_{0.15}Ga_{0.85}As$ (15 nm)/GaAs, (b) GaAs/$In_{0.2}Ga_{0.8}As$ (10 nm)/GaAs, and (c) GaAs under a constant tensile stress of τ = 7.25 MPa at 670 K. **g** = [220], bar = 200 nm.

The dislocation clusters shown above are seen to be varied, but there is one common feature that can be found among them, that is the direction of their motion. As can be seen in sections 6.1.1 and 6.1.2.1, the dislocation clusters formed during thermal processing or bending tests all take the line (if one considers them as lines) directions of <110>. For individual dislocations, the line directions are varied which results in the variety of dislocation configurations seen in Fig. 6.7 and Fig. 6.8. During thermal processing or bending tests, all of these dislocation clusters moved towards to a certain direction. Dislocation clusters seems to be constrained to move only along this direction and there was not any drift from it. Such a motion produced a dislocation region which has a distinct directional boundary dividing it from the undislocated crystal area, and appears as a line when observed by CL or TEM at low magnifications. Therefore, the line directions of these dislocation clusters are actually the directions of motion of these dislocations, and the line direction which can be assigned to these dislocation clusters only resulted from their motion, which had been restricted to a specific direction. Although the mechanisms of motion of such dislocation clusters are unclear, this directionality is characteristic of dislocation behaviour in these crystals under elevated temperatures or an applied stress.

6.1.4 Difference in dislocation velocity between GaAs/$In_{0.2}Ga_{0.8}As$ /GaAs and GaAs

Distance of dislocation motion in the same time scale (1 second at the targeted temperature) in GaAs/$In_{0.2}Ga_{0.8}As$(h = 10 nm)/GaAs and GaAs, as listed in Table 6.1, were measured based on CL observations of dislocations formed during thermal processing or bending tests. As noted in section 2.7, these have not been expressed as a velocity because the duration of motion cannot be accurately determined.

Dislocation motion in GaAs/$In_xGa_{1-x}As$/GaAs and GaAs is thermally activated and is sensitive to temperature. Fig. 6.9 shows the temperature dependence of dislocation motion in these structures during thermal processing. It can be seen that the distances of dislocation motion in both GaAs/$In_{0.2}Ga_{0.8}As$/GaAs and GaAs increase

exponentially with temperature. Dislocation motion in GaAs is faster than that in GaAs/$In_{0.2}Ga_{0.8}As$/GaAs, approximately by a constant factor of 2.

Table 6.1. Distance of dislocation motion in GaAs/$In_{0.2}Ga_{0.8}As$(h = 10 nm)/GaAs and GaAs calculated based on CL observations of dislocations formed during thermal processing and bending test (applied tensile stress τ = 7.25 MPa).

Temperature	GaAs/$In_{0.2}Ga_{0.8}As$/GaAs (μm)		GaAs (μm)	
(K)	Annealing	Bending test	Annealing	Bending test
473	4	4.5	7	7
573	6	7.5	11	14.5
673	10.5	12	20.5	27.5
743		18		40
773	15		30	
873	20		44	

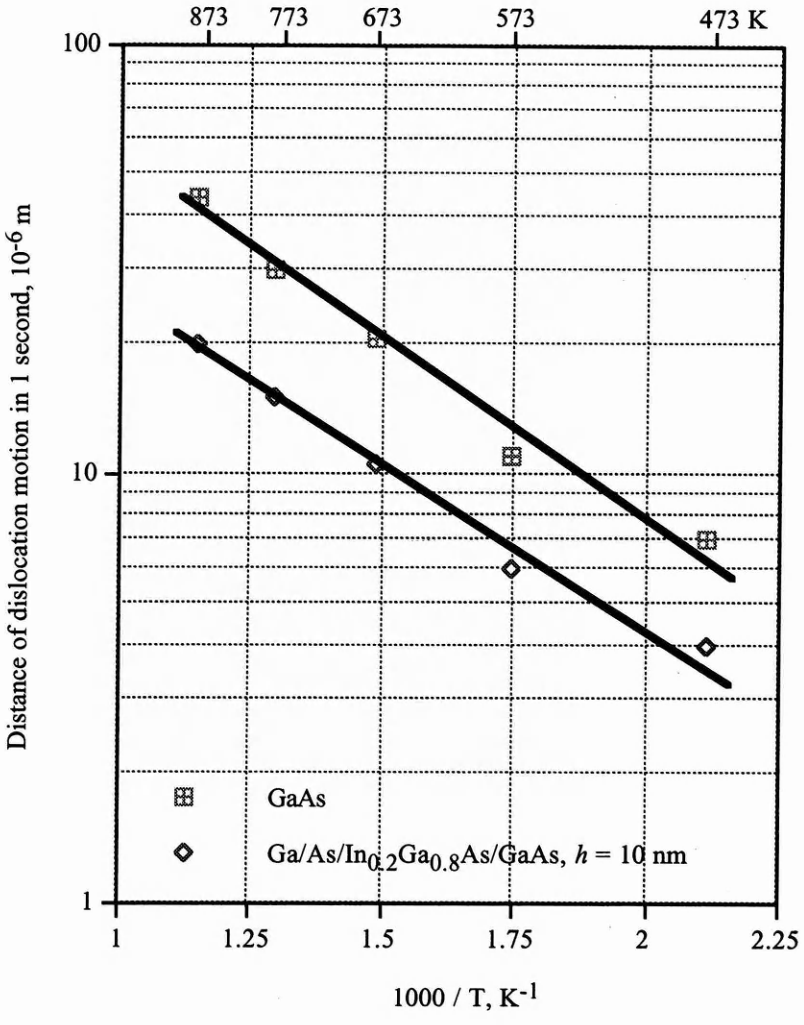

Fig. 6.9. Comparison of the temperature dependence of dislocation motion in GaAs/$In_{0.2}Ga_{0.8}As$ (h = 10 nm)/GaAs and GaAs during thermal processing.

Fig. 6.10 shows the temperature dependence of dislocation motion under a constant tensile stress of τ = 7.25 MPa in GaAs/$In_{0.2}Ga_{0.8}As$ (h = 10 nm)/GaAs and GaAs. Compared with the experimental results of thermal processing, a tensile stress made dislocation motion faster in both structures. For example, at 673 K, the distance of dislocation motion were 20.5 μm for GaAs and 10.5 μm for GaAs/$In_{0.2}Ga_{0.8}As$ (h = 10 nm)/GaAs during thermal processing. Under an applied tensile stress of τ = 7.25 MPa, these distances increased to 27.5 and 12 μm respectively at the same temperature. That is, under the applied stress, the distance of dislocation motion increased 34% for GaAs

and 14% for GaAs/$In_{0.2}Ga_{0.8}As$/GaAs. This indicates that GaAs is more sensitive to an applied stress than GaAs/$In_{0.2}Ga_{0.8}As$/GaAs.

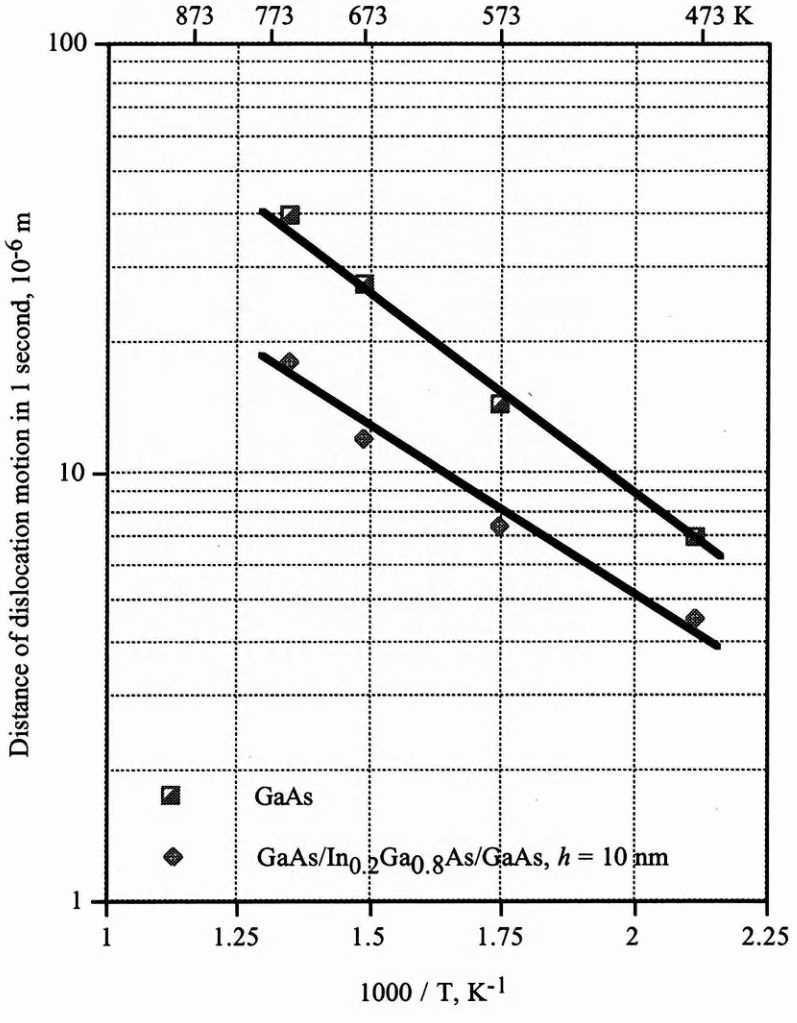

Fig. 6.10. Comparison of the temperature dependence of dislocation motion in GaAs/$In_{0.2}Ga_{0.8}As$ (h = 10 nm)/GaAs and GaAs at a constant tensile stress of τ = 7.25 MPa.

It can be seen from these experimental results that dislocation motion in GaAs is faster than that in the strained-layer structure GaAs/$In_{0.2}Ga_{0.8}As$ (h = 10 nm)/GaAs in both thermal processing and bending tests.

The existence of indium in GaAs/$In_xGa_{1-x}As$/GaAs is not merely a compositional factor. For GaAs/$In_xGa_{1-x}As$/GaAs, indium also changes the structure, from an

unstrained structure to a strained-layer structure. Therefore, the difference in dislocation motion shown by these results reflects the difference not only between two compositions but also between two kinds of structures of strained and unstrained.

Waters *et al* found [Waters_90, Waters_91] that, in strained-layer InGaAs and InAlGaAs quantum well heterostructure lasers, dislocations appeared in the form of dark line defects (DLDs). Growth along <100> directions was practically eliminated while the much slower growth along <110> still occurred compared with the situation of DLDs in unstrained AlGaAs lasers. Although no dislocation cluster (DLDs) growth along <100> directions was observed in both GaAs and GaAs/$In_xGa_{1-x}As$/GaAs here, inhibition of dislocation motion along <110> directions in a strained-layer structure is apparent from the experimental results above and in agreement with Waters *et al* .

6.1.5 Difference in dislocation motion between GaAs/$In_{0.2}Ga_{0.8}As$ /GaAs and GaAs/$In_{0.15}Ga_{0.85}As$ /GaAs

Table 6.2 is the distance of dislocation motion within 1 second in GaAs/$In_{0.15}Ga_{0.85}As$(h = 15 nm)/GaAs during thermal processing and bending tests.

Table 6.2. Distance of dislocation motion of GaAs/$In_{0.15}Ga_{0.85}As$(h = 15 nm /GaAs calculated based on CL observations of dislocations formed during thermal processing and bending test (applied tensile stress τ = 7.25 MPa).

Temperature (K)	GaAs/$In_{0.15}Ga_{0.85}$/GaAs, (μm)	
	Annealing	Bending test
473	4.5	5.5
573	9.5	11
673	15.5	19.5
743		29.5
773	18	
873	27.5	

For the strained-layer structure GaAs/$In_xGa_{1-x}As$/GaAs, the indium content also exerts an influence on dislocation motion. As shown in Fig. 6.11 for thermal processing, the increase of indium content from x = 0.15 to 0.2 slowed down the dislocation motion, for example, from 15.5 to 10.5 μm at 673 K.

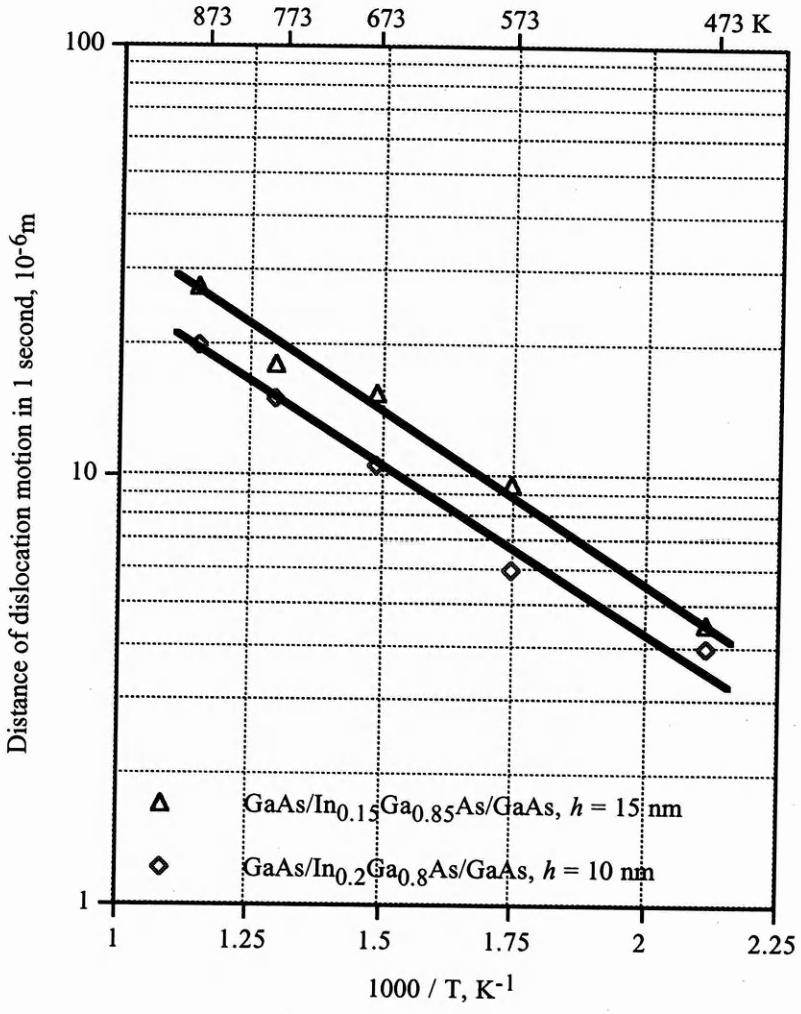

Fig. 6.11. Comparison of dislocation motion in GaAs/$In_{0.2}Ga_{0.8}As$(h = 10 nm)/GaAs and GaAs/$In_{0.15}Ga_{0.85}As$(h = 15 nm)/GaAs during thermal processing.

Comparison of dislocation motion under an applied tensile stress of τ = 7.25 MPa when the indium content x changed from 0.15 to 0.2 for GaAs/$In_xGa_{1-x}As$/GaAs is shown in Fig. 6.12. Slowing down of dislocation motion caused by the increase of indium fraction observed in bending tests is also apparent in thermal processing, for example, at 673 K, from 19.5 μm for x = 0.15 to 12 μm for x = 0.2.

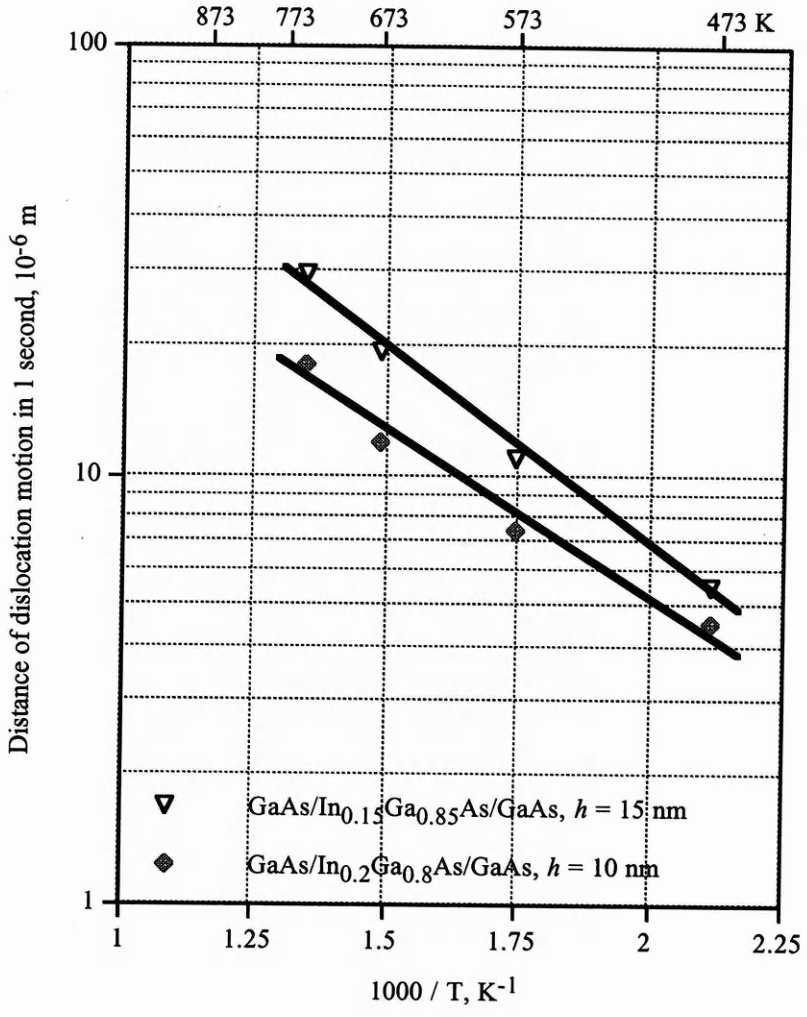

Fig. 6.12. Comparison of dislocation motion in GaAs/$In_{0.2}Ga_{0.8}As$(h = 10 nm)/GaAs and GaAs/$In_{0.15}Ga_{0.85}As$(h = 15 nm)/GaAs at a constant applied stress τ = 7.25 MPa.

These results show that an increase in the indium content in GaAs/$In_xGa_{1-x}As$/GaAs, which increases the misfit strain, slows down dislocation motion.

6.1.6 Effects of indium on dislocation motion

There is no doubt from the experimental results above that either by altering structure or composition, indium plays an role in influencing dislocation motion in GaAs/$In_xGa_{1-x}As$/GaAs. As shown in Fig. 6.13, dislocation motion slows down as indium content increases whether comparing GaAs/$In_{0.2}Ga_{0.8}As$/GaAs with GaAs, that

is, two different structures, or comparing GaAs/$In_{0.2}Ga_{0.8}As$/GaAs with GaAs/$In_{0.15}Ga_{0.85}As$/GaAs, the same structure but with different indium content. It merits attention that, with the increase of indium content, i.e. an increase of misfit stress in GaAs/$In_xGa_{1-x}As$/GaAs, dislocation motion is slowed down and the differences in dislocation motion between thermal processing and bending tests become narrowed.

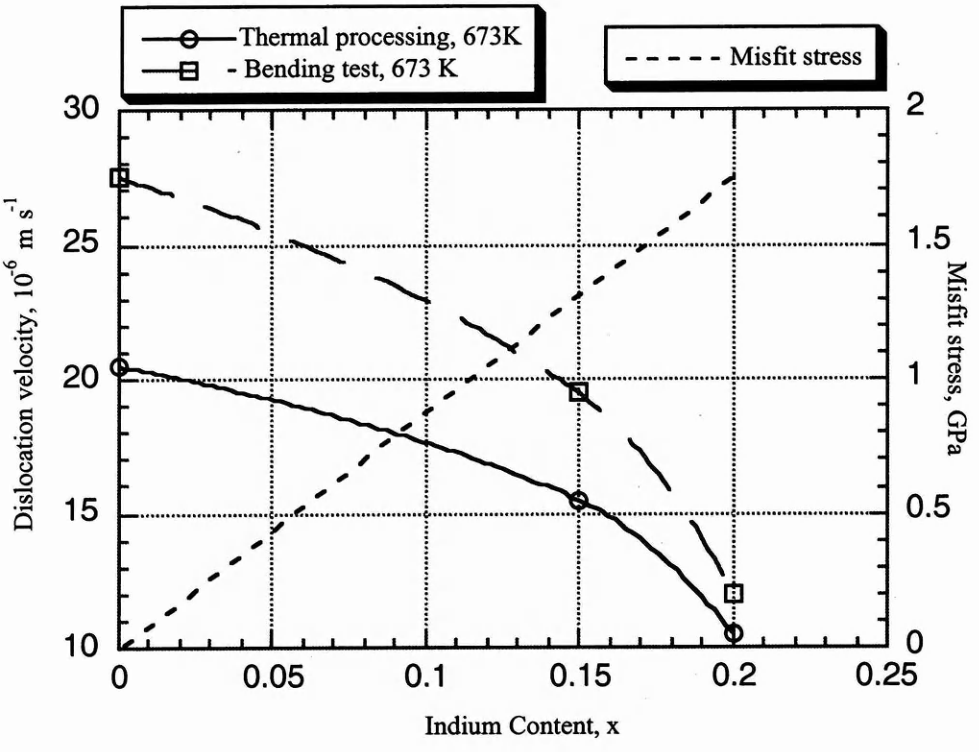

Fig. 6.13. Comparison of dislocation motion in GaAs/$In_xGa_{1-x}As$/GaAs when x = 0, 0.15, and 0.2 in terms of indium content, and the increase of misfit stress with indium in GaAs/$In_xGa_{1-x}As$/GaAs.

An increase of indium content means an increase of misfit. From Vegard's law, the lattice parameter varies linearly with alloy composition. For $In_xGa_{1-x}As$ grown on GaAs, the misfit is the function of indium content x and can be found to be

$$f(x) = \frac{a_{In_xGa_{1-x}As} - a_{GaAs}}{a_{GaAs}}$$

$$= \frac{xa_{InAs} + (1-x)a_{GaAs} - a_{GaAs}}{a_{GaAs}}$$

$$= \frac{x(a_{InAs} - a_{GaAs})}{a_{GaAs}}$$

$$= 0.0717x, \qquad (6.1)$$

taking the lattice parameters of GaAs and InAs to be 0.565325 and 0.60584 nm respectively [Stringfellow_93]. This results in the increase of misfit stress in $In_xGa_{1-x}As$/GaAs with the indium content, x, as expressed by the equation (1.1) and shown in Fig. 6.13.

Therefore, the change of crystal structure resulting from indium and the misfit stress due to lattice mismatch must be considered when assessing the effects of indium on dislocation behaviour and discussing the difference in dislocation motion between GaAs and GaAs/$In_xGa_{1-x}As$/GaAs.

6.1.7 Two aspects of the effects of misfit stress

Misfit stress due to lattice mismatch between a film and its substrate has been discussed more often as the driving force for the formation of misfit dislocations. Its influence on other dislocations has been less considered.

Dislocation motion in crystals is basically the displacement of atoms. It is well known that an applied stress, the Peierls stress, is needed for dislocation motion to overcome the lattice resistance. It arises as a direct consequence of the force-distance relationship between individual atoms [HullD_92]. For a crystal having atomic planes as illustrated as Fig. 6.14(a), the force-distance relationship between individual atoms must have been changed when it was compressed to become a strained-layer structure as illustrated by Fig. 6.14(b).

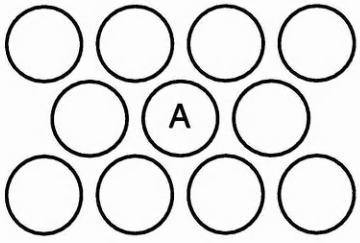

(a)

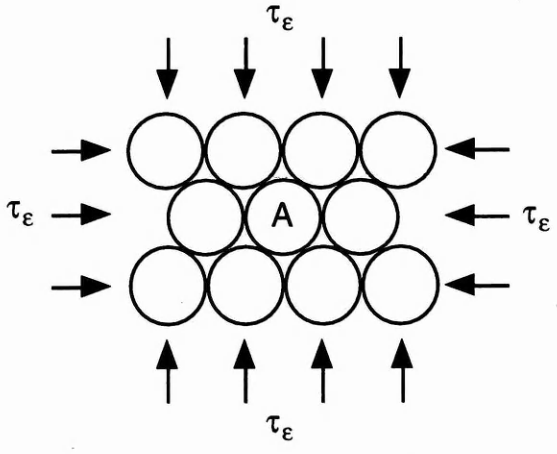

(b)

Fig. 6.14. Illustration of effects of misfit stress τ_ε on the displacement of an atom *A* in a strained-layer structure (b) compared with that in an unstrained crystal structure (a).

Considering the atom *A* in Fig. 6.14(a), after the crystal lattice is compressed, as in the case of a compressive strained layer, besides all the factors which may affect its displacement when the crystal is in an unstrained state and which still exist, a new factor emerges because of the compression of crystal lattice, i.e. because of the existence of misfit stress τ_ε as illustrated in Fig. 6.14(b). Assuming that the stress due to misfit strain is uniform and isotropic, the resulting force will act as a binding force to constrain the atoms to become closer to each other. Any displacement of the atoms, any dislocation motion in such a crystal, now has one more resistant force compared with that in normal structure, and this resistance takes effect in the direction opposite to dislocation motion as soon as the dislocation motion begins. The atom *A* in Fig. 6.14(b)

can be imagined as a rigid ball restrained by springs which are uniformly distributed around it and produce the forces towards the centre of the ball from outside. The ball rests in a balance restrained by these springs and any tendency to move away from its equilibrium position will cause a reacting force to keep it from movement. In this way, atoms become more stable in their lattice positions in a strained structure than that in a normal structure. Thus, for dislocation motion, which results from the displacement of atoms from their equilibrium lattice positions (even for the equilibrium set up within a strained-layer structure) and is not the case of the formation of misfit dislocations, misfit stress is intrinsically a friction force. This force causes lattice hardening [Waters_91], which was used to describe the phenomenon of dislocations being suppressed in strained-layer structures, and therefore hinders the development of dislocation motion.

The experimental results also show differences in dislocation motion in the same kind of specimens when they were subjected to different tests, that is, thermal processing and bending tests. Dislocation motion in bending tests was faster than that in thermal processing. This difference is very clear for GaAs, from the distance of dislocation motion of 20.5 μm in thermal processing to 27.5 in bending test, as $x = 0$ (GaAs) shown in Fig. 6.13. However, it can be well recognised that this difference became narrowed with the increase of indium content, as can be seen in Fig. 6.13 where the distance changed from 15.5 μm in thermal processing to 19.5 in bending test for $x = 0.15$, and from 10.5 μm in thermal processing to 12 in bending test for $x = 0.2$. The differences in the distance of dislocation motion between thermal processing and bending tests at the same temperature are 7 μm for $x = 0$, 4 μm for $x = 0.15$, and 1.5 μm for $x = 0.2$. This means that, compared with the change of the distance of dislocation motion in thermal processing, dislocation motion is slowed down much more by the same increase of indium content when the structures were subjected to an applied stress. In other words, dislocation motion in GaAs/$In_xGa_{1-x}As$/GaAs became much slower and was more resistant to an applied stress when the indium content increased. Decrease of

sensitivity to an applied stress, or, increase of resistance to an applied stress reflects the accumulation of a counter force inside the crystal which offsets the effects of applied stress on dislocation motion. Weakening of the effects of an applied stress emphasises the increase of effects of the counter force. Such a counter force can only be attributed to misfit stress, because any other factor which may affect dislocation motion would not cause the difference in dislocation motion to respond to an applied stress in this way.

It was suggested by Waters *et al* [Waters_90] that the inhibited DLD growth in strained-layer InGaAs and InAlGaAs quantum well heterostructures was possibly due to dislocation pinning by indium atoms, as was originally proposed by Kirkby [Kirkby_75]. This seems to be a reasonable explanation of the experimental results showing the dislocation velocity in inverse proportion to the increase of indium content. However, because their experimental results showed that DLD growth along <100> directions was practically eliminated while the much slower growth along <110> still occurred, and it is generally accepted that <100> DLDs propagate by dislocation climb and <110> DLDs propagate by dislocation glide [Ueda_88], it is not clear from this explanation why the climb mechanism would be affected but not the glide mechanism [Hopgood_94]. Furthermore, if it was the pinning taking effect, it should behave the same whether under an applied stress or not. At least, it should not cause dislocation motion to become immune to an applied stress but not to thermal treatment.

Hopgood [Hopgood_94] proposed a vacancy-controlled model of degradation in compressive strained-layer heterostructure lasers. The model proposed that, when compared with an unstrained structure in which the vacancies migrate towards dislocations and cause them to climb, the vacancies in strained-layer lasers act as strain relievers, thus reducing the energy of their formation and this reduction causes the vacancies to remain as isolated point defects rather than to contribute to DLD growth. The consideration of misfit stress acting as a resistance to dislocation motion strengthens this model. If the atom *A* in Fig. 6.14(a) and (b) is taken as a vacancy, it can also be seen that the vacancies in a strained-layer structure are constrained by misfit

stress to become more stable and less mobile than those in an unstrained structure. Misfit stress has a linear increase in relationship to the indium content as can be seen from equation (6.1) and Fig. 6.13. Therefore, the more indium, the greater misfit stress, the less mobility of atoms or vacancies, and the lower dislocation velocity. Both the elimination of dislocation climb or the inhibition of dislocation glide can thus be expected, and the effects of misfit stress are intensified with the increase of indium content in GaAs/$In_xGa_{1-x}As$/GaAs, as revealed by the difference in dislocation motion not only between GaAs/$In_{0.2}Ga_{0.8}As$/GaAs and GaAs but also between GaAs/$In_{0.2}Ga_{0.8}As$/GaAs and GaAs/$In_{0.15}Ga_{0.85}As$/GaAs.

Certainly, the prerequisite to the consideration of misfit stress acting as resistance to dislocation motion in a strained-layer structure is that the structure should not be in the conditions which lead to the loss of coherence. In fact, misfit dislocations and other dislocations are dominated by different mechanisms. As has been seen in Chapter 4, an experimental condition which can cause dislocations to propagate away from indentations cannot make misfit dislocations follow the same route to generate and propagate. Even at conditions which have led to the introduction of misfit dislocations into the structure, the dislocation growth from indentations, the pre-existing dislocation sources, still do not have misfit dislocation features and are still affected by the factors which play a role in dislocation motion when the experimental conditions are not favourable for the formation of misfit dislocations. For example, under an applied stress of τ = 7.25 MPa, many misfit dislocations were introduced into a specimen of GaAs/$In_{0.15}Ga_{0.85}As$(h = 15 nm)/GaAs at 710 K as seen in Fig. 4.9(c), but the trend of dislocation motion changing with temperature was still kept the same as that from 473 to 673 K. This means that the formation of misfit dislocations did not affect dislocation motion proceeding in its own way. When misfit stress became capable, by thermal or mechanical means, of driving the generation and propagation of misfit dislocations, it still kept the same effects on the motion of other dislocations. The effects of misfit stress on dislocation motion might be weakened in concordance with the relaxation

caused by the formation of misfit dislocations, but this weakening was not serious enough to eliminate its effects on the motion of other dislocations. Because a strained-layer structure can never be fully relaxed [Goodhew_99], the effects of misfit stress on dislocation motion can never be totally eliminated due to relaxation.

So, misfit stress has two aspects of behaviour. It is the driving force for the formation of misfit dislocations. Thus, it is a factor making the structure unstable. However, it also restrains the mobility of atoms, thus inhibiting dislocation motion. Therefore, with respect to dislocation motion, misfit stress is also a factor making the devices more reliable when a strained-layer structure is adopted.

6.1.8 Effects of strained-layer thickness on dislocation motion

The thickness is crucial for relaxation of strained-layer structures, but it does not have a strong effect on dislocation motion as can be seen from Fig. 6.15. For GaAs/$In_{0.2}Ga_{0.8}As$/GaAs, when strained-layer thickness increased from 4 nm to 10 nm, the distance of dislocation motion, for example, only changed from 11.5 to 10.5 μm at 673 K.

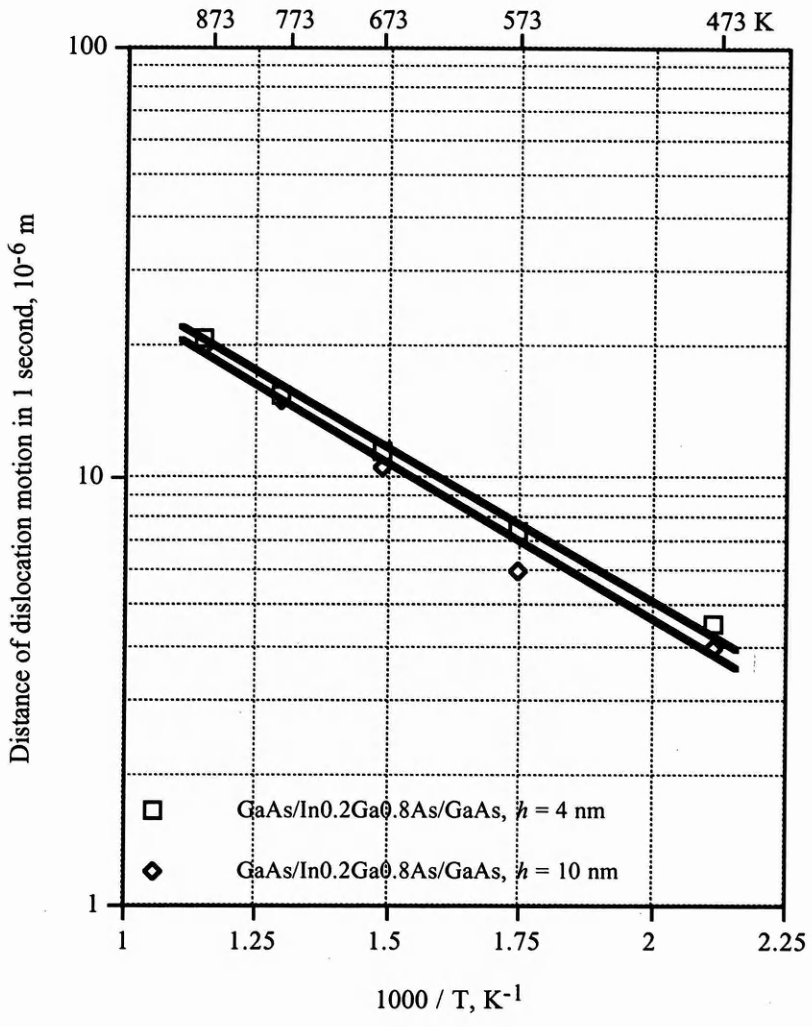

Fig. 6.15. Comparison of dislocation motion when the thickness of strained layer changed from 4 nm to 10 nm for GaAs/$In_{0.2}Ga_{0.8}As$/GaAs

6.2 Different dislocation configurations under an applied stress

Dislocations discussed in this section are those which were generated (by both thermal and mechanical means) homogeneously all over the specimens. They are not the dislocations which propagated from indentations.

It has been shown in Chapter 4 that a dislocation network consisting of orthogonal misfit dislocation lines was formed in GaAs/$In_xGa_{1-x}As$/GaAs during [100] bending tests. Only a few of threading dislocations, or the dislocations which penetrate the

specimens can be found, as shown in Fig. 4.13. This indicates that, for strained-layer structures subjected to an applied stress, dislocations are mainly formed at the interfaces in the manner of misfit dislocations. They could propagate along interfaces quite a long way without threading to reach surfaces by moving in the direction perpendicular to interfaces. This produces a distribution of dislocations mainly along specific planes — interfaces. The density of dislocations in the direction perpendicular to interface, i.e., on the cross section of the specimen, in these circumstances is quite low.

Under the same applied stress during the same [100] bending test, the dislocations formed in GaAs are present in a different configuration, as shown in the TEM plan-view image of a GaAs specimen after [100] bending in Fig. 6.16. The difference in dislocation configurations between an unstrained structure and a strained-layer structure after the same bending test is apparent and significant. Dislocations in GaAs are not present as straight directional lines forming a regular dislocation network at the specific planes (interfaces) as misfit dislocations in strained-layer structures. Dislocations caused by [100] bending in GaAs are irregular and do not have any directionality. All these dislocations are short and do not run too long within the structure before the ends of them reach surfaces. This configuration indicates that, unlike misfit dislocations whose activities only take place at specific crystal planes — the interfaces, the dislocations in GaAs take the whole structure as their scope of activities.

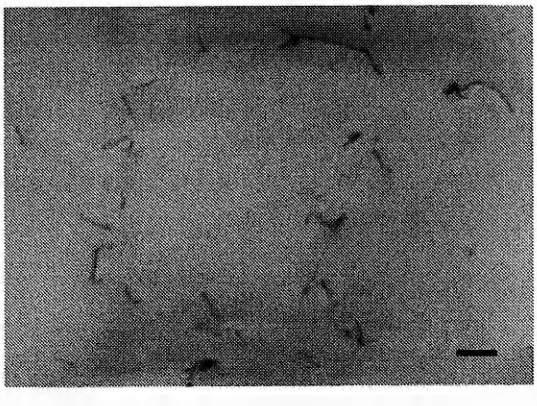

Fig. 6.16. Dislocations caused by [100] bending in GaAs. Bar = 500 nm.

Under an applied stress, when the mechanisms of dislocation formation operates, as discussed in Chapter 4, the dislocations produced in a strained-layer structure are misfit dislocations resulting from both relaxation and deformation. Dislocation motion in strained-layer structures is thus constrained within interfaces resulting in a distribution of dislocations mainly along interfaces. For unstrained structures, there are not any limits or restraints in principle for the direction and scope of dislocation motion when this motion takes place on a slip system. Dislocations can propagate along all glide directions in all slip planes. Thus, they can be present anywhere all over the structure. Therefore, the existence of a strained layer effectively restrains the activities of dislocations within the specific planes — interfaces, and avoids the propagation of dislocations all over the structure. In this way, a strained layer acts as a filter of dislocations.

6.3 Dislocation motion stimulated by electron beam irradiation on TEM

Dislocations can be caused to move by the effects of electron beam irradiation [Friedel_67, Hirsch_56, Pashley_59, Matthews_89]. After high-stress deformation, dislocations in GaAs has been found to be able to move during irradiation in TEM [Kuesters_86]. Owing to their different natures, misfit dislocations and other dislocations exhibit different behaviours under the irradiation of electron beam, that is a significant comment on the energy states of both themselves and the systems they belong to.

6.3.1 Motion of dislocations

Fig. 6.17 (a) and (b) are successive (with a time interval of several minutes) TEM images of dislocations at the same observation area in a previously bending tested GaAs specimen. It can be seen from the micrographs that most of these dislocations have undergone some changes under electron beam irradiation. Dislocations *a* and *b* in image (a) become shorter. Dislocation *c* has disappeared from the observation area.

Dislocations *d* and *e* in (a) combined to form dislocation *f* in (b). Dislocation node *n* was more stable, although its dislocation lines have changed a little.

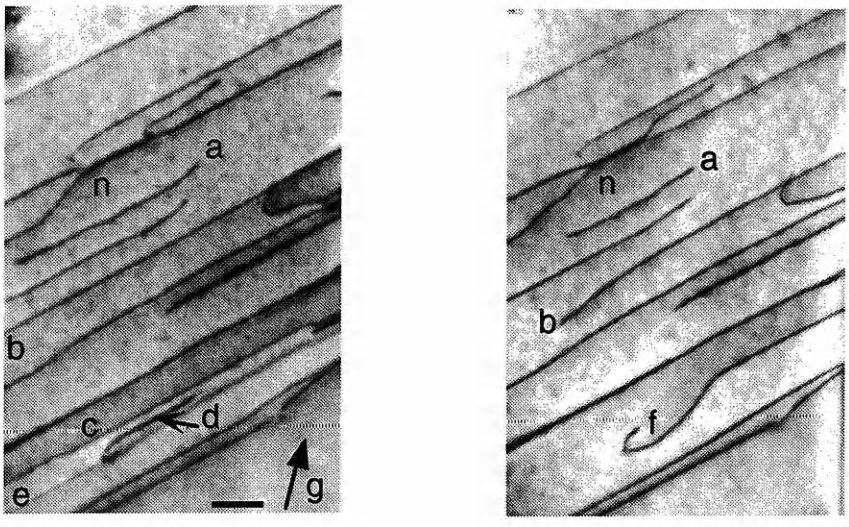

(a) (b)

Fig. 6.17. Dislocation motion simulated by electron beam during TEM observation in a GaAs specimen after a bending test. Image (a) is the dislocation configuration before motion and (b) is after. **g** = [220], bar = 200 nm.

Similarly, dislocations introduced by thermal processing or bending testing in GaAs/$In_xGa_{1-x}As$/GaAs could also be stimulated to move by an electron beam. Fig. 6.18 (a), and (b) are successive TEM images showing dislocation motion under electron beam irradiation in a GaAs/$In_{0.2}Ga_{0.8}As$/GaAs specimen after a bending test. It can be seen that, by comparing (b) with (a), the tip *a* and *b* shrunk a little under electron beam irradiation. But nothing happened to dislocation line *c*, it remains the same as before electron beam irradiation.

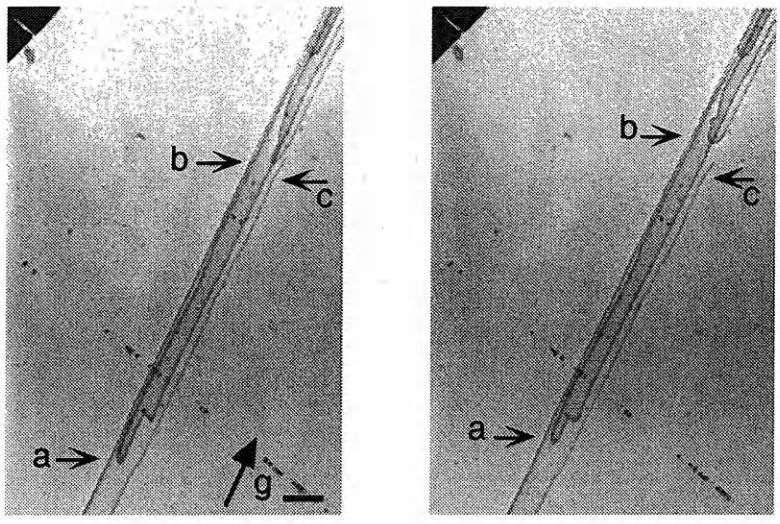

(a) (b)

Fig. 6.18. Dislocation motion stimulated by the electron beam during TEM observation in a bending tested GaAs/$In_{0.2}Ga_{0.8}As$/GaAs specimen. Dislocation tip *a* and *b* in (a) shrunk a little becoming a shape in (b). Dislocation *c* in (a) remains unchanged after irradiation as shown in (b). **g** = [220], bar = 500 nm

6.3.2 Motion of misfit dislocations

In general, misfit dislocations, regardless of whether they were grown in during fabrication of the structure or introduced by thermal processing or bending test, are stable under electron beam irradiation as shown in Fig. 6.19. Fig. 6.19(a) is the misfit dislocation before and (b) after 16 hours electron beam irradiation within TEM. After irradiation for as long as 16 hours, it kept its original state without any change.

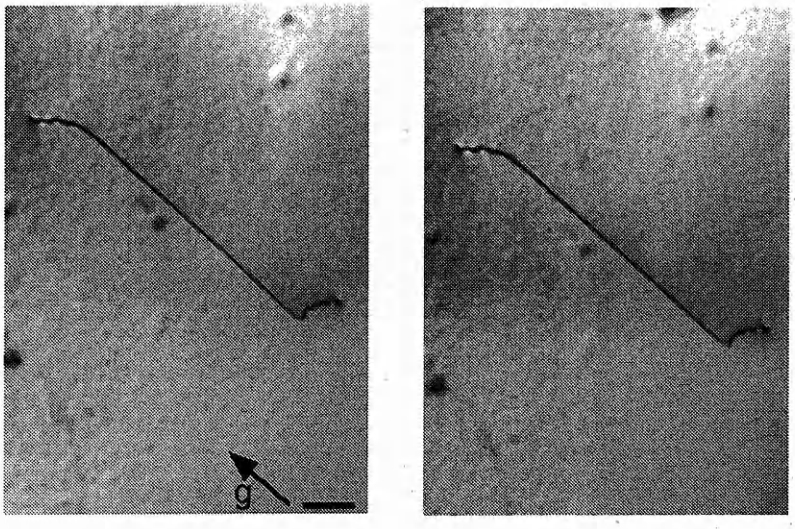

(a) (b)

Fig. 6.19. Effects of electron beam irradiation on misfit dislocations. (a) A misfit dislocation present in a bending tested specimen of GaAs/$In_{0.15}Ga_{0.85}As$/GaAs. (b) After 16 hours electron beam irradiation, there was no change. **g** = [220], bar = 200 nm.

In some cases, some changes can be found in misfit dislocations after irradiation of the electron beam. Fig. 6.20(a) is a group of misfit dislocations with their original state. After 16 hours under irradiation by the electron beam, as shown in Fig. 6.20(b), some changes occurred. For comparison, Fig. 6.2 (a) and (b) were printed by overlapping as shown in Fig. 6.21. Most apparently, the threading segments of misfit dislocations *B* and *C* shifted a little by changing their angles to the main misfit dislocation line. But these threading segments are not misfit dislocations. Their movement of this kind does not have any significant relation to misfit dislocation themselves. What is more important is the shifting of misfit dislocations from their original positions. If one takes the misfit dislocation *A* as a reference, the line position of misfit dislocation *B*, *C*, and *D* all shifted a little towards it. This shift might have resulted from two factors which all related to the raising of temperature due to electron beam irradiation. Firstly, raising the temperature might cause distortion of the specimen. Secondly, the different thermal coefficients caused the interfacial structure to

adjust in accordance with the change of temperature. In any case, these shifts of their line position do not have significance for the whole structure.

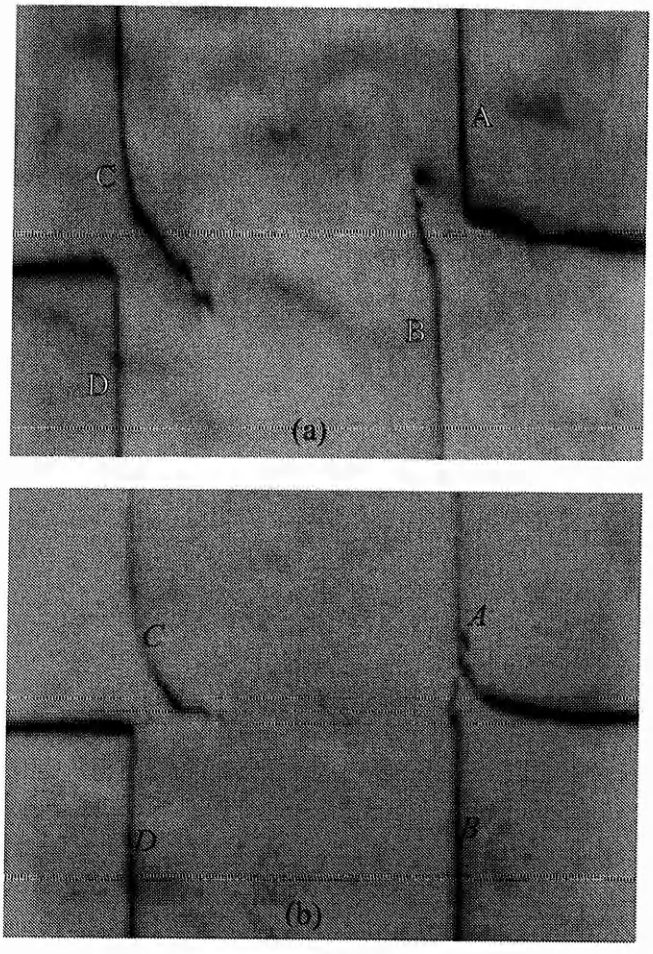

Fig. 6.20. Misfit dislocations under electron beam irradiation. (a) The original state. (b) After electron beam irradiation for 16 hours.

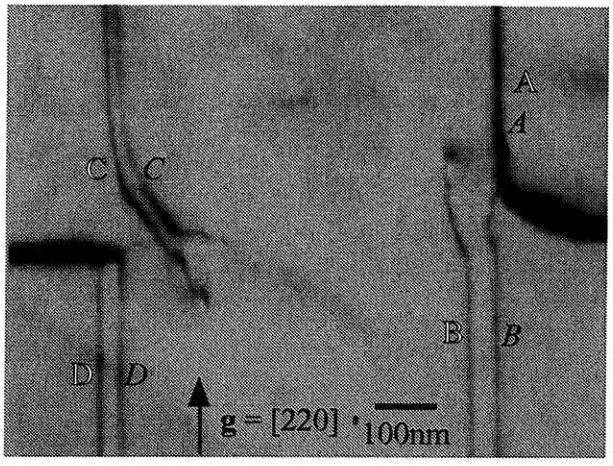

Fig. 6.21. Superimposed photographs showing the comparison of the misfit dislocations before and after electron beam irradiation. Outline letters mark the original position of dislocations (Fig. 6.20(a)). Italic letters mark the shifted position of the same dislocations after electron beam irradiation for 16 hours (Fig. 6.20(b)).

Motion of a misfit dislocation shown in Fig. 6.22 is the only observation in this research showing the mobility of misfit dislocations under electron beam irradiation in TEM. This motion was different in principle from that occurring in other dislocations. As has been seen in Fig. 6.17, dislocations in GaAs were mobile under electron beam irradiation resulting in their shortening or even disappearing. The motion of a misfit dislocation shown in Fig. 6.22 is not to shorten the dislocation itself. On the contrary, this motion resulted in an additional length of dislocation line to be introduced into the structure by this motion.

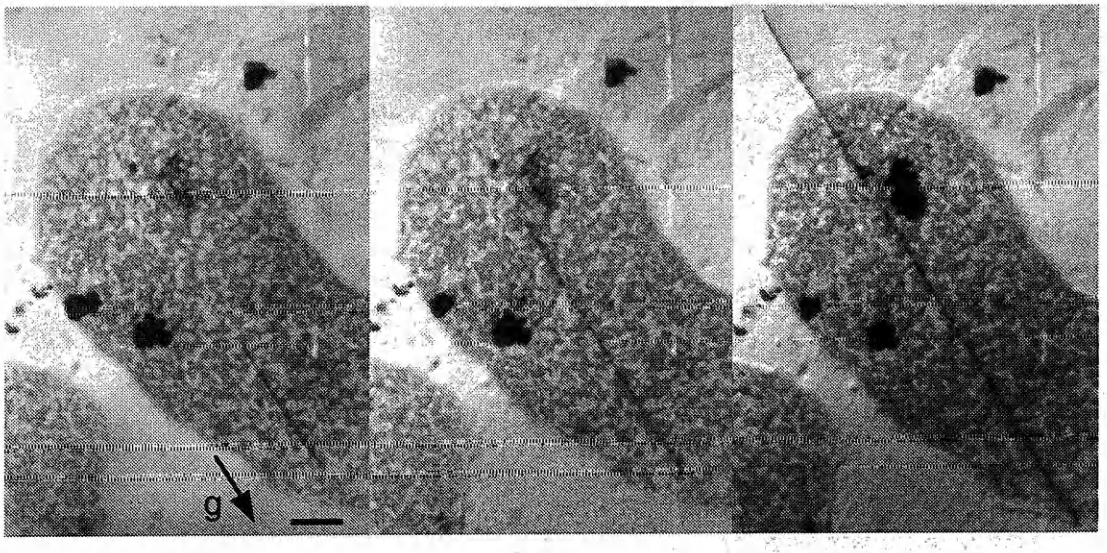

(a) (b) (c)

Fig. 6.22 Elongation of a misfit dislocation line under electron beam irradiation. g = [220], bar = 500 nm. (a) first photograph, (b) one minute later, (c) two minutes after the first photograph. **g** = [220], bar = 1μm.

The specimen in which the elongation of a misfit dislocation occurred was a piece of GaAs/$In_{0.15}Ga_{0.85}As$/GaAs subjected to a bending test. The bending test might have caused some additional strain energy to be stored around the misfit dislocation line which took effect when the specimen was irradiated by electron beam. This could also have happened to dislocations in the GaAs specimens. Thus the motion of dislocations in GaAs/$In_{0.15}Ga_{0.85}As$/GaAs and GaAs may have the same origin regarding electron beam irradiation after a bending test. The consequences of their motion should always be a lowering of the energy of the system. However, this was achieved in different ways. It is because they are non-misfit dislocations that they lower the system energy only by shortening themselves. And it is because they are misfit dislocations that they lower the system energy only by elongating themselves. A key factor of misfit strain makes things different.

The motion of a misfit dislocation in Fig. 6.22 is actually elongation of that misfit dislocation. The ends of the dislocation shifted, so were not pinned, when the

dislocation was elongating. This suggests that, as has been pointed out in Chapter 3, the elongation of misfit dislocations does not follow the M-B model, in which the threading segments of a misfit dislocation were pinned while the segment within strained layer drags misfit dislocations to elongate at interfaces.

6.3.3 Strain energy related to dislocations and misfit dislocations

The internal energy of a crystal body is increased by strain. For an unstrained crystal, the existence of distortion around a dislocation implies that a crystal containing dislocations has extra strain energy. As illustrated in Fig. 6.23, the strain energy is created by a dislocation when it is introduced into an unstrained crystal and causes distortion among the neighbouring atoms which contain it. The total strain energy of a dislocation may be divided into two parts [Hull_92],

$$E_{total} = E_{core} + E_{elastic\ strain}. \tag{6.2}$$

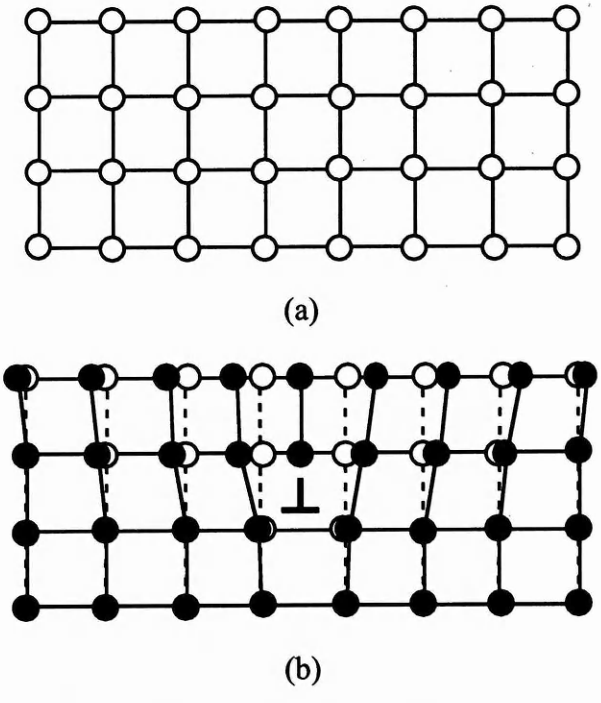

(a)

(b)

Fig. 6.23. A sketch illustrating a dislocation is introduced into a crystal and creates distortion. (a) A normal crystal. (b) The crystal with a dislocation. ○ marks the original position of an atom and ● marks the dislocated position.

The elastic part, stored outside the core in an element of volume dV per unit length of dislocation is

$$dE_{elastic\ strain} = \frac{1}{2} dV \sum_{i=x,y,z} \sum_{j=x,y,z} \sigma_{ij} e_{ij}, \tag{6.3}$$

where σ_{ij} is the components of stress and e_{ij} is the components of strain.

It should be noted that, in an unstrained structure, the strain e_{ij} is created by the formation of a dislocation and the strain energy results from the creation of the dislocation. Therefore, non-misfit dislocations in both unstrained and strained-layer structures were activated by the electron beam to move so as to reduce the strain energy stored. The experimental results have shown several possible ways in which dislocation motion achieved this. The strain energy of a dislocation is proportional to its length and a decrease in length results in decrease of strain energy [HullD_92]. Most dislocation motion stimulated by the electron beam shown above, such as dislocations *a*, *b*, and *c* in Fig. 6.17 and dislocation tips *a* and *b* in Fig. 6.18, was dominated by this mechanism. If dislocations have an interaction energy, they will come together and annihilate one another or combine to form a single dislocation [Read_53], this is how dislocation *f* was formed in Fig. 6.17 (b) by interactions among dislocations *d* and *e* in (a). All dislocation motion shown above resulted in a decrease of dislocation length. This characteristic of dislocation motion is determined by the nature of these dislocations. As has been mentioned in Chapter 1, dislocations always increase the energy in an unstrained structure, so they are not required by thermodynamics. The direction of thermodynamic stability of such a crystal containing dislocations is lowering the strain energy by shortening or eliminating dislocations. This makes it possible to lower the dislocation density in an unstrained crystal by annealing.

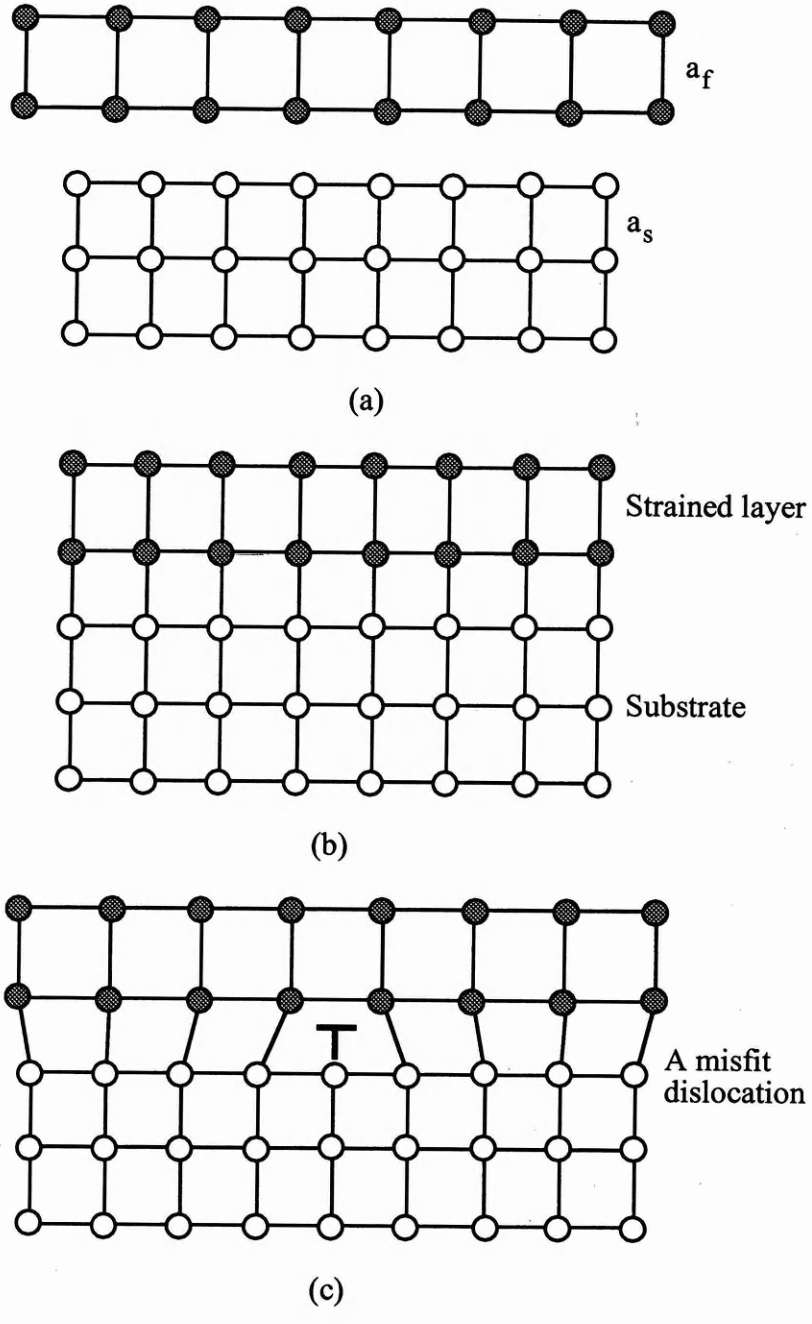

Fig. 6.24. Building up of a strained-layer structure and introduction of a misfit dislocation to relax such a strained-layer structure. a_f is the lattice parameter of overlayer, a_s the lattice parameter of substrate, and $a_f > a_s$.

However, for misfit dislocations, the story is totally different.

Firstly, in a misfit dislocation-free strained-layer structure, there has been a strain energy before the formation of misfit dislocations. When a overlayer of which the

lattice parameter is a_f is grown on a substrate with the lattice parameter of a_s, and $a_f > a_s$, as shown in Fig. 6.24(a), the overlayer is strained as shown in Fig. 6.24(b). The strain energy is created by the fabrication of the structure, and this strain energy makes the structure thermodynamically unstable. Secondly, because there has been a strain energy, the direction of thermodynamic stability of the structure is lowering this strain energy and the most important way to do so is the creation of misfit dislocations. When a misfit dislocation is created, as shown in Fig. 6.24(c), the structure achieves relaxation — the lowering of the energetic state of the structure.

As the result of the formation of misfit dislocations, the components of strain e_{ij} in (6.3) associated with a misfit dislocation become the recovery from the pre-existing strain due to lattice mismatch, their value will be negative if not zero (compared with the original dimensions of the lattices of strained layer) after the relaxation has occurred. If the strain energy E'_{total} associated with misfit dislocations can still be divided into two parts, then it should be

$$E'_{total} = E_{core} + (-E_{elastic\ strain}). \tag{6.4}$$

So, the elastic part of the total energy becomes negative after the formation of misfit dislocations because the creation of misfit dislocations reduces the elastic strain. Therefore, the total energy associated with a misfit dislocation in a strained-layer structure has the intrinsic and essential difference from the total energy of a dislocation in an unstrained crystal.

The formation of misfit and non-misfit dislocations are driven by different factors which produce different thermodynamic requirements of the structure. This basic difference is well distinguished by their behaviours under electron beam irradiation. Unlike non-misfit dislocations shown in Fig. 6.17 and 6.18, misfit dislocations, under electron beam irradiation, were transformed in the opposite direction. They were either quite stable, as shown in Fig. 6.19, or become longer as shown in Fig. 6.22. Non-misfit dislocations can be eliminated by annealing [Nadgornyi_88], but misfit dislocations

cannot. Instead, they can be generated during thermal processing, like the 60° misfit dislocations generated in the structures of $h < h_c$ and $h_c < h < H_c$ shown in Chapter 4 and the edge misfit dislocations generated in the structures of $h > H_c$ shown in Chapter 5. It is their different natures that determines that non-misfit dislocations and misfit dislocations follow different, actually opposite, ways to lower the total strain energy of the system and thus to realise the thermodynamic requirements of the structures.

The line tension of a dislocation is the increase in energy per unit increase in the length of a dislocation line, which is based on the consideration that the strain energy created by a dislocation line is proportional to its length [HullD_92]. As analysed above, a misfit dislocation in a strained-layer structure does not have the same strain energy as that of a non-misfit dislocation in an unstrained crystal, and the formation of a misfit dislocation results in the lowering of strain energy, not as a non-misfit dislocation which results in creation of strain energy. The concept of line tension established on the basis of the strain energy created by a dislocation in a normal crystal thus becomes invalid for a misfit dislocation because a misfit dislocation does not create the strain energy from which line tension arises, but, on the contrary, eliminates the strain energy which has been created by the fabrication of strained-layer structure. The line tension of a non-misfit dislocation and the line tension of a misfit dislocation are not the same. It neglects the intrinsic and essential difference between the strain energy created by a non-misfit dislocation and the strain energy associated with a misfit dislocation, therefore, it neglects the intrinsic and essential difference between a non-misfit dislocation and a misfit dislocation to take the line tension of a dislocation as the main resistant factor for the formation of a misfit dislocation.

6.4 Conclusions

Differences in dislocation behaviours between GaAs/$In_xGa_{1-x}As$/GaAs and GaAs have been investigated in this chapter. The first is the difference in dislocation (non-misfit dislocation) motion and resultant dislocation configuration between strained-

layer structures and unstrained structures, which reflects the impact of a strained layer on dislocation motion. The second is the difference between non-misfit dislocations and misfit dislocations when they are activated to move by electron beam irradiation, which reflects the different thermodynamic requirements of the strain energy created by non-misfit dislocations and the strain energy associated with misfit dislocations.

Misfit stress has been well recognised as the driving factor for the introduction of misfit dislocations into the structure resulting in relaxation. However, in a compressive strained-layer structure, the force resulting from misfit stress constrains the atoms closer to each other. This is an additional resistant force to dislocation motion which is not present in unstrained structures and opposes dislocation motion as soon as the dislocation motion initiates. Even when misfit dislocations has formed, this force is still working. Therefore, when the misfit stress drives the formation of misfit dislocations resulting in relaxation, it also plays a role in resisting dislocation motion which will result in crystal defects. The dislocation motion in GaAs/$In_xGa_{1-x}As$/GaAs is slower than that in GaAs, and the sensitivity of the dislocation motion in GaAs/$In_xGa_{1-x}As$/GaAs to an applied stress proved the two aspects of the effects of misfit stress. Further research is needed to investigate if this is true for a tensile strained-layer structure.

The existence of a strained layer makes the interfaces the most energetically favourable venue for the activities of dislocations. Under conditions which cause the generation and multiplication of dislocations in a strained-layer structure, these dislocations adopt the form of misfit dislocations, resulting in both the deformation of the crystal and the relaxation of the structure. In this way, dislocations are confined to interfaces unlike in GaAs A strained layer provides protection from dislocation propagation all over the structure.

Non-misfit dislocations and misfit dislocations behave in different ways under electron beam irradiation, tending to shorten and elongate respectively. These

differences are determined by their own strain energies and the different thermodynamic requirements of an unstrained structure and a strained-layer structure. A dislocation creates strain energy in an unstrained structure while a misfit dislocation relaxes the strain energy which has existed in a strained-layer structure before the formation of any misfit dislocations. The behaviours of both non-misfit dislocations and misfit dislocations are dominated by strain energy, but the thermodynamic requirement for the lowest energy state of the system is met in different way. The longer a non-misfit dislocation, the higher the strain energy of the system. Thus, a non-misfit dislocation tends to shorten and line tension works to keep it to the shortest length. In contrast, the longer a misfit dislocation is, the more strain energy it relaxes, and the greater the decrease in strain energy achieved by the system. Thus, a misfit dislocation always tends to elongate, fulfilling the lower energy state for a strained-layer structure. Line tension cannot help this process because it works on a dislocation to keep it as short as possible. Therefore, the expression of the line tension derived from a non-misfit dislocation is no longer valid for a misfit dislocation.

Chapter 7 : Summary, conclusions and suggestions for further research

7.1 Summary

Understanding of relaxation through the formation of misfit dislocations and the effects of misfit stress on the reliability of the structure is vital to the development of reliable devices based on semiconductor strained-layer heterostructures. In this thesis, semiconductor strained-layer GaAs/$In_xGa_{1-x}As$/GaAs heterostructures have been investigated and the stability of the structures have been assessed with respect to dislocations.

Firstly, as-grown specimens have been examined in terms of critical thickness, which provides the basis for understanding relaxation of strained-layer structures and for assessment of stability of the structures with respect to misfit dislocations. Threading dislocations are found to transform from a straight threading geometry in GaAs into different geometries in GaAs/$In_xGa_{1-x}As$/GaAs:

a). threading dislocations with a misfit segment in GaAs/$In_xGa_{1-x}As$/GaAs when the strained-layer thickness is smaller than the critical thickness predicted by the M-B model for single strained-layer heterostructure ($h < h_c$);

b). elongated misfit dislocations in GaAs/$In_xGa_{1-x}As$/GaAs with the strained-layer thickness smaller than the critical thickness for double heterostructure ($h_c < h < H_c$); and

c). a misfit dislocation network in GaAs/$In_xGa_{1-x}As$/GaAs when $h > H_c$.

These results confirm the mechanism of formation of misfit dislocations from threading dislocations as a means of relieving misfit stress in strained-layer structures, in accordance with the M-B model. However, these results also indicate that the misfit segments have been introduced into the structure by transformation of threading

dislocations when the strained-layer thickness is below the critical thickness predicted by the M-B model. Analysis shows that threading dislocations may be able to glide on the interface to form a misfit dislocation segment even though the critical thickness predicted by the M-B model has not been reached. After the generation of misfit dislocations from threading dislocations, compared with the change of the excess stress based on the M-B model, a sudden increase of the misfit dislocation density is found in the development of misfit dislocations with increasing strained-layer thickness. This provides the evidence that there are different stages of relaxation, i.e., the local and global relaxation, in a strained-layer structure during fabrication. The generation of misfit dislocations on threading dislocations is only the behaviour of individual dislocations, and the relaxation resulted from this process is not related to the energy status of the whole structure. Therefore, the mechanism proposed by the M-B model only works for the local relaxation although this model cannot predict the real critical condition for relaxation; the global relaxation is dominated by a separate mechanism.

Secondly, the stability of strained-layer structures is studied by investigation of the response of misfit dislocations to thermal and mechanical stimuli. For structures in which the strained-layer thicknesses are below the critical thickness and the misfit dislocation network had not formed during the fabrication of the structures, thermal processing and an applied stress bring about misfit dislocations. Although they are originally coherent in their as-grown state for either $h < h_c$ or $h_c < h < H_c$ and are generally thought to be either thermodynamically stable or metastable, these structures have all been proved to be relaxable. The formation of misfit dislocations in these structures is found to be thermally activated and sensitive to an applied stress. The generation and propagation of misfit dislocations does not show reliance on pre-existing dislocation sources and each individual dislocation generates and propagates independently. The mechanism which generates edge misfit dislocations is active at high temperature and has produced edge misfit dislocations in these structures with a variable configuration.

Thermal processing introduces a new kind of misfit dislocation into strained-layer structures which have been relaxed by the formation of a 60° dislocation network in their as-grown state. Further relaxation of the structures is found to occur during post-growth thermal processing by the introduction of edge misfit dislocations into the structures. This discovery leads to a new approach to understanding the relaxation of strained-layer structures through the formation of misfit dislocations. The newly-formed dislocations are all in pairs protruding from the pre-existing 60° dislocations. They are all at 45° to the pre-existing 60° dislocations from which they originate. These characterise them as edge type misfit dislocations with a Burgers vector of a/2<101> perpendicular to their line direction of <010>. Based on the difference in lowering the strain energy between 60° and edge dislocations, the misfit stress acting on 60° dislocations, and the vacancies as strain relievers, a model is proposed in which the formation process of edge type misfit dislocations is ascribed to vacancy-producing jogs arising from the pre-existing 60° dislocations and their motion trailing dislocation dipoles.

Finally, as dislocations are the main mechanism of failure of semiconductor devices, the difference in dislocation motion between strained-layer structures and unstrained structures has been investigated. The difference in dislocation motion between the strained-layer structures (GaAs/$In_xGa_{1-x}As$/GaAs) and the unstrained structure (GaAs) is confirmed. Dislocation motion in a strained-layer structure is found to be slower than that in a unstrained normal structure. Distance of dislocation motion decreases with the increase of misfit stress and this decrease is intensified when the compressive strained-layer structures are subjected to an applied stress. This is explained by the two aspects of the effects of misfit stress as follows. Misfit stress is the driving force for the formation of misfit dislocations, but it also provides an additional force to resist the motion of dislocations. The inhibition of dislocation motion in a compressive strained-layer structure results from the lattice compression which strengthens the resistance of atoms to displacement. Also, dislocations formed in a

strained-layer structure lie along the interfaces and are present mainly in interfaces, differing from those in an unstrained structure which are present all over the structure. In this way, a strained layer provides protection against damage to the whole structure resulting from dislocation propagation.

Dislocations investigated in this thesis include non-misfit dislocations and misfit dislocations. It is very important to understand that they differ from each other by their natures, which are manifested by their different behaviours under electron beam irradiation. When activated to move by an electron beam, non-misfit dislocations tend to shorten and misfit dislocations tend to elongate. This reflects their inherent difference and the different thermodynamic requirements of the structures containing different dislocations. A non-misfit dislocation creates strain energy in a system while a misfit dislocation relaxes the strain energy which has been created by building up of the strained-layer system. Considering the change of the total strain energy brought about by them, misfit dislocations are a sink for the strain energy which has been created by fabricating the strained-layer structure and which existed before the formation of misfit dislocations. Non-misfit dislocations are the source of the strain energy which is created by the dislocations themselves. When their motion is driven by the thermodynamic requirement to lower the total strain energy of the systems in which they are located, the resultant strain energy after motion of either non-misfit dislocation or misfit dislocation must be lower than before. Otherwise, this motion is impossible. To achieve this, a non-misfit dislocation has to shorten, while a misfit dislocation has to elongate. The line tension created by a dislocation and the line tension associated with a misfit dislocation can not be treated in the same way based on the strain energy analysis of a dislocation in a normal crystal.

The massive formation of misfit dislocations shown in Chapter 4 and 5 has an implication for understanding the causal relationship between the relaxation of the structure and the formation of misfit dislocations. The formation of misfit dislocations is due to the transition that occurs when the structure passes through a crucial point

which determines the state, coherent or incoherent, of the structure. This transition results in the formation of misfit dislocations. Therefore, misfit dislocations are the result, not the cause, of the transition of a strained-layer structure from coherent to incoherent. The behaviour of individual dislocations, which only has local significance, thus cannot be taken as the criterion to decide whether or not this transition will occur. Understanding of this causality is important for the investigation of relaxation of strained-layer structures through the formation of misfit dislocations because it decides the basis for the theoretical model.

7.2 Conclusions

7.2.1 Relaxation through the formation of misfit dislocations and critical thickness

There is always the possibility of relaxation of strained-layer structures through the formation of misfit dislocations, and there are different stages for this relaxation. The first stage is relaxation during fabrication of structures resulting from the glide of threading dislocations along the interfaces generating 60° misfit dislocations The second is the relaxation resulting from the formation of the 60° misfit dislocation network, which can take place either during growth of the structure or during the post-growth thermal or mechanical experience. The latter is the relaxation resulting from the formation of edge misfit dislocations generated on the pre-existing 60° misfit dislocations. This process only takes placed after the formation of 60° misfit dislocations, or during the post-growth thermal experience, because of the reliance of their formation on the pre-existing 60° misfit dislocations and high temperature.

The relaxation of strained-layer structures can actually be achieved through the formation of different kinds of misfit dislocations. The formation of 60° dislocations is the first option, because the mechanism involved in this process adopts glide which is the easiest way for the introduction of dislocations into structures. Because 60° dislocation can only relax a limited part of the whole misfit strain energy, there are still

thermodynamic requirements that the 60° dislocation relaxed-structures are relaxed further by the formation of new misfit dislocations. These new misfit dislocations are dislocations of edge type generated on pre-existing 60° dislocations. Therefore, relaxation of strained-layer structures through the formation of misfit dislocations involves the mechanisms of both glide and climb. Climb presupposes the existence of 60° dislocations, that is, dislocation climb as a stage of relaxation follows glide. However, this following is not an event immediately. It needs a new condition — thermal activation.

The relaxation realised by the generation of misfit dislocations on threading dislocations, as proposed by the M-B model, has only local significance, because it is only the behaviour of individual dislocations. Comparing with the increase of excess stress, the elongation of such 60° dislocations after their onset is very limited with increasing strained-layer thickness. Because of the sudden increase of misfit dislocation density after the generation and elongation of misfit dislocations on threading dislocations, and of the unlikelihood of the formation of misfit dislocations on the pre-existing dislocation sources during bending tests, the mechanism dominating the global relaxation through the formation of a misfit dislocation network cannot be the one suggested by the M-B model. Even for the misfit dislocations generated as proposed by the M-B model, glide of threading dislocations along the interfaces has been observed to actually begin at strained-layer thicknesses which are smaller than the prediction of the M-B model. Also, the configuration of resultant misfit dislocations is different from that suggested by the M-B model, implying that the practical process of misfit dislocation elongation by glide of threading dislocations along interfaces proceeds in synchronism with the process of MBE growth and occurs at interfaces one after the other.

How individual misfit dislocations develop into a network remains unclear. However, it has been shown that the pre-existing dislocation sources are not crucial for the formation of a 60° misfit dislocation network, and that the formation of the network

results from the independent development of individual dislocations. The interaction between individual misfit dislocations is not significant for the multiplication of misfit dislocations, and is thus not significant for relaxation. A model of the relaxation through the formation of a misfit dislocation network should consider the crucial point at which, under the effects of the misfit stress, the transition of the whole structure towards a lower energy status becomes possible by displacing the atoms adjacent to the interfaces to create misfit dislocations homogeneously.

The formation of misfit dislocations as the result of relaxation is temperature dependent. This means that the critical thickness, if it is defined by the consideration of the global relaxation through the formation of misfit dislocations, is temperature dependent. For a strained-layer structure coherent in its as-grown state, even if it has been considered to be thermodynamically stable or metastable according to the M-B model, relaxation can occur depending on the temperature. An applied stress is an effective means of stimulating this process, significantly decreasing the required temperature. Also, when a strained-layer structure has passed one criterion for relaxation, such as the formation of 60° dislocation network, there is another criterion which decides the next stage of relaxation, such as the further relaxation of the 60° dislocation-relaxed structures.

7.2.2 Stability of strained-layer structures with respect to non-misfit dislocations

The stability of strained-layer structures with respect to non-misfit dislocations is improved by the existence of a strained layer. Misfit stress exists in strained-layer structures with two aspects of its effects on dislocations. The lattice mismatch between an overlayer and its substrate creates misfit stress which drives the formation of misfit dislocations, and also, for a compressive strained-layer structure, this misfit stress produces an additional force which constrains the atoms of strained layer to be more stable in their lattice positions. This makes the displacement of atoms, which is the basic mechanism for dislocation motion, more difficult. In addition, the existence of a

strained layer provides protection from damage to the structure resulting from dislocation propagation. Interfaces in a strained-layer structure trap dislocations keeping them from propagating all over the structure as they do in an unstrained structure.

The effects of the relaxation through the formation of misfit dislocations on the stability of coherent strained-layer structures need not cause concern because it occurs only at temperatures which are too high for general applications. However, caution should be exercised where any possible external stress may be involved, because an applied stress significantly decreases the temperature needed for the formation of misfit dislocations.

7.3 Suggestions for further research

Some of the results obtained in this thesis may provide clues to other questions. The methodology devised in this research has been proved to be effective and efficient. It has potential for further research to solve some unsolved puzzles which are significant to the development of reliable devices based on semiconductor strained-layer structures.

7.3.1 Generality of the duality of misfit stresses

The duality of misfit stress is proposed only based on the compressive strained-layer InGaAs/GaAs heterostructures. To test the general applicability of this concept, other compressive strained-layer structures and tensile strained-layer structures should be examined.

7.3.2 Generation and multiplication of misfit dislocations

Almost all misfit dislocations previously reported are those which had been formed during fabrication of the structure, and investigations into their generation and development were all based on this kind of configuration of misfit dislocations. It has been a puzzle since the emergence of the strained-layer structure how misfit

dislocations generate and develop to form a network. With the methodology devised in this thesis, by careful design and technique, misfit dislocations could be introduced step by step into the structure at the stages of their generation, multiplication, and formation of network, enabling their development to be investigated in detail. So, it can be expected that the puzzle will be solved. This could be a significant contribution to the development of semiconductor strained-layer structures.

7.3.3 Computer simulation of dislocations

The formation of misfit dislocations has not been well understood. For example, why are edge dislocations but not 60° dislocations introduced as further relaxation in the 60° dislocation-relaxed structures during thermal processing? Computer simulations might be able to provide a means of understanding how an edge misfit dislocation can be generated on a 60° dislocation but the 60° dislocations cannot extend further.

Computer simulations could also be expected to simulate the transformation of threading dislocations to generate misfit segments, and to distinguish the strain energy created by a dislocation in an unstrained structure from that associated with a misfit dislocation in a strained-layer structure. Thus, the proposed inapplicability of the traditional line tension concept in dealing with misfit dislocations can be proved.

Appendix A: MBE growth of GaAs/$In_xGa_{1-x}As$/GaAs

[Wang_97, Wang_99, Usher_99]

(1) MBE systems are a Riber 32p and a highly modified Varian MBE-360.

(2) Growth temperature is 793 K for InGaAs and 873 K for others.

(3) Growth rate is ~1 μm/hour.

(4) Layer thickness and composition are caliberated by using RHEED.

(5) The composition of strained layer is also determined by X-ray diffraction.

(6) The accuracy for the indium fraction, x, and layer thickness is ±5%.

(7) All specimens are Si uniformly doped, doping level is about 1×10^{18} cm^{-3}.

Appendix B: Measurement of layer thickness on TEM[Augustus_98]

(1) Method

(a) The specimen should be made as illustrated in Fig. App.B1.

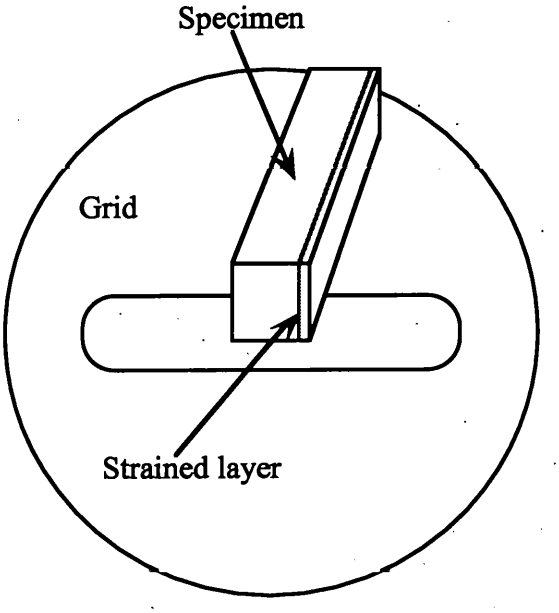

Fig. App.B1. TEM specimen for measurement of strained layer.

(b) Play the specimen on TEM and tilt it to 45°, as shown in Fig. App.B2, so the specimen can be viewed through either edge of the thin wedge.

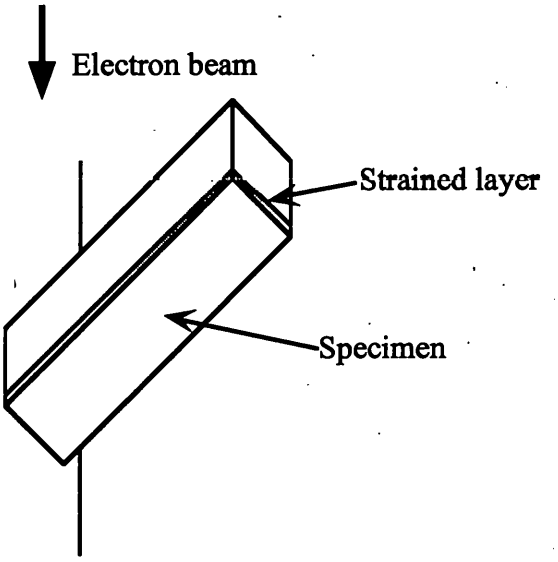

Fig. AppB.2. Measurement of strained-layer thickness on TEM

(c) Go to [010] pole and get (200) reflection.

(d) Observe and photograph the specimen with dark filed imaging.

(2) Measurements

The measurements of the strained-layer thicknesses of GaAs/$In_xGa_{1-x}As$/GaAs specimens are listed in Table App. B1.

Table App. B1. Measurements of the strained-layer thicknesses of GaAs/$In_xGa_{1-x}As$/GaAs specimens

Specimen	Designed thickness (nm)	Measured thickness (nm)
1	4	4.6 ± 0.5
2	6	6.4 ± 0.5
3	6	7.4 ± 0.5
4	6	7.4 ± 0.5

References

Abrahams_65: M. S. Abrahams and C. J. Bujocchi, *J. Appli. Phys.*, **36**, 2855-2863 (1965)

Adachi_96: S. Adachi, in Properties of Gallium Arsenide, third edition, edited by M. R. Brozel and G. E. Stillman, INSPEC, p23-38, 1996

Adams_86: A. R. Adams, *Electron. Lett.*, **22**, 249-250 (1986)

Alexander_68: H. Alexander and P. Haasen, *Solid State Physics*, **22**, 27-158 (1968)

Antonelli_89_A: A. Antonelli and J. Bernholc, *Phys. Rev. B*, **40**, 10643-10646 (1989)

Antonelli_89_B: A. Antonelli and J. Bernholc, *Mater. Res. Soc. Symp. Proc.*, **61**, 289 (1989)

Augustus_98: P. Augustus, a private communication, 1998

Beanland_97: R. Beanland, M. A. Lourenco and K. P. Homewood, *Inst. Phys. Conf. Ser.* **No. 157**, 145-148 (1997)

Born_88: M. Born and K. Huang, Dynamical Theory of Crystal Lattices, Oxford, 1988

Beeston_73: B. E. P. Beeston, Robert W. Horne and Roy Markham, Electron Diffraction and Optical Diffraction Techniques, North-Holland Publishing Company, 1973

Bouillet_93: C. Ulhaq-Bouillet and A. Leffbvre, *Phil. Mag. A*, **68**, 1273-1294 (1993)

Breen_89: K. R. Breen, P. N. Uppal, and J. S. Ahearn, *J. Vac. Sci. Technol.*, **B7**, 758-763 (1989)

Breen_90: K. R. Breen, P. N. Uppal, and J. S. Ahearn, *J. Vac. Sci. Technol.*, **8**, 730-735 (1990)

Brenchley_97: M. E. Brenchley, M. Hopkinson, A. Kelly, P. Kidd, and D. J. Dunstan, *Phys. Rev. Lett.*, **78**, 3912-3194 (1997)

Chu_85: S. N. G. Chu, A. T. Macrander, K. E. Strege, and W. D. Johnston, Jr., *J. Appl. Phys.*, **57**, 249-257 (1985), *J. Appl. Phys.*, **60**, p1238 (1986)

Cohen_94_A: G. Cohen-Solal. F. Bailly, and M. Barbe, *J. Cryst. Growth*, **138**, 68-74 (1994)

Coleman_91_A: J. J. Coleman, R. G. Waters, and D. P. Bour, **SPIE Vol. 148** *Laser Diode Technology and Applications III*, 318-327 (1991)

Demeester_93: P. Demeester, I. Pollentier, P. De Dobbelaere, C. Brys, and P. Van Daele, *Semicond. Sci. Technol.*, **8**, 1124-1135 (1993)

Dixon_90: R. H. Dixon and P. J. Goodhew, *J. Appl. Phys.*, **68**. 3163-3168 (1990)

Dodson_87: B. W. Dodson and J. Y. Tsao, *Appl. Phys. Lett.*, **51**, 1325-1327 (1987)

Dodson_88: B. W. Dodson and J. Y. Tsao, *Appl. Phys. Lett.*, **52**, p852 (1988)

Downes_94: J. R. Downes, D. J. Dunstan, and D. A. Faux, *Semicond. Sci. Technol.*, **9**, 1265-1267 (1994)].

Downes_97: J. R. Downes, D. J. Dunstan, and D. A. Faux, *Phil. Mag.*, **76**, 77-81 (1997)

Drigo_89_A: A. V. Drigo, A. Aydinli, A. Carnera, F. Genova, C. Rigo, C. Ferrari, P. Franzosi, and G. Salviati, *J. Appl. Phys.*, **66**(5), 1975-1983 (1989)

Dunstan_97: D. J. Dunstan, *J. Materials Science:Materials in Electronics*, **8**, 337-375 (1997)

Erofeeve_94: S. A. Erofeeve, *Phil. Mag.*, **70**, 943-950 (1994)

Esquivel_73: A. L. Esquivel, W. N. Lin, and D. B. Wittry, *Appl. Phys. Lett.*, **22**, 414-416 (1973)

Felbeck_84: D. K. Felbeck and A. G. Atkins, Strength and Fracture of Engineering Solids, Prentice-Hall, Inc., 1984

Fitzgerald_89: E. A. Fitzgerald, G. P. Watson, R. E. Proano, D. G. Ast, P. D. Kirchner, G. D. Pettit, and J. M. Woodall, *J. Appl. Phys.*, **65**(6), 2220-2237 (1989)

Fitzgerald_91: E. A. Fitzgerald, *Mater. Sci. Rep.*, **7**, 87-142 (1991)

Fox_90: B. A. Fox and W. A. Jesser, *J. Appl. Phys.*, **68**, 2801-2808 (1990)

Frank_49_A: F. C. Frank and J. H. van der Merwe, *Proc. Roy. Soc.*, **A198**, 205-216 (1949)

Frank_49_B: F. C. Frank and J.H.van der Merwe, *Proc. Roy. Soc.*, **A198**, 216-225 (1949)

Freund_90: L. B. Freund, J. *Mech. Phys. Solids*, **38**, 657-679 (1990)

Friedel_67: J. Friedel, Dislocations, Pergamon Press, 1967

Fritz_87_A: I. J. Fritz, P. L. Gourly, and L. R. Dawson, *Appl. Phys. Lett.*, **51**, 1004-1006 (1987)

Fritz_87_B: I. J. Fritz, *Appl. Phys. Lett.*, **51**, 1080-1081 (1987)

Gillin_94: W. P. Gillin and D. J. Dunstan, *Phys. Rev. B*, **50**, 7495-7498 (1994)

Goodhew_88: P. J. Goodhew and F. J. Humphreys, Electron Microscopy and Analysis, Taylor & Francis, 1988

Goodhew_94: P. J. Goodhew, *J. Physics and Chemistry of Solids*, **55**, 1107-1114 (1994)

Goodhew_97: P. J. Goodhew and G. MacPherson, Institute of Physics Conference Series, No.157, 111-120 (1997)

Goodhew_99: P. J. Goodhew and K. Giannakopoulos, *Micron*, **30**, 59-64 (1999)

Grundmann_89: M. Grundmann, U. Dienert, D. Bimberg, A. Fischer-Colbrie, and J. N. Miller, *Appl. Phys. Lett.*, **55**, 1765-1767 (1989)

Grundy_76: P. J. Grundy and G. A. Jones, Electron Microscopy in the Study of Materials. Edward Arnold, 1976

Hagen_78: W. Hagen and H. Strunk, *Appl. Phys.*, **17**, 85-87 (1978)

Haasen_68: P. Haasen, in Materials Science Engineering Series: Dislocation Dynamics, McGraw-Hill Book Company, New York, p701-722, 1968

Hearn_77: E. J. Hearn, Mechanics of Materials, Pergamon Press, 1977

Heimendahl_80: Manfred Von Heimendahl, Electron Microscopy of Materials: An Introduction, Academic Press, 1980

Hirsch: P. B. Hirsch, R. W. Horne, and M. J. Whelan, *Phil. Mag.*, **1**, 677-684 (1956)

Hopgood_94: A. A. Hopgood, *J. Appl. Phys.*, **76**(7), 4068-4071 (1994)

Howard_91: D. J. Howard, D. C. Paine, and R. N. Sacks, *J. Electron. Microsc. Technol.*, **18**, 117-120 (1991)

Hull.D_92: D. Hull and D. J. Bacon, Introduction to Dislocations, 3rd edition, Pergamom Press, 1992

Hull.R_92: R. Hull and J.Bean, *Critical Reviews in Solid State and Materials Science*, **17**, 507-546 (1992)

Hull.R_96: R. Hull and E. A. Stach, *Current Opinion in Solid State and Materials Science*, **1**(1), 21-28 (1996)

Hutchinson_75: P. W. Hutchinson, P. S. Dobson, S. O'Hara, and D. H. Newman, *Appl. Phys. Lett.*, **26**, 250-252 (1975)

Jain_94: S. C. Jain, Ge-Si Strained Layers and Heterostructures, Academic Press, London, 1994

Jesser_67: W. A. Jesser and J. W. Matthews, *Phil. Mag.*, **15**, 1097-1106 (1967)

Jesser_68_A: W. A. Jesser and J. W. Matthews, *Phil. Mag.*, **17**, 461-473 (1968)

Jesser_68_B: W. A. Jesser and J. W. Matthews, *Phil. Mag.*, **17**, 595-602 (1968)

Jesser_90_A: B. A. Jesser and W. A. Jesser, *J. Appl. Phys.*, **68**, 2801-2808 (1990),

Jesser_90_B: W. A. Jesser and B. A. Fox, *J.Electron. Mater.*, **19**, 1289-1297 (1990)

Kanagai_78: M. Kanagai, M. Sugimoto, and T. Takahashi, *J. Crys. Growth*, **45**, 277-280 (1978)

Kelly_63: A. Kelly and R. B. Nicholson, *Prog. in Materials Science*, **10**, 149-392 (1963)

Kidd_93: P. Kidd, P. F. Fewster, N. L. Andrew, and D. J. Dunstan, *Inst. Phys. Conf. Ser.*, **134**, 585-588 (1993)

Kirkby_75: P. A. Kirkby, *IEEE J. Quantum Electron.*, **QE-11**, 562-568 (1975)

Kishino_76: S. Kishino, N. Chinone, H. Nakashima, and R. Ito, *Appl. Phys. Lett.*, **29**, 488-490 (1976)

Kovacs_73: I. Kovacs and L. Zsoldos, Dislocations and Plastic Deformation, Pergamon Press, 1973

Kuesters_86: K. H. Kuesters, B. C. De Cooman, and C. B. Carter, *Phil. Mag. A*, **53**, 141-159 (1986)

Laidig_84: W. D. Laidig, P. J. Caldwell, Y. F. Lin, and C. K. Peng, *Appl. Phys. Lett.*, **44**, 653-655 (1984)

Lefebvre_91: A. Lefebvre, C. Herbeaux, and J. Di Persio, *Philos. Mag.*, **A63**, 471-485 (1991)

LeGoues_96: F. K. LeGoues, *MRS Bulletine*, **21**, 38-44 (1996)

Loretto_94: M. H. Loretto, Electron Beam Analysis of Materials, 2nd edition, Chapman & Hall, p15-26, 1994

Lourenco_94: M. A. Lourenco, K. P. Homewood, and L. Considine, *Mater. Sci. Eng.*, **B28**, 507-509 (1994)

Maree_87: P. M. J. Maree, J. C. Barbour, J. F. van der Veen, K. L. Kavanagh, C. W. T. Bulle-Lieuwma, and M. P. A. Viegers, *J.Appl. Phys.*, **62**, 4413-4420 (1987)

Matthews_66: J. W. Matthews, *Phil. Mag.*, **13**, 1207-1221 (1966)

Matthews_70_A: J. W. Matthews, S. Mader, and T. B. Light, *J. Appl. Phys.*, **41**, 3800-3804 (1970)

Matthews_70_B: J. W. Matthews and J. L. Crawford, *Thin Solid films*, **5**, 187-198 (1970)

Matthews_74: J. W. Matthews and A. E. Blakeslee, *J. Crystal Growth*, **27**, 118-125 (1974)

Matthews_75_A: J. W. Matthews, *J. Vac. Sci. Thecnol.*, **12**, 126-133 (1975)

Matthews_75_B: J. W. Matthews and A. E. Blakeslee, *J. Cryst. Growth*, **29**, 273-280 (1975)

Matthews_76: J. W. Matthews, A. E. Blakeslee, and S. Mader, *Thin Solid film*, **33**, 253-273 (1976)

Matthews_79: J. W. Matthews, "Misfit dislocations" in *Dislocations in Solids*, edited by F. R. N. Nabarro, North-Holland Publishing Company, 462 - 545, 1979

Matthews_89: J. W. Matthews, K. R. Breen, P. N. Uppal, and J. S. Ahearn, *J. Vac. Sci. Technol.*, **B7**, 758(1989)

Merwe_91: J. van der Merwe, *Critical Reviews in Solid State and Materials Sciences*, **17**, 187-209 (1991)

Merwe_91B: J. van der Merwe, *J. Electronic Materials*, **20**, 793-803 (1991)

Miller_80: D. C. Miller and G. A. Rozgonyi, Hand book on Semiconductord, Vol. 3, edited by S. P. Keller, North-Holland, Amsterdam, p217, 1980

Nabarro_67: F. R. N. Nabarro, Theory of Crustal Dislocations, Oxford University Press, 1967

Nadgomyi_88: E. Nadgornyi, Progress in Materials Science: Dislocation Dynamics and Mechanical Properties of Crystals, Pergamon Press, 1988

Nix_89_A: W. D. Nix, *Met.allurgical Transactions A-Physical Metallurgy and Materials Science*, **20**, 2217-2245 (1989)

Paine_90: D. C. Paine, D. J. Howard, D. Luo, R. N. Sacks, and T. C. Eschrich, Mater. *Res. Soc. Symp. Proc.*, **160**, 123-128 (1990)

Pashley_59: D. W. Pashley, *Phil. Mag.*, **4**, 324-335 (1959)

Pashley_65_A: D. W. Pashley, *Adv. in Physics*, **14**, 327-416 (1965)

Paufler_87: P. Paufler, P, Rotsch, and G. Wagner, *Phil. Mag. A*, **56**, 533-551 (1987)

People_85: R. People and J. C. Bean, *Appl. Phys. Lett.*, **47**, 322-324 (1985)

People_86: R. People and J. C. Bean, *Appl. Phys. Lett.*, **49**, p229(1986)

Petroff_73: P. Petroff and R. L. Hartman, *Appl. Phys. Lett.*, **23**, 469-471 (1973)

Pichaud_98: B. Pichaud, M. Putero, and N. Burle, *J. Phys. IV France (Journal De Physique IV)*, **8**, (Pr4)227-236 (1998)

Pichaud_99: B. Pichaud, M. Putero, and N. Burle, *Physica Status Solidi A - Applied Research*, **171**, 251-265 (1999)

Pinardi_98: K. Pinardi, U. Jain, S. C. Jain, H. E. Maes, R. van Overstraeten, and M. Willander, *J. Appli. Phys.*, **83** (9), 4724-4733 (1998)

Price_91: G. L. Price, *Phys. Rev. Lett.*, **66**, 469-472 (1991)

Rajan_87: K.Rajan and M.Denhoff, *J. Appl. Phys.*, **62**, 1710-1712 (1987)

Radulescu_89: D. C. Radulescu, *J. Vac. Sci. Technol.*, **B7**, 111-115 (1989)

Read_53: W. T. Read, Dislocations in Crystals, McGraw-Hill Book Company, Inc., 1953

Rhan_96: H. Rhan. in III-V Quantum Wells and Superlattices, edited by P. Bhattacharya, INSPEC, 1996

Ralls_76: K. M. Ralls, T. H. Courtney, and J. Wulff, Introduction to Materials Science and Engineering, John Wiley & Sins, Inc., 1976

Stringfellow_93: G. B. Stringfellow, in Properties of Lattice-Matched and Strained InGaAs, edited by P. Bhattacharya, INSPEC, 1993

Strunk_79: H.Strunk, W.Hagen, and E.Bauser, *Appl. Phys.*, **18**, 67-75 (1979)

Sugiura_94: L.Sugiura, K.Shigenaka, F.Nakata, and K.Hirahara, *J. Crystal Growth*, **145**, 547-551 (1994)

Sutton_95: A. P. Sutton and R. W. Balluffi, Interfaces in Crystalline Materials, Clarendon Press, Oxford, 1995

Takahashi_93: N. S. Takahashi and M. Matsuura, in Properties of Lattice-Matched and Strained InGaAs, edited by A Bhattacharya, INSPEC, 1993

Thijs_89: P. J. A. Thijs and T. van Dongen, *Electron. Lett.*, **25**, 1735-1737 (1989)

Thijs_95: P. J. A. Thijs, L. F. Tiemeijer, J. J. M. Binsma, and T. van Dongen, *Philips J. Res.*, **49**, 187-224 (1995)

Tsao_87: J. Y. Tsao, B.W.Dodson, S. T. Picraux, and D. M. Cornelison, *Physical Review Letters*, **59**, 2455-2458 (1987)

Tsao_88: J.Y.Tsao and B.W.Dodson, *Appl. Phys. Lett.*, **53**, 848-850 (1988)

Twigg_90: M. E. Twigg, *J. Appl. Phhys.*, **68**, 5109-5114 (1990)

Ueda_88: O. Ueda, *J. Electrochem. Soc.: Rev. News*, 135, C11-C22 (1988)

Usher_99: B. F. Usher, a private communication, 1999

Vodhanel_89: R. S. Vodhanel, R. I. Laming, V. Shah, L. Curtis, D. P. Bour, W. L. Barnes, J. D. Minelly, E. J. Tarbox, and F. J. Tarbox, *Electron. Lett.*, **25**, 1386-1388 (1989)

Wang_96: J. N. Wang, *Acta Mater.*, **44**, 1541-1546 (1996)

Wang_97: H. Wang, a private comunication, 1997

Wang_99: H. Wang, a private comunication, 1999

Waters_90: R. G. Waters, D. P. Bour, S. L. Yellen, and N. F. Ruggieri, *IEEE Photon. Technol. Lett.*, **2**, 531-533 (1990)

Waters_91: R. G. Waters, R. J. Dalby, J. A. Baumann, J. L. Sanctis, and A. H. Shepard, *IEEE Photon Technol. Lett.*, **3**, 409-411 (1991)

Weertman_92: J. Weertman and J. R. Weertman, Elementary Dislocation Theory, Oxford University Press, 1992

Whaley_90: G. J. Whaley and P. I. Cohen, *Mater. Res. Soc. Symp. Proc.*, **160**, 35-46 (1990)

Whitehouse_93: C. R. Whitehouse, S .J. Barnett, B. F. Usher, A. G. Cullis, A. M. Keir, A. D. Johnson, G. F. Clark, B. K. Tanner, W. Spirkl, B. Lunn, W. Hagston, and C. Hogg, *Inst. Phys. Conf. Ser.* **134**, 563-568 (1993)

Williams_96: D. B. Williams and C. B. Carter, Transmission Electron Microscopy, Plenum Press, 1996

Yablonovitch_86: E. Yablonovitch and E. O. Kane, *J. Lightwave Technol.*, **LT-4**, 504-506 (1986)

Zaumseil_96: P. Zaumseil, G. G. Fischer, Ch. Quick, and A. Misiuk, P*hys. Stat. Sol. (a)*, **153**, 401-408 (1996)

Zuo_93: J. Zuo and D. J. H. Cockayne, *J. Appl. Phys.*, **73**, 619-626 (1993)